EXPLICIT NUMERICAL STUDY OF AEROSOL-CLOUD INTERACTIONS IN BOUNDARY LAYER CLOUDS

Irena T. Paunova

Department of Atmospheric and Oceanic Sciences

McGill University, Montréal

May 2006

A thesis submitted to McGill University in partial fulfillment

of the requirements of the degree of Doctor of Philosophy

Your file Votre référence
ISBN: 978-0-494-25226-0
Our file Notre référence
ISBN: 978-0-494-25226-0

Abstract

Aerosol-cloud interactions, the mechanisms by which aerosols impact clouds and precipitation and clouds impact aerosols as they are released upon droplet evaporation, are investigated by means of explicit high-resolution (3 km) numerical simulations with the Mesoscale Compressible Community (MC2) model. This model, which is non-hydrostatic and compressible, was extended by including separate continuity equations for dry and activated multi-modal aerosol, and for chemical species. The sources and sinks include: particle activation, solute transfer between drops, generation of extra soluble material in clouds via oxidation of dissolved SO_2, and particle regeneration. The cloud processes are represented by an advanced double-moment bulk microphysical parameterization.

Three summertime cases have been evaluated: a marine stratus and a cold frontal system over the Bay of Fundy near Nova Scotia, formed on 1 Sep 1995 and extensively sampled as a part of the Radiation, Aerosol, and Cloud Experiment (RACE); and a continental stratocumulus, formed over the southern coast of Lake Erie on 11 July 2001. The marine stratus and the frontal system have been examined for the effects of aerosol on cloud properties and thoroughly evaluated against the available observations. The frontal system and the continental stratocumulus have been evaluated for the effects of cloud processing on the aerosol spectrum.

The marine stratus simulations suggest a significant impact of the aerosol on cloud properties. A simulation with mechanistic activation and a uni-modal aerosol showed the best agreement with observations in regards to cloud-base and cloud-top height, droplet concentration, and liquid water content. A simulation with a simple activation parameterization failed to simulate essential bulk cloud properties: droplet concentration was significantly underpredicted and the vertical structure of the cloud was inconsistent with the observations. A simulation with a mechanistic parameterization and a bi-modal aerosol, including a coarse mode observed in particle spectra below cloud, showed high sensitivity of droplet concentration to the inclusion of the coarse mode. There was a significant reduction in droplet number relative to the simulation without the coarse mode. A similar change occurred in the precipitating system preceding the stratus formation, resulting in an enhancement of precipitation in the weaker (upstream) part of

the system while the precipitation in the more vigorous (downstream) part of the system remained almost unaffected.

Aerosol processing via collision-coalescence and aqueous chemistry in the non-drizzling stratocumulus case suggests that impact of the two mechanisms is of similar magnitude and can be as large as a 3-5 % increase in particle mean radius. A more detailed analysis reveals that the impact of chemical processing is oxidant-limited; beyond times when the oxidant (H_2O_2) is depleted (~ 40 minutes), the extent of processing is determined by supply of fresh oxidant from large-scale advection (fresh gaseous emissions are not considered). Aerosol processing via drop collision-coalescence alone suggests, as expected, sensitivity to the strength of the collection process in clouds. Larger particle growth, up to 5-10 %, is observed in the case of the frontal clouds, which exhibit stronger drop collection compared to that in the stratocumulus case. The processed aerosol exerted a measurable impact on droplet concentrations and precipitation production in the frontal clouds. For the case modeled here, contrary to expectations, the processed spectrum (via physical processing) produced higher droplet concentration than the unprocessed spectrum. The reasons explaining this phenomenon and the resulting impact on precipitation production are discussed.

The current work illustrates the complexity of the coupled system at the cloud system scales, revealed earlier at much smaller large eddy scales. If future parameterizations of the regional effect of aerosols on clouds are to be developed, careful consideration is required of the many of feedbacks in the boundary layer.

Résumé

Les intéractions entre aérosols et nuages (ie. les mécanismes par lesquels les aérosols influencent les nuages et la precipitation et les nuages influencent les aérosols qui sont dechargés pendant l'évaporation des goutelettes) sont étudiées à l'aide de simulations numériques explicites à haute résolution (utilisant un pas de grille de 3 km) avec le modéle méso-échelle-compressible-communautaire, MC2. Le modéle qui est non-hydrostatique et compressible, a été ajusté pour inclure les équations de continuité pour des aérosols secs, des aérosols activés et multimodals et des espéces chimiques. Les gains et pertes comprennent: l'activation des particules, le transfert des substances entre les gouttes, la production du matiériel soluble dans les nuages par oxidation de SO_2 dissous, et la régénération des particules. Les processus nuagueux sont représentés par une paramétrisation avancée basée sur la microphysique en deux moments.

Trois cas de nuages d'été ont été évalués: un stratus marin et un système frontal froid au dessus de la Baie de Fundy près de Nouvelle Ecosse, qui se sont formés le 1 Septembre 1995 et qui ont été beaucoup échantilloné pendant l'expérience RACE (Expérience de Radiation, d'Aérosol et des Nuages); et un cas stratocumulus continental qui s'est formé sur le côte sud du lac Erie le 11 Juillet 2001. Dans le cas du stratus marin et le cas du système frontal froid, on a comparé les effets des aérosols sur les propriétés des nuages avec les observations disponibles. Dans le cas du système frontal froid et le cas du stratocumulus continental, on a étudié l'effet du traitement des nuages sur le spectre des aérosols.

Le traitement des aérosols dans un système pluvieux a aussi été évalué afin de le comparer avec le traitement dans les stratocumulus qui ne produisent pas de bruine. L'impact des aérosols traités sur les nuages et la précipitation a été évalué.

Les simulations des nuages du type stratus marin suggèrent un impact important des aérosols sur les propriétés des nuages. Une simulation où l'activation mécaniste et des aérosols uni-modals ont été appliqués, a démontré un meilleur accord avec les observations en ce qui concerne la base des nuages, l'altitude de leurs sommets, la concentration des goutelettes et le LWC. Une simulation où une simple parametrization de l'activation a été appliquée, a échoué à reproduire les propriétés fondamentales des nuages: la concentration de goutelettes a été fortement sous-estimé et la structure verticale des nuages ne representait pas la structure revélée par les observations. Une simulation avec une parametrization mécaniste et un aérosol bimodal qui contient un

mode additionnel observé dans le spectre des particules au-dessous des nuages, a démontré de haute sensibilité à la concentration des goutelettes dans ce dernier mode. La sensibilité s'exprime comme une réduction considérable du nombre de goutelettes comparativement à la simulation où le mode n'est pas inclus. Une évolution similaire s'est produit dans le systéme pluvieux qui a précédé la formation du nuage type stratus. Elle a fini avec une augmentation de la précipitation dans la partie faible (en amont) du système tandis que la précipitation dans la partie du système plus vigoureuse (aval) est restée presque insensible.

Le traitement des aérosols par les mécanismes de collision-coalescence et de chimie aqueuse dans les nuages qui ne produisent pas de bruine, demontre un petit impact de la même grandeur pour les deux mécanismes, chacun résultant à une augmentation jusqu' à 3-5 % du rayon moyen. Une analyse plus detaillée a revelé que l'impact du traitement chimique est controlé par l'oxidant; au-delà d'une période d'environ 40 min qu'il prend pour que l'oxidant (H_2O_2) soit épuisé, l'ampleur du traitement est décidé par l'approvisionnement de nouveau oxidant par l'advection aux grandes échelles (les nouvelles émissions gazeuses n'étant pas considerées). Comme prévu, le traitement des aérosols seuleument par collision-coalescence des gouttes, a démontré de la sensibilité à l'intensité du processus de collection dans les nuages. La croissance des particules est jusqu'à 5-10 % plus grande dans le cas des nuages frontaux pour lesquels la collection des gouttes est accentuée, comparativement au cas des nuages du type stratocumulus. Pour les nuages frontaux on trouve que l'aérosol traité exerce un impact mesurable sur les concentrations de goutelletes et sur la production de précipitation. Contre nos attentes dans le cas qu'on a simulé, le spectre traité par processus physique a donné une plus grande concentration des goutelettes que le spectre non traité. Les causes qui peuvent expliquer ce phénomène et l'impact qui se produit sur la production de précipitation sont discutés.

Le travail dénote la complexité du systéme couplé à l'échelle des nuages, qui a déjà été démontré pour les échelles plus petites comme celles des tourbillons. Pour développer la paramétrization des effets régionaux des aérosols sur les nuages, des études prudentes sur la rétroactions des aérosols dans la couche limite sont requises.

Statement of Originality

The following aspects of this study are considered original:

(1) The first explicit high-resolution (3 km) mesoscale numerical simulation of aerosol-cloud feedbacks in boundary-layer clouds achieved by implementation of a balanced approach for dry and activated aerosol and chemical species commensurate in complexity with the representation of cloud microphysics and dynamics. This was achieved by including the following components:
   a. prognostic equations for dry and activated multi-modal (lognormal) aerosol and for selected chemical species
   b. sources and sinks consisting of particle activation, solute transfer between drop categories, aqueous sulfate chemistry, and particle regeneration.

(2) The attainment of realistic droplet concentration in marine stratus cloud by the addition of a mechanistic parameterization of the activation process.

(3) The demonstration of the sensitivity of the marine stratus and that of a precipitating system to giant cloud condensation nuclei at intermediate spatial scales resolving the cloud system.

(4) Explicit simulation of the impacts on the particle spectrum of collision-coalescence and aqueous chemistry processing in continental stratocumulus at the intermediate (cloud system) scales, which have not been previously evaluated.

(5) Isolating the relative contributions to particle growth of the two processing mechanisms at the above scales.

(6) The demonstration that it is necessary to consider multi-modal representation of both the dry and the activated particle spectra to simulate realistically cloud processing of CCN using the modal approach.

(7) The simulation of the impacts of the processed aerosol (via collision-coalescence) on precipitation production in frontal clouds at the cloud system scales

(8) The demonstration of the complexity of the coupled system, revealed earlier at much smaller large eddy scales, at intermediate cloud system scales.

Acknowledgements

I would like to thank my supervisor Prof. Henry G. Leighton for suggesting this research project and allowing great academic freedom to go about the research. His directional suggestions and constructive criticism at various stages of this work have been invaluable. I also would like to thank him for his editorial comments, which have improved this manuscript immensely. I enjoyed working with him and look forward to future collaborations. I also would like to thank my other committee members, Prof. Peter (M. K.) Yau and Prof. John Gyakum for discussions and their critical suggestions regarding different aspects of this research. In the beginning of this project I greatly benefited from Dr. Badrinath Nagarajan who helped me get started with the MC2 modeling system and his constant guidance on various model related issues. Dr. Jason Milbrandt is acknowledged for providing the source code of the microphysical scheme and for discussions on the scheme. I wish to thank my colleague and friend Dr. Lily Ioannidou for the French translation of the abstract.

I also would like to thank people who provided data for this research. Mark Couture and Richard Leaitch of the Meteorological Service of Canada – Downsview are acknowledged for providing aircraft cloud microphysical and aerosol data and for their helpful comments on the measurements; Richard Leaitch is also acknowledged for suggesting the Lake Erie case and discussions on the cloud chemistry part of this work. Alexander Trishchenko of the Canadian Space Agency is acknowledged for providing satellite data.

I am thankful to the members of my research group for the very friendly atmosphere, which prevailed during our weekly meetings. I would like to thank my colleagues and friends in the Department of Atmospheric and Oceanic Sciences who have always been cheerful and friendly to me.

Lastly, I would like to thank my family who have always helped me to push the envelop of my abilities and who have taken such delight in my accomplishments.

Contents

List of Figures

altitude 1050 m. Vertical distribution of b) LWC (shading; g m^{-3}) and raindrop radius (contours; μm) and c) cloud concentration (shading; cm^{-3}) and raindrop concentration (contours; dm^{-3}). The vertical cross section is taken along track ABC. Panels are valid at 18 UTC.

Figure 4.5: Various fields in experiment CTRL: a) horizontal distribution of rain rate (mm hr^{-1}) and horizontal winds; the line EF indicates the vertical cross section in b); b) vertical cross-section of vertical velocity (m s^{-1}; positive values in shading negative in contours) along line EF; solid contour shows the cloud boundary. Panels are valid at 9 UTC.

Figure 4.6: Same as: a) Fig.4.3a; b) Fig. 4.3b; c) Fig. 4.3d but for experiment M1.

Figure 4.7: Same as Fig. 4.4 but for experiment M1.

Figure 4.8: Various fields in experiment M1: a) change of rain rate (mm hr^{-1}) relative to experiment CTRL; b) change in LWP (mm) relative to experiment CTRL; and c) change in column-average droplet concentration (cm^{-3}) relative to experiment CTRL. Panels are valid at 9 UTC.

Figure 4.9: Same as: a) Fig.4.3a; b) Fig. 4.3b; and c) Fig. 4.3d but for experiment M2.

Figure 4.10: Same as: a) Fig. 4.4b; and b) Fig. 4.4c but for experiment M2.

Figure 4.11: Various fields in experiment M2: a) change of rain rate (mm hr^{-1}) relative to experiment M1; b) change in LWP (mm) relative to experiment M1; and c) change in column-average droplet concentration (cm^{-3}) relative to experiment M1. Panels are valid at 9 UTC.

Figure 5.1: Geometric mean radius (nm) (in terms of number) in shading and total number concentration (cm^{-3}) in contours of first processed mode in experiment S0. Panels are valid at: a) 0900 UTC, b) 1200 UTC, and c) 1500 UTC. Solid contour shows the cloud boundary. The cross section is taken along line EF.

Figure 5.2: Reduction (%) in the geometric mean radius (in terms of number) in shading of the background aerosol mode in experiment S0. Panel is valid at 1200 UTC. Solid contour shows the cloud boundary. The cross section is taken along line EF.

Figure 5.3: Change (%) in geometric mean radius (in terms of number; in shading) in experiment S1 relative to S0 and in total number concentration (in contours) in

experiment S0 relative to S1 of the first regenerated mode. Panels are valid at: a) 0900 UTC; b) 1200 UTC; and c) 1500 UTC. Solid contour shows the cloud boundary. The cross section is taken along line EF.

Figure 5.4: Geometric mean radius (in terms of number; μm; in shading) and total number concentration (dm^{-3}; in contours) of the second regenerated modes in experiment S1. Panels are at: a) 0900 UTC, b) 1200 UTC, and c) 1500 UTC. Solid line shows the cloud boundary. The cross section is taken along line EF.

Figure 5.5: Changes (%) of geometric mean radius (in terms of number) in shading and number concentration in contours of the first regenerated mode in experiment S1 relative to M1. Panel is valid at 1500 UTC. Solid contour shows the cloud boundary. The cross section is taken along line EF.

Figure 5.6: Changes (%) in geometric mean radius (in terms of number) of a) first and b) second regenerated modes in experiment M1 relative to S1. Panels are valid at 1200 UTC. Solid contour shows the cloud boundary. The cross section is taken along line EF.

Figure 5.7: a) Changes in cloud LWC ($g\ m^{-3}$; in shading) and droplet concentration (cm^{-3}; in contours) in experiment M1 relative to S1. The cross section is taken along line EF. b) Changes in precipitation rate ($mm\ hr^{-1}$; in shading) in experiment S1 relative to M1. Panels are valid at 0900 UTC.

Figure 6.1: Various fields in experiment S0: a) cloud LWP (mm) and horizontal winds ($m\ s^{-1}$); line CD indicates the vertical cross-section in b); b) vertical velocity ($m\ s^{-1}$) in shading (positive values) and in contours (negative values); the solid contour shows the cloud boundary. Panels are valid at 1800 UTC.

Figure 6.2: Various fields in experiment S0: a) cloud LWP (mm); the arrow indicates cross section CD in the remaining panels; b), c) and d) show cloud LWC ($g\ m^{-3}$) in shading and raindrop radius (μm) in contours. Panels are valid at: a) 1500 UTC, b) 1800 UTC, c) 2100 UTC, and d) 2400 UTC.

Figure 6.3: Same as Fig. 6.2 but for cloud droplet concentration (cm^{-3}) in shading and raindrop concentrations (dm^{-3}) in contours.

Figure 6.4: Various fields in experiment S0: a) vertical velocity ($m\ s^{-1}$; positive values in shading, negative in contours) and horizontal winds ($m\ s^{-1}$); b) background aerosol mode

geometric mean radius (in terms of number; nm; in shading) and number concentration (cm^{-3}; in contours); and c) solute content in cloud drops ($\mu g\ m^{-3}$). Panels are valid at 2100 UTC. Solid contour shows cloud boundary. The cross-section is taken along line CD.

Figure 6.5: Geometric mean radius (in terms of number, nm) (in shading) and number concentration (cm^{-3}) (in contours) of first regenerated mode (without processing). Panels are valid at a) 1500 UTC, b) 1800 UTC, c) 2100 UTC and d) 2400 UTC. The solid contour shows the cloud boundary. The cross-section is taken along line CD.

Figure 6.6: Solute content in cloud category (in shading) and in large hydrometeor category (in contours) ($\mu g\ m^{-3}$). The cross-section is taken along line CD.

Figure 6.7: Change of the total number concentration (cm^{-3}) of first processed mode in experiment S0 relative to S1. Panels are valid at a) 1500 UTC, b) 1800 UTC, c) 2100 UTC and d) 2400 UTC. The black contour shows the cloud boundary. The cross-section is taken along line CD.

Figure 6.8: Geometric mean radius (in terms of number, μm) in shading and number concentration (cm^{-3}) in contours of second regenerated mode. Panels are valid at a) 1500 UTC, b) 1800 UTC, c) 2100 UTC and d) 2400 UTC. The solid contour shows the cloud boundary. The cross-section is taken along line CD.

Figure 6.9: Various chemical species in experiment SO1: a) SO_2 (ppbv) b) NH_3 (ppbv) c) H_2O_2 (ppbv) and d) pH units. Panels are valid at 1800 UTC. The cross-section is taken along line CD.

Figure 6.10: Change of the geometric mean radius (in terms of number; nm) of first processed mode in experiment SO1 relative to S1. Panels are valid at a) 1500 UTC, b) 1800 UTC, c) 2100 UTC and d) 2400 UTC. The black contour shows the cloud boundary. The cross-section is taken along line CD.

List of Tables

Chapter I

Introduction

1.1 Effects of aerosols on clouds

Observational studies have firmly established that anthropogenic aerosols exert an impact on clouds due to the fact that aerosols can act as cloud condensation nuclei (CCN). The effect of anthropogenic CCN on cloud radiative properties, and thus on the radiative budget of the atmosphere, is referred to as the indirect aerosol effect. This effect can take place via different mechanisms: (1) via change in droplet concentration in clouds, a phenomenon originally suggested by Twomey (Twomey, 1971, 1977; Twomey et al., 1984) and referred to as the first indirect effect; and (2) via change in precipitation production in clouds resulting in change in cloud lifetime and cloud liquid water path (LWP), as first suggested by Albrecht (1989) and referred to as the second indirect effect. The net indirect aerosol forcing (including the first and the second indirect effects) has potentially the same magnitude as the clear-sky (direct) aerosol forcing but is highly uncertain (Penner et al., 1994; 2001). The uncertainty, which ranges from –1.1 W m^{-2} to –3.2 W m^{-2}, arises from interaction between aerosols and clouds that is complex in a number of respects. First, the magnitude of the indirect aerosol effect depends on the significance of the albedo change in clouds, which varies with cloud optical thickness (Platnick and Twomey, 1994). The albedo of thin stratiform cloud decks that are formed through weak updrafts and hence have smaller LWP and smaller droplet concentrations is more susceptible to

changes in droplet concentration than the albedo of deep convective clouds. Second, the magnitude and the sign of the effect vary with the composition and the size distribution of the CCN. For example, anthropogenic sulfate, which typically resides in the accumulation mode of particle spectrum, increases droplet number and suppresses precipitation (Warner et al., 1968; Rosenfeld, 2000). On the other hand, sea spray, inhabiting the coarse mode of particle spectrum, tends to enhance precipitation by providing giant CCN, which cause stronger drop collection in clouds (Rosenfeld et al., 2002). Finally, absorption of solar radiation by black carbon within clouds can result in a local reduction of cloud cover; in clear regions, this mechanism can inhibit cloud formation (semi-direct effect), as modeling studies suggest (e.g., Ackerman et al., 2000; Lohmann and Feichter, 2001). It is important is to understand these individual effects for those cloud types of radiative importance. Thus, one of the objectives of the present study is to assess the sensitivity of selected cloud types of radiative importance to the atmospheric aerosol and to investigate the mechanisms responsible for it via detailed high-resolution numerical simulations.

The first case considered in this study is that of mid-latitude summertime marine stratus. This cloud type is the focus of the study for several reasons. The Canadian Radiation, Aerosol, and Cloud Experiment (RACE), conducted in August and September 1995, took measurements by aircraft in marine stratus over the mid-latitude North Atlantic off the eastern coast of Canada. The measurements of cloud microphysical and radiative properties taken in-situ as well as the measurements of particle spectra below the cloud form a dataset that can be useful for closure studies of the effects of aerosols on clouds. Due to the fact that this region of the mid-latitude North Atlantic is frequently affected by air masses with widely varying aerosol and trace-gas loading originating from the eastern North American continent (Banic et al. 1996), this dataset is particularly relevant for studying the influence of anthropogenic aerosol on stratus cloud

properties. Surface-based climatology of low stratus (Klein and Hartmann, 1993) reveals that during the summer the amount of stratus over the mid-latitude oceans is comparable to that in the subtropical stratus region. For example, for June, July, and August, stratus amounts greater than 60 % over the North Atlantic and greater than 80 % over the North Pacific are common (Fig. 1.1). Data from the Earth Radiation Budget Experiment reveal that these oceanic regions exhibit the greatest net cloud forcing (defined as the difference in the net radiative fluxes between cloudy and cloud-free atmospheres) with monthly mean cloud forcing of as much as -100 W m^{-2} (Ramanathan et al., 1989; Fig.1.2) and a two-year mean cloud forcing on the order of -40 W m^{-2} (Klein and Hartmann, 1993; Fig. 1.3). Therefore, changes in the atmospheric aerosol that may modify the radiative properties of these clouds and their coverage can have a pronounced impact on the global radiative budget, as suggested by Slingo (1990).

The summertime marine stratus selected for the present study was observed on 1 Sep 1995 over the Bay of Fundy near Nova Scotia. This case was the focus of previous work which simulated the stratus at high-resolution with a mesoscale model using a simple bulk one-moment microphysical parameterization (Guan et al., 2000). The simulated cloud properties were in reasonable agreement with satellite imagery and the aircraft observations taken during the RACE campaign on that day. Differences were found, however, between the simulated cloud base and thickness and those obtained from the aircraft and lidar observations. These discrepancies were attributed to inconsistencies in the feedback between the clouds and the radiation in the model. Rather than testing if a more accurate simulation could be obtained, the aim of the current study is to investigate the feedbacks between the aerosol and the cloud. This was achieved by taking advantage of the extensive aerosol and cloud microphysical measurements available from the RACE campaign on that day and by utilizing them for initialization and evaluation of numerical

simulations of the phenomenon. The formation of the stratus over the Bay of Fundy was preceded by the passage of an occluded (warm) frontal system. The precipitating system provides a mechanism – via the drop collection process – for physical processing of the aerosol, which is also of interest for this study, as described in section 1.2.

In a numerical model, it is desirable to capture two characteristics of a mid-latitude summertime stratus. First, the model needs to be able to capture the large-scale dynamics and thermodynamics, which trigger and maintain the low stratus cloud. Klein and Hartmann (1993) indicate that mid-latitude summertime marine stratus typically forms over oceans with relatively cold sea surface temperatures and beneath a strong temperature inversion that caps the boundary layer, in analogy with the trade wind inversion capping the marine subtropical stratus. This inversion is maintained by mid-tropospheric subsidence and limits the stratiform convection to the boundary layer, ensuring that the clouds remain thin. At the mesoscale model grid the cloudy eddies are not resolved but an important test for the model is the extent to which it can reproduce the large-scale dynamic (e.g., surface divergence, mid-tropospheric subsidence) and thermodynamics (e.g., air-sea temperature contrast, inversion strength) driving the stratus formation. Second, the model needs to be able to produce an accurate portrayal of an unbroken stratus deck as well as the bulk cloud properties, LWC, droplet number, cloud thickness, and drizzle, which should be within bounds established by observations. The need for a reasonable representation of the large-scale flow and the cloud microphysics of boundary layer clouds in numerical models is supported by the suggested strong sensitivity of these clouds to large-scale divergence and drizzle formation (Wang et al., 1993).

Modeling studies of boundary-layer clouds and of the aerosol-cloud interactions in these clouds have taken a variety of approaches. Three-dimensional large eddy simulation (LES)

models and their two-dimensional counterparts, the eddy-resolving models (ERM), can simulate explicitly boundary layer cloud characteristics (e.g., Kogan et al., 1995; Feingold et al., 1996a, 1997). The emphasis in these models is on dynamics and microphysics through a coupling of a dynamical model that resolves the large eddies with a microphysical model that explicitly resolves (sectional representation) the CCN and drop spectra. Such models are extremely useful for detailed process studies and in particular for examining the processes involved in the interaction between aerosols and clouds. In that regard, LES models have been further developed by adding to their sophisticated dynamics fully coupled components consisting of size-resolved dry and activated aerosol, size-resolved microphysics, and size-resolved aqueous chemistry. This approach has significantly increased the understanding of the many feedbacks involved in the interaction on large eddy scales of the order of few hundred meters and on temporal scales of the order of few seconds.

On the other extreme, the evaluation of the indirect aerosol effects on global and regional climate scales (the order of one to a few hundred kilometers) has attracted particular attention in recent years. This has lead to substantial development in these models in regard to representation of aerosols, clouds, and the sulfur cycle. These models have been continuously extended by including new components of the aerosol-cloud interaction, such as the inclusion of an increasing number of bulk or size-segregated multicomponent aerosol species (sulfate, sea salt, dust, and carbonaceous species; e.g., Lohmann et al., 2000; Gong, 2003), or improving the existing ones. The representation of clouds and precipitation has also improved substantially by adding droplet concentration to the cloud prognostic quantities and by linking it to the precipitation formation (e.g., Ghan, 1997, Lohmann, 1999a,b) and even by adding prognostic ice nuclei concentrations (Lohmann, 2002). One of the challenges in the GCM modeling of the indirect aerosol effects,

however, still remains the representation of clouds. To describe the cloud field within the model grid box, typically on the order of a few 100 km, GCMs need sub-grid parameterizations to account for the spatial variability of the cloud over such a large areas. At the same time, predicting droplet concentrations over such a large grid box requires knowledge of the sub-grid distribution of vertical velocity, responsible for generating the local supersaturations that govern droplet activation. Nevertheless, the developments in GCMs have lead to substantial improvement of the global estimates of the first and the second indirect aerosol effects. Each of these approaches is valid and useful in increasing the understanding of particular aspects of the problem of interaction between aerosols and clouds at the extreme ends of the spatial and temporal scales.

The estimates of the indirect aerosol effects at the intermediate mesoscales, however, have been lagging behind. This seems odd since the regional effects of the aerosol can vary substantially from region to another. These scales, characterized by spatial dimensions of the order of a few kilometers and temporal scales of the order of tens of seconds, are small enough to resolve a cloud system and the domain sizes are large enough to cover phenomena of interest for regional climate change; they are also the spatial and the temporal scales of interest for Numerical Weather Prediction (NWP) models. One of the advantages of mesoscale models is that they can achieve a relative dynamical and microphysical realism and thus can provide insight into the aerosol effects dominating at these intermediate scales. In addition, they can serve for the development of parameterizations for global and regional climate models. Such models have been widely used to simulate precipitation events but mesoscale simulations of cloud-topped boundary layers (CTBLs) are rare. In studies of non-drizzling CTBLs, where the focus is on the BL processes that are not affected by cloud microphysics, the use of simple

microphysical parameterizations, such as those of Kessler (1969), Berry (1967), Berry and Reinhardt (1974) etc., is acceptable. However, when one is concerned with drizzling boundary layers, the burden placed on the microphysics is great and simple schemes are not able to capture the cloud and the boundary layer evolution adequately (e.g., Feingold, 1996b). Feingold et al. (1998) addressed special problems that arise in stratocumulus simulations; in particular, the need to include drop collection at low LWC and the importance of correctly simulating drop sedimentation in weak updrafts (0.1-1 m s^{-1}). The authors devised a new approach that uses a double basis (i.e., for cloud and drizzle) lognormal representation of the drop spectra and applied it in an ERM simulating drizzling stratocumulus deck. By comparing the new two-moment approach to other simplified schemes, the authors demonstrated the importance of detailed representation of droplet collection (particularly autoconversion) and differential (size-dependent) drop sedimentation in stratocumulus clouds. Mechem and Kogan (2003) applied another two-moment microphysical scheme, that of Khairoutdinov and Kogan (2000), in a mesoscale model and ran it in a nested configuration with the finest grid spacing of 2 km to simulate a stratocumulus cloud field. They demonstrated that such a scheme is able to mimic the diurnal cycle of the stratocumulus fields and can produce a drizzle-induced transition from pure, unbroken stratocumulus to boundary layer cumulus over a period of a few hours. The authors demonstrated sensitivity of the cloud to the efficiency of drizzle production. That study was the first one to use a regional model to demonstrate mesoscale organization arising from the effects of drizzle.

The use of advanced microphysical schemes is also important for adequate representation of aerosol effects on stratocumulus clouds. The CCN concentration determines the colloidal stability of clouds and the possibility of drizzle formation (Feingold, 1996b). Drop collection

reduces the number of CCN and creates larger aerosol particles when the original cloud evaporates (e.g., Hudson, 1993; Flossmann, 1994; Feingold et al., 1996).

Previous work leads to the conclusion that it is fully justified to examine the aerosol-cloud interactions in boundary layer clouds with a mesoscale model using an advanced bulk double moment microphysical scheme, similar to those devised by Feingold et al. (1998) or by Cohard and Pinty (2000a; hereafter referred to as CP00). As computer power increases, it becomes possible to run such models with horizontal grid spacing similar to that of the LES domain size (~1-3 km) and it becomes important to address whether at such fine scales these models are correctly representing the boundary layer cloud properties and the interaction of the cloud with the aerosol.

In this work, I continue with the approach taken by the detailed mesoscale studies. An extended version of the Canadian Mesoscale Compressible Community (MC2) model (Benoit et al., 1997) is used. Like other modeling studies, the current one simplifies the representation of some aspects of the problem but strives for a reasonable balance. Most importantly, it couples the mesoscale dynamics with explicit bulk double-moment microphysics, recently introduced to the model, explicit bulk double-moment aerosol, and bulk cloud chemistry. The aerosol and gas-phase concentrations are initially prescribed for illustrative purposes, thus neglecting gas-phase sources and sinks of species. The simulations discussed in this work were conducted at sufficiently high resolution (3 km in the horizontal; 50 m in the vertical) to resolve boundary layer clouds. The predicted cloud microphysical quantities are total cloud water mass and droplet concentration as well as water mass and number concentration of large drops, both assumed to follow generalized gamma distributions.

The aerosol processes in the aqueous phase are accounted for by introducing prognostic equations for the total mass and number concentration of aerosol, which are assumed to follow multi-modal lognormal distributions. In addition, prognostic equations for the mass and number concentration of CCN within cloud droplets and raindrops are also introduced. While the mass and the number concentration of aerosol and CCN are predicted independently, the spread of the distribution is kept fixed. The microphysical processes affecting the aerosol and the CCN include cloud nucleation, drop collisions and coalescence, and new particle regeneration following evaporation of cloud droplets and large drops. In its original formulation, the double-moment cloud microphysical scheme makes use of an activity-spectrum based, "Twomey"-type (Twomey, 1959) CCN activation parameterization (Cohard et al., 1998). For the purposes of the current study, the mechanistic CCN activation parameterization of Abdul-Razzak et al. (1998; 2000; henceforth referred to as A98/00) is introduced and coupled to the double-moment microphysics. The mechanistic activation predicts the number and the mass concentration of CCN activated in clouds, from which the impact of nucleation scavenging on the dry aerosol can be determined.

1.2 Mechanisms for cloud processing of aerosol

There is increasing evidence that the atmospheric aerosol, and particularly those particles that serve as CCN, not only impact clouds but also clouds, in turn, modify the aerosol size distributions. The influence of clouds on the size and the concentration of the aerosol particles has implications for the aerosol-cloud interactions and the related climate feedbacks: the modified aerosol size spectra can change the drop size distribution in subsequent cloud cycles and can either enhance or suppress the drop concentrations.

Clouds impact the abundance and the characteristics of atmospheric aerosol through different mechanisms including drop collisions followed by coalescence (e.g. Hudson, 1993; Flossmann, 1994; Garret and Hobbs, 1995; Feingold et al., 1996), addition of sulfate mass in droplets via aqueous-phase chemical reactions (e.g. Hegg and Hobbs, 1982; Chameides, 1984; Liu et al., 1996; Bower and Choularton, 1993; Feingold et al., 1998) and precipitation scavenging. Other cloud processing mechanisms such as homogeneous nucleation of sulfuric acid particles at relatively high humidity, found in the 'halo' around marine clouds and responsible for the high concentrations of CCN measured near the tops of these cloud (e.g., Hegg et al., 1990), may be important but are not well understood and are omitted from this study. The various cloud-processing mechanisms can have competing effects. Drop collision-coalescence steadily reduces drop and aerosol concentrations because subsequent evaporation of droplets produces one aerosol particle per droplet (Mitra et al. 1992), increases particles size and activated drop size, and increases the likelihood of stronger collision-coalescence in subsequent cloud cycles (e.g., Feingold et al., 1996). Aqueous chemistry adds sulfate mass to already activated particles, thereby generating larger particles. In subsequent cloud cycles, this process can both increase and decrease drop concentrations and suppress and enhance drizzle depending of the properties of the aerosol and the clouds (Bower et al., 1997; Feingold and Kreidenweis, 2000).

The outcome of cloud processing has been extensively studied in stratocumulus-capped marine boundary layer. Numerical studies show that it depends strongly on the trace gas concentrations, cloud LWC, input aerosol distribution and contact time with a cloud, which is, in turn, closely tied to boundary layer dynamics and cloud type (e.g., Feingold et al., 1996a). Bower and Choularton (1993) demonstrated that processing of the CCN spectrum by the aqueous

chemistry occurring in a hill cap cloud results in a bimodal size distribution downwind of the processing cap cloud. The size of a particle at the peak of the large end of the bimodal distribution is determined by the extra sulfate mass generated as a result of the aqueous oxidation, which, in turn, is determined by the concentration of SO_2 and, for large SO_2 concentrations, the availability of oxidant. The principal oxidants are H_2O_2 and, if NH_3 gas is present to act as a buffer, O_3. The effect of drop collision-coalescence and aqueous chemistry on the mass-mean size of CCN as it is cycled in the stratocumulus marine boundary layer in the absence of wet deposition was investigated by Feingold et al. (1996a) in a 2-D eddy resolving model (ERM) coupled with size-resolved aerosol, size-resolved microphysics, and solute transfer between drop size bins. Using trajectory analysis of in-cloud residence times, the authors compared the relative importance of the two mechanisms for remote marine conditions. They concluded that at low LWC (0.1 g m^{-3}) aqueous chemistry would dominate whereas above some threshold LWC (> 0.5 g m^{-3}) collision-coalescence would become the dominant aerosol processing mechanism; at intermediate LWC, the two mechanisms would likely produce comparable rates of increase of the mass mean size of the CCN. The initial conditions used in the simulations represent those in a remote marine boundary layer with initial lognormal CCN spectrum: $N_{CCN} = 50$ cm^{-3}, $a_{CCN} = 0.08$ μm and $\sigma_{CCN} = 1.8$; and initial gas phase concentration of SO_2 of 55 pptv. These clearly represent a small subset of the conditions for aqueous chemistry and physical processing that may exist in the atmosphere. The authors admit that the relative importance of the two mechanisms may vary substantially upon change in these conditions. Feingold and Kreidenweis (2000) investigated the effect of aqueous chemistry processing on the number of drops activated in a subsequent cloud cycle in an adiabatic parcel model with size-resolved chemistry. They examined a broad range of input lognormal CCN spectra ($N_{CCN} = 100$-

5000 cm^{-3}, a_{CCN} =0.03-0.07 μm and σ_{CCN} =1.5-1.8) and updraft velocities (0.2-3 m s^{-1}) in the subsequent cloud cycle and showed that aqueous chemistry can either enhance or suppress the number of drops activated depending on these conditions. Enhancements of drop concentrations occurred at lower updraft velocities (< 1 m s^{-1}), with the enhancement being more pronounced at small a_{CCN}, and reductions of drop concentrations occurred at high updraft velocities (>1 m s^{-1}) although these reductions tended to be more modest than the enhancements in the droplet number. Finally, the effect of aqueous chemistry on drizzle production in a subsequent cloud cycle was explored by Feingold and Kreidenweis (2002) in a large eddy resolving (LES) model with coupled size-resolved aerosol, size-resolved microphysics, and aqueous chemistry. The authors investigated the sensitivity of drizzle production to the CCN size distributions that changed as a result of aqueous chemistry, collision-coalescence, and drizzle. The conclusion was that aqueous chemistry processing enhances drizzle at intermediate CCN concentrations (N_{CCN} > 150 cm^{-3}) of relatively small size (a_{CCN} = 0.05 μm), suppresses drizzle at intermediate CCN concentrations of relatively large size (a_{CCN} = 0.1 μm), and does not substantially affect drizzle at relatively low CCN concentrations (N_{CCN} < 100 cm^{-3}).

Detailed modeling studies like the ones cited above illustrate the complexity of the feedbacks determining the cloud processing in the boundary layer and indicate that cloud-processing mechanisms modify the dynamics and microphysics of stratocumulus clouds. Rather than exploring the myriad of feedbacks in greater detail, the aim of the current study is to focus on the effect cloud processing by drop collision and coalescence and aqueous chemistry (the two main processing mechanisms) has on the aerosol spectrum by. While previous studies focused on examining the contributions of the principle mechanisms at cloud scales (few 100 m) the current study investigates these mechanisms at the cloud-system scales (a few km), for selected real-case

clouds with and without precipitation, and examines the spatial distribution of the processed CCN during the development and the evolution of the cloud systems. The first case selected in the present study is that of a stratocumulus cloud exhibiting negligible wet deposition, occurring downwind of Lake Erie on 11 July 2001. The interest in this case was motivated by the fact that the Great Lakes region typically experiences frequent occurrence of stratocumulus clouds due to lake effects and is often characterized by polluted continental conditions for atmospheric aerosol (N_A of the order of few 1000 cm^{-3}) and for trace gases (Isaac et al., 1998). Observational evidence for production of sulfate in stratocumulus clouds in this region has also been reported (e.g., Liu et al., 1993). Provided there is presence of relatively simple airflow, the effects of processing are likely to be immediately evident downstream of the cloud and as such should be easily identifiable and verifiable by field experiments. The results for the stratocumulus case are compared to the precipitating case. Neither case attempts to serve as case studies of events but rather they provide a representative dynamical framework within to explore the processes of interest. However, to ensure that each numerical simulation is physically reasonable, the structure of the boundary layer produced in the model is examined for each case. In the precipitating case, drop collision and coalescence can significantly reduce droplet number, thus modifying the spectrum of the regenerated CCN, compared to the non-precipitating case. In the non-precipitating case, the effect of chemical processing on the aerosol spectrum is examined and compared to that with physical processing. The spatial variation of the changes in CCN spectrum due to chemical processing is also examined. Finally, I investigate how the obtained results, representative at the cloud-system scales, compare with results from prior work at the much finer cloud scales.

Including the mechanisms for cloud physical and chemical processing of aerosol requires another major modification of the MC2 model. First of all, an algorithm that calculates the properties of CCN in solution is required. This is true for studies of both aqueous-chemistry and collision-coalescence processing. Prior studies have included some level of knowledge of drop solute. Pioneering work by Flossmann et al. (1985) calculated bulk properties of solute (e.g., total mass) whereas later work by Trautmann (1993) and Chen and Lamb (1994) solves for the two-dimensional drop size distribution $n(x,a)$, where x represents drop mass and a represents CCN mass. These techniques provide a more complete description of the CCN-drop interactions than the bulk approach. Nevertheless, they are computationally extremely expensive and to date have only been employed in one-dimensional models or in kinematic models with prescribed flow. For the purposes of the study presented here, a bulk treatment of solute has been chosen, though solute from each dry particle mode is tracked individually in cloud drops. Solute within cloud drops is transferred to large drops via collision-coalescence at a transfer rate determined by the collection kernel for drops. In large drops, only the total solute (sum of all modes) is considered.

The treatment of regeneration of CCN following drop evaporation is central to the current investigation and will be discussed here in some detail. A number of regeneration schemes for size-resolved representation of the CCN and drop spectra have been tested in the literature. Bin representation of the CCN and drop spectra has commonly been used in simple model settings or in complex model setting, such as LES models, over spatial domains and for integration times with limited dimensions; its implementation in mesoscale models, however, is prohibitively expensive. Nevertheless, a review of the bin approaches for CCN regeneration is helpful. Generally, the methodology used by the different schemes follows the principle that one particle

is regenerated for every evaporated drop. The reconstruction of the regenerated spectrum, however, varies between the schemes. The first type of scheme assumes bulk (monodisperse) treatment of solute within each bin of the droplet spectrum and regenerates particles in a manner commensurate with the degree of depletion of a given CCN bin (Cotton et al., 1993; Feingold et al., 1996a). Since large CCN are more readily activated, the bins representing the larger CCN have a higher probability of receiving regenerated particles than smaller-sized bins. The second type of regeneration scheme, computationally more demanding, distributes the regenerated mass and number of particles in each bin according to a lognormal distribution with a variable breadth parameter (Ackerman et al., 1995; Feingold et al., 1996a). This type of scheme is based on the representation of the solute size distribution by three of its moments: CCN number, mass, and, typically, surface area (the second moment with respect to radius) although another moment of the size distribution can also be chosen. Thus the standard deviation of the regenerated spectra varies according to the ratio of the three moments. This approach is computationally demanding because it requires a prognostic equation for an additional moment in each aerosol bin as well as a prognostic equation for tracking the property of the solute within each drop bin. Results from the two types of regeneration schemes have been compared in Feingold et al. (1996a). All these schemes provide a more complete description of CCN regeneration. They conserve total mass and number and hence regenerate the correct global mass mean radius of the aerosol. An alternative approach, which is also mass conserving and has been adopted in the present study, redistributes the total regenerated mass and number of particles in a global sense rather than in each bin, according to a lognormal distribution with a fixed geometric standard deviation.

Given the complexity of the coupled system and the broad range of conditions, prior numerical studies have tended to simplify certain aspects of the problem. This was usually

achieved by considering simple kinematic flows or adiabatic parcel models (e.g., Bower and Choularton, 1993; Gurciullo and Pandis, 1997; Feingold et al., 1998), so as to focus on the aerosol-cloud interface. In so doing these studies have separated the microphysics and the chemistry from the dynamics. Other studies have considered one- or two-dimensional Eulerian parcel models (e.g., Flossmann, 1994; Wurzler et al., 2000) and, therefore, have captured the coupling between dynamics, microphysics, and chemistry. However, the large number of processes that need to be treated typically limits the spatial dimensions of the model and sometimes the accuracy of resolving a phenomenon. The current approach is to include a simple bulk sulfate chemistry fully coupled to the bulk double-moment aerosol and the bulk double-moment microphysics. Continuity equations were added for the concentrations of selected gas-phase species, SO_2 and ammonia (NH_3) as well as for the concentration of oxidant, in this case hydrogen peroxide (H_2O_2). Other gas phase species and oxidant are present in the system but are kept fixed. Gas-phase and oxidants concentrations change (1) due to dissolution into the aqueous phase, thus affecting the drop pH and the oxidizing capacity of the cloud water, and (2) as the oxidation proceeds, due to aqueous production of sulfate.

1.3 Objectives of the thesis

The purpose of this work is to physically model CCN concentration and aerosol processing in boundary-layer clouds at fine scales. The present approach is through explicit high-resolution mesoscale simulations of real case clouds using the MC2 model. Specifically, the scientific objectives are to:

(1) obtain realistic simulations of the two selected cases of boundary layer clouds;

(2) evaluate the 1 Sep 1995 marine stratus simulation against thermodynamic and microphysical measurements taken as a part of the RACE campaign on that day;

(3) determine the sensitivity of the marine stratus and that of the large-scale precipitation preceding the stratus formation to the presence of giant CCN, found below cloud in observed particle spectra during the RACE campaign;

(4) examine the impacts of collision-coalescence processing on aerosol spectrum and its sensitivity to the strength of droplet collection in clouds; identify locations where the aerosol changes are most significant;

(5) examine the relative impacts of collision-coalescence and aqueous-chemistry processing on the aerosol spectrum in non-drizzling stratocumulus; identify locations of the most significant impacts;

(6) evaluate the effect of processed aerosol on droplet concentration and precipitation in clouds subsequently forming on these particles.

The main part of the thesis is organized as follows: Chapter 2 provides an overview of the cases selected for discussion; Chapter 3 describes the improvements made to the model and the modeling strategy; Chapter 4 examines the aerosol impacts on cloud properties for the RACE case; Chapter 5 investigates aerosol processing via drop collision-coalescence in the precipitating frontal clouds in the RACE case; Chapter 6 provides insight into aerosol processing via aqueous chemistry for the stratocumulus case near Lake Erie; Chapter 7 summarizes the main results and conclusions and briefly mentions ideas for future work.

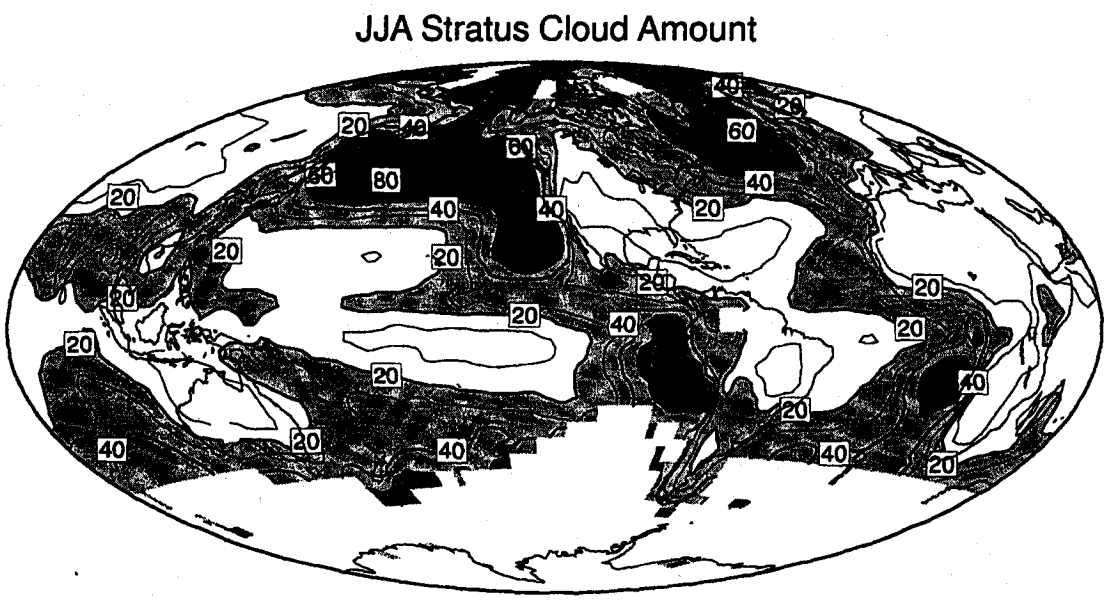

Figure 1.1: Averaged stratus, stratocumulus, and sky-obscuring fog cloud amount in percent for June, July, and August averaged over two years from 1986 to 1988. Contour interval is 10 % (from Klein and Hartmann, 1993).

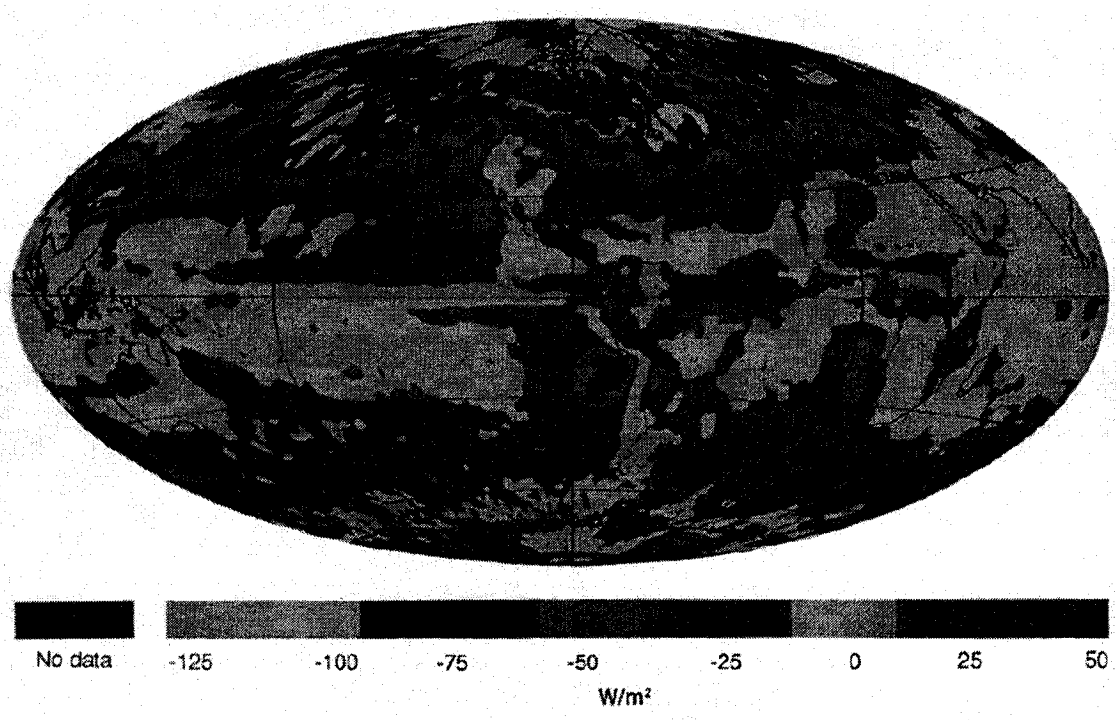

Figure 1.2: Net (short wave + long wave) radiative cloud forcing (W m^{-2}) for April 1985 as seen by the Earth Radiation Budget Experiment. The positive values of cloud forcing, including those seen in North America and the polar regions, do not exceed 25 W m^{-2} (from Ramanathan et al., 1989).

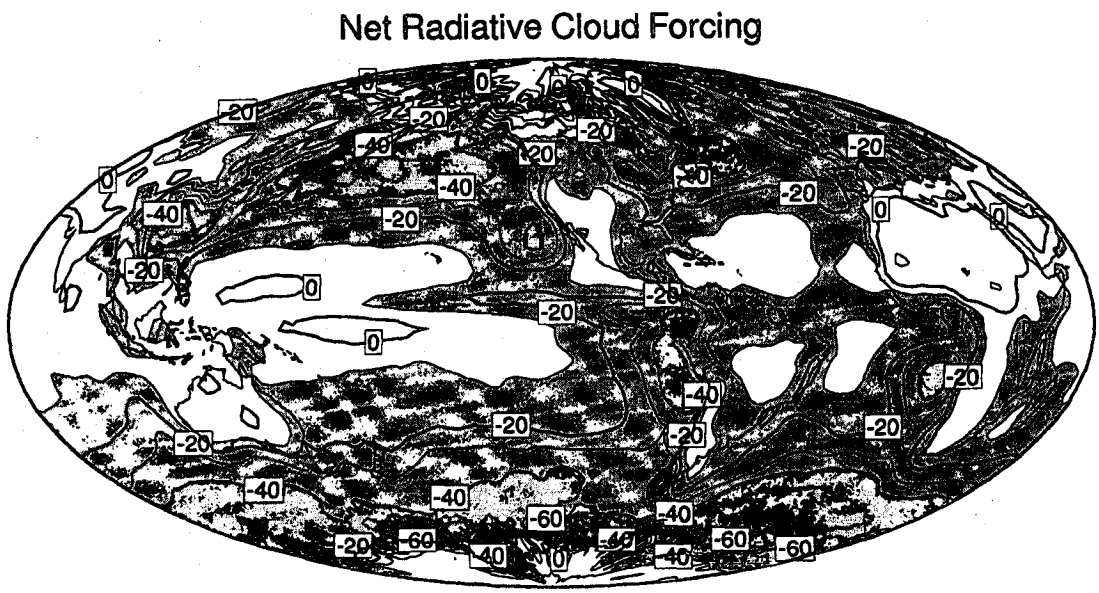

Figure 1.3: Net radiative cloud forcing (W m^{-2}) as seen by the Earth Radiation Budget Experiment averaged over the two years from February 1985 through January 1987. Contour interval is 10 W m^{-2} (from Klein and Hartmann, 1993).

Chapter II

Cases overview

2.1 RACE case overview

a) Synoptic Situation

The Canadian Meteorological Center (CMC) surface analyses at 0000 and 1200 UTC on 1 Sep 1995 illustrate the synoptic conditions prior to the stratus formation (Fig. 2.1). The area upstream of Bay of Fundy was dominated by the passage of a cold frontal system. The stratus cloud formed at around 1800 UTC in the region of the Bay of Fundy following the passage of the front. The CMC low-level (850 hPa) and the upper level (500 hPa) regional analyses (at 50 km horizontal resolution and 16 pressure levels) are shown in Fig. 2.2. At low levels the region of Bay of Fundy was influenced by geostrophic warm temperature advection from the southwest and strong Q-vector convergence, indicative of large-scale upward motion (Bluestein, 1992). At upper levels, ridging and Q-vector divergence dominated the Bay region, indicative of large-scale mid-tropospheric subsidence. The low-level warm temperature advection and the upper level Q-vector divergence both favor the formation of low stratus cloud.

a) Satellite imagery and flight plan

A visible image from the Advanced Very High Resolution Radiometer (AVHRR) on the NOAA-14 satellite at 1733 UTC on 1 Sep 1995 shows the cloud (Fig. 2.3). Bay of Fundy is located in the rectangular box. The stratus cloud can be seen extending from the coast of New

Brunswick (to the north-west of the Bay), where it was thicker and relatively inhomogeneous, to the Bay itself where it appeared less bright and unbroken. The southwestern end of the Bay was cloud free. A narrow band of clear air was also present in the middle of the Bay, separating the Bay of Fundy cloud from the cloudy region over the Nova Scotia peninsula. The presence of broken convective-like cloudiness over Maine and New Brunswick indicates the presence of convective instability in the cold air mass behind the cold front.

The aircraft data that are used in this study were collected on 1 Sep 1995 on Flight 13C of the RACE campaign (Banic et al., 1996b). The sampling platform was the National Research Council of Canada Twin Otter aircraft with an operating airspeed of 50-70 m s^{-1}, which undertook a flight in Bay of Fundy between 1720 UTC to 1910 UTC with horizontal and the vertical tracks shown in Figure 2.4. The flight pattern consisted of vertical soundings and level flights. Soundings between heights of 100 m and 1500 m were completed at the beginning (ascent profile AB at 1730 UTC) and in the middle of the flight (descent profile at point B at 1820 UTC) to assess cloud base and cloud top heights. The lateral cloud boundary was encountered at point C. Level runs were performed in the middle of the Bay (segment BC). The vertical soundings together with the timing and positioning of the level runs relative to the cloud are indicated in Fig. 2.4 b (the horizontal position is indicated with letters). The mean heights of cloud top (5 penetrations) and cloud base (5 penetrations) were found to be 829 m and 1108 m, respectively. During the earlier ascent profile over the coast (1730 UTC), a two-layer cloud was encountered with cloud base height of 665 m and cloud top height of 861 m for the lower layer and cloud base height of 864 m and cloud top height of 1210 m for the upper layer. During the later descent profile over the Bay (1820 UTC), a single layer cloud was present with cloud base and cloud top heights of 873 m and 1112 m, respectively, very close to the flight mean values.

The measurements of thermodynamic and microphysical properties of the Bay of Fundy stratus cloud provide a good database for verification of numerical simulations of the stratus cloud.

c) Temperature and humidity measurements

The vertical thermodynamic structure at 1730 UTC (solid lines) and 1820 UTC (dashed lines) is illustrated in Fig. 2.5. The earlier sounding sampled the air over the coast while the later sounding was taken over the Bay. Some systematic variation across the experimental area due to large-scale gradients is apparent in the measurements. During the descent over the Bay (1820 UTC), the vertical variation of the equivalent potential temperature was small up to cloud top where there was a 3°C temperature inversion. Above this level, the humidity minimum causes the temperature to decrease. The observed temperature and dew point temperature discontinuity at cloud top are typical for stratus cloud decks.

The temperature inversion at the top of the boundary layer is an important feature of the summertime mid-latitude marine stratus cloud. It is caused by mid-tropospheric subsidence in analogy to the trade wind inversion capping the subtropical stratocumulus (Klein and Hartmann, 1993). The subsidence is usually associated with the descending branches of monsoon-like circulations between the much warmer continent and the colder ocean. In the present case, the larger-scale forcing at the upper levels (ridging and Q-vector divergence) also supports mid-tropospheric subsidence.

The inversion at the top of the boundary layer affects the existence of stratus in several ways. It is believed to cause moisture evaporated from the sea surface to gradually accumulate in the boundary layer. A moderate updraft (typically less than 1 m s^{-1}) helps the moisture trapped in the boundary layer to reach saturation. Once the cloud has formed, convection is easily

maintained, primarily due to the strong radiative cooling at cloud top. Because the cloudy eddies are unable to penetrate the inversion the cloud is confined to the boundary layer.

d) Cloud microphysical measurements

LWC was measured by the PMS[1] King probe and droplet number concentration by the Fast Scattering Spectrometer Probe (FSSP-100)[2] in the diameter range 1.31-28.58 μm. Figure 2.6 shows the vertical variations of LWC, droplet number and droplet mean volume diameter for the two profiles. The ascent profile of LWC indicates a two-layer cloud exhibiting large variations in LWC and droplet number. The upper cloud layer had peak values of LWC about 0.9 g m^{-3}, drop concentration of the order of 700 cm^{-3}, and mean volume diameter about 14 μm. The lower cloud layer had smaller values of LWC with a peak value of 0.3 g m^{-3} and smaller mean volume diameter with a peak value of 9 μm, while the peak droplet concentration was similar to that in the upper layer. The descent profile at 1820 UTC indicates a shallower one-layer cloud exhibiting a triangular LWC profile (Noonkester, 1984) and a uniform drop number profile commonly observed in non-precipitating stratiform clouds. The peak values of LWC and drop concentration were smaller during the ascent profile with values of about 0.5 g m^{-3} and 350 cm^{-3}, respectively. The increase in LWC with height was accounted for by an increase in the mean volume radius of the drops rather than an increase in concentration, as shown in Fig. 2.6. Such systematic behavior suggests that the condensation process dominated droplet growth in this part of the spectrum. These data are similar to those described by Slingo et al. (1982) and Nicholls (1984) for a similar layer of marine stratocumulus.

[1] Particle Measuring Systems, Inc., Boulder, CO

e) Aerosol measurements

Aerosol particles were measured by the PMS Passive Cavity Aerosol Spectrometer Probe (PCASP) in the diameter range 0.1-2.8 μm and by the FSSP in the diameter range 1.3-28.6 μm. Since the FSSP probe is designed to measure cloud droplets, in order to estimate aerosol particle concentration, only data collected at RH below 85% is considered. Figure 2.7 shows the observed aerosol size spectra from the two probes averaged over every 100 m altitude from the surface to 1500 m. Two distinct aerosol modes were present, an accumulation-mode with a mean radius of about 50 nm and a coarse-mode with mean radius of about 1 μm. The mismatch between the aerosol spectra from the two probes is due, first, to the fact that, unlike PCASP, the FSSP does not dry the particles, and second, to the uncertainty in the sizing of the first FSSP channel. No FSSP spectra are plotted between 500-1000 m because the RH was greater than 85 % in this layer. Due to the limited size range of the PCASP, particles smaller than 70 nm in radius remain undetected. Such small particles do not add much to the aerosol mass concentration though they contribute significantly to the aerosol number concentration. The observed spectra can be fitted with a bi-modal lognormal distribution:

$$\frac{dN_A}{d\ln a} = n_L(\ln a) = \sum_{i=1}^{2} \frac{N_{A,i}}{\sqrt{2\pi}\ln\sigma_{A,i}} \exp\left(-\frac{\ln^2(a/a_{m,i})}{2\ln^2\sigma_{A,i}}\right) \qquad (2.1)$$

with parameters $N_{A,i}$ total number concentration, $a_{m,i}$ geometric-mean radius, and $\sigma_{A,i}$ geometric standard deviation of aerosol mode i = 1,2. The variation with height of the lognormal parameters is shown in Table 2.1. As the values suggest, the case corresponds to a heavily polluted situation with particle concentration in the accumulation mode reaching 1200-1500 cm^{-3} in the vicinity of the cloud base (between 600 m and 800 m). The particle concentration in

[2] Detailed information about the FSSP can be found in Dye and Baumgardner (1984), Baumgardner et al. (1985), Brenguier (1989), and Baumgardner and Spowart (1990)

the coarse mode ranged between 6-10 cm^{-3} at the level of the cloud base. Notably, the measurements of the coarse mode are highly variable.

2.2 Lake Erie case overview

a) Synoptic situation

The second case presented in this study occurred on 11 July 2001 downwind of Lake Erie. An almost stationary cyclone was centered northeast of Lake Erie with a northerly flow (northwesterly flow at the upper levels) over the Lake, as illustrated in Fig. 2.8, which shows the CMC surface analysis on that day at 0000 UTC and at 1200 UTC. A low stratocumulus cloud covered the area downwind of Lake Erie, as shown in the satellite image in Fig. 2.9.

This case of almost stationary long-lasting continental stratocumulus clouds represents a typical summertime situation in the region of the Great Lakes. This case is not intended as a case study of the event but rather as a suitable framework to study aerosol processing.

b) Aerosol concentrations

The region of the Great Lakes is often exposed to high aerosol loading caused by the anthropogenic emissions originating from the highly industrialized regions in eastern and central North America (e.g., Liu et al., 1996). The aerosol distribution shown in Figure 2.10 was collected in the region of the Great Lakes (Richard Leaitch, MSC, Downsview, personal communications). The lognormal parameters of the distribution are listed in Table 2.2. This distribution is representative of a continental aerosol in highly polluted conditions with total particle concentration reaching almost 5000 cm^{-3}. The geometric mean radius of the distribution, 44 nm, is representative of the accumulation mode in the particle spectrum. The existence of a

pronounced second larger-size mode in the particle spectrum raises the possibility of processing of CCN in clouds or a weak source of large particles. The effect of cloud processing on this particle spectrum in the idealized framework of the stratocumulus cloud will be evaluated.

Table 2.1: Variation with height of the log-normal parameters of the aerosol spectra shown in Fig. 2.7. The standard deviation of the accumulation mode is $\sigma_{A,1}$=1.7 and that of the coarse mode is $\sigma_{A,2}$=1.21.

Altitude (m)	$N_{A,1}$ (cm^{-3})	$a_{m,1}$ (nm)	$N_{A,2}$ (cm^{-3})	$a_{m,2}$ (μm)
0	4000	50	90	1.1
100	4000	50	90	1.1
200	3500	50	30	1.05
300	3000	50	20	1.05
400	2500	50	15	1.05
500	2000	50	12	1.05
600	1800	55	10	1.05
700	1400	55	8	1.05
800	1200	55	6.5	1.05
900	1000	55	5	1.05
1000	800	60	3.3	1
1100	600	60	2	1
1200	500	60	1	1
1300	400	60	0.04	1
1400	300	60	0.05	0.95
1500	300	60	0.05	0.9
1600-25000	200	60	0.0	-

Table 2.2: Parameters of the log-normal distributions fitted to the observed aerosol distribution shown in Fig. 2.10.

Aerosol mode	N_A (cm^{-3})	a_m (nm)	σ_A
Mode 1	4982	44	1.83
Mode 2	5	300	1.9

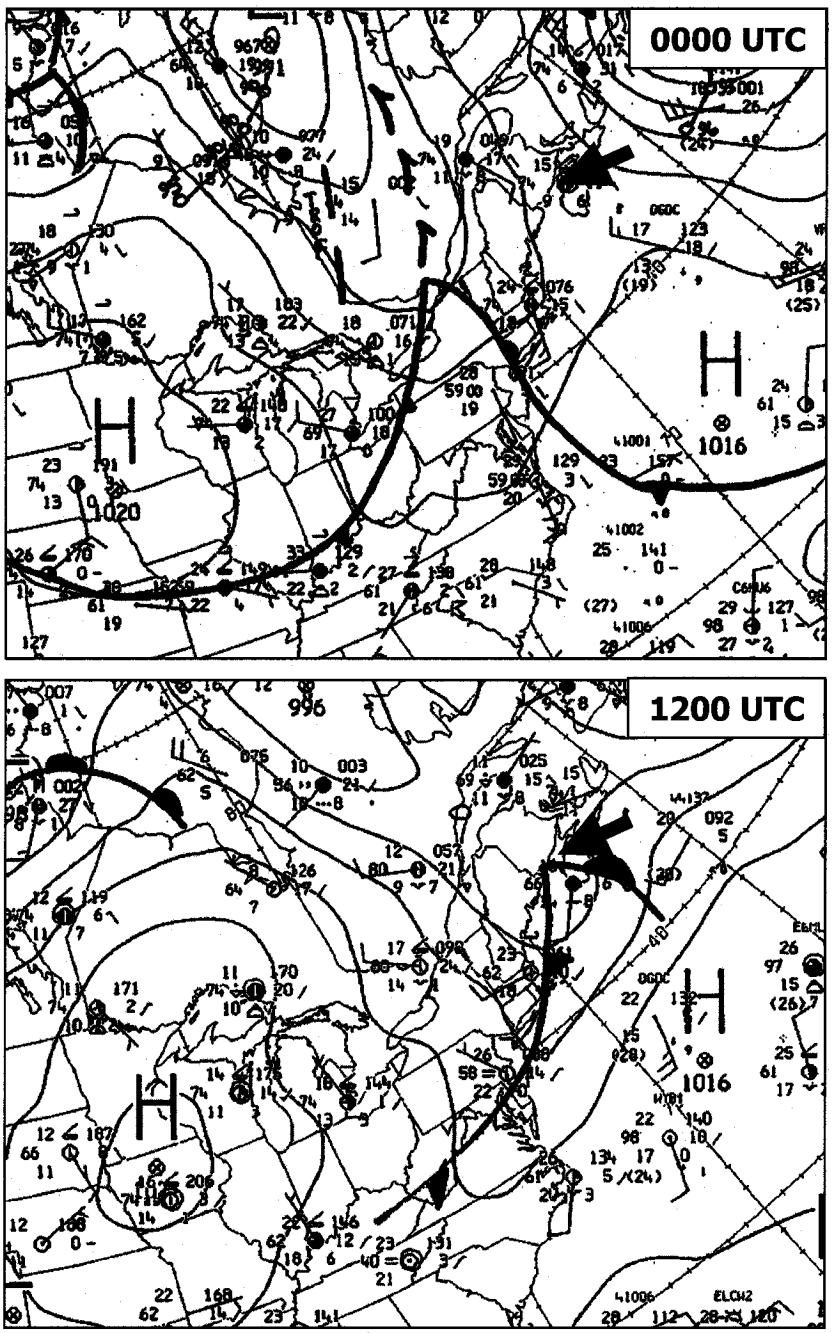

Figure 2.1: CMC surface analysis at 0000 and 1200 UTC, 1 Sep 1995. The location of the surface fronts is indicated. The arrows show the location of Bay of Fundy.

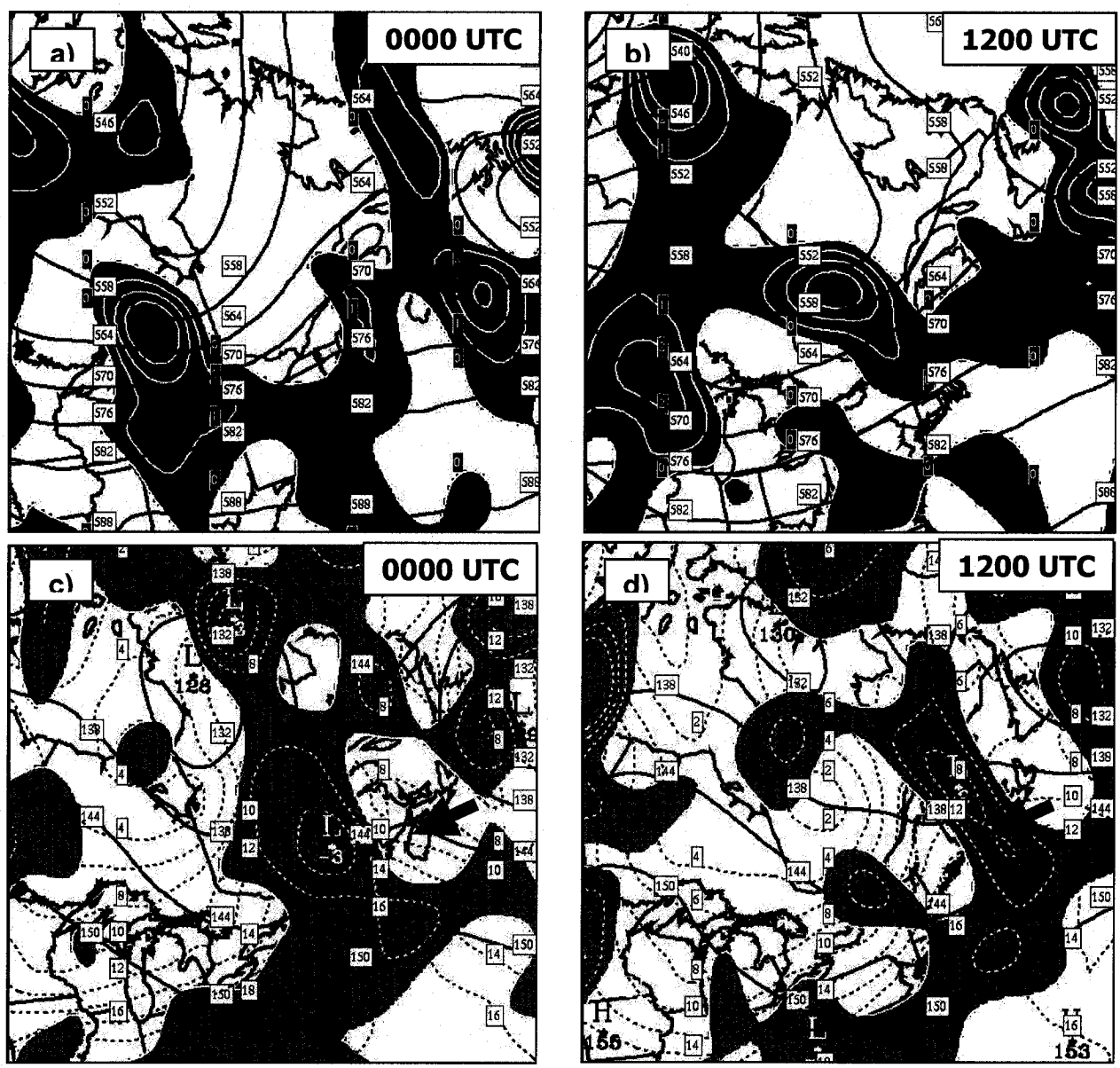

Figure 2.2: CMC analysis on 1 Sep 1995. Upper row shows 500 hPa map of geopotential height in black solid lines (contours every 6 dam) and Q-vector divergence in shading and in white solid lines indicating 1, 2, and 3 unit contours (1 unit = 10^{-13} kg m^{-2} s^{-3}) at a) 0000 UTC and b) 1200 UTC, respectively. Lower row shows 850 hPa map of geopotential height in black solid lines (contours every 6 dam), temperature in black dashed lines (contours every 2°C), and Q-vector convergence in shading with white dashed lines showing -1, -2, and -3 unit contours.

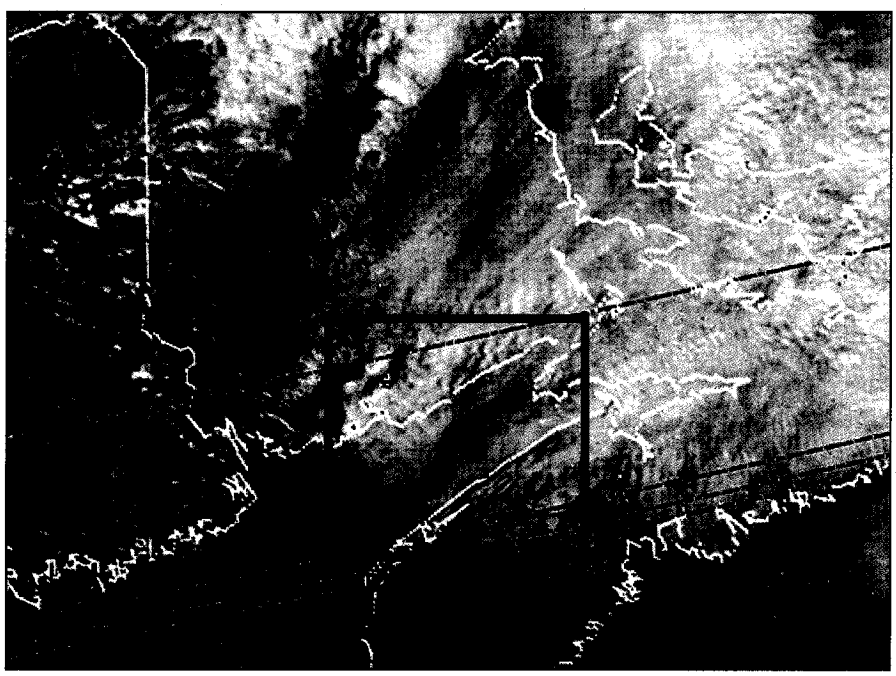

Figure 2.3: AVHRR visible image taken at 1733 UTC, 1 Sep 1995. The box shows the location of Bay of Fundy.

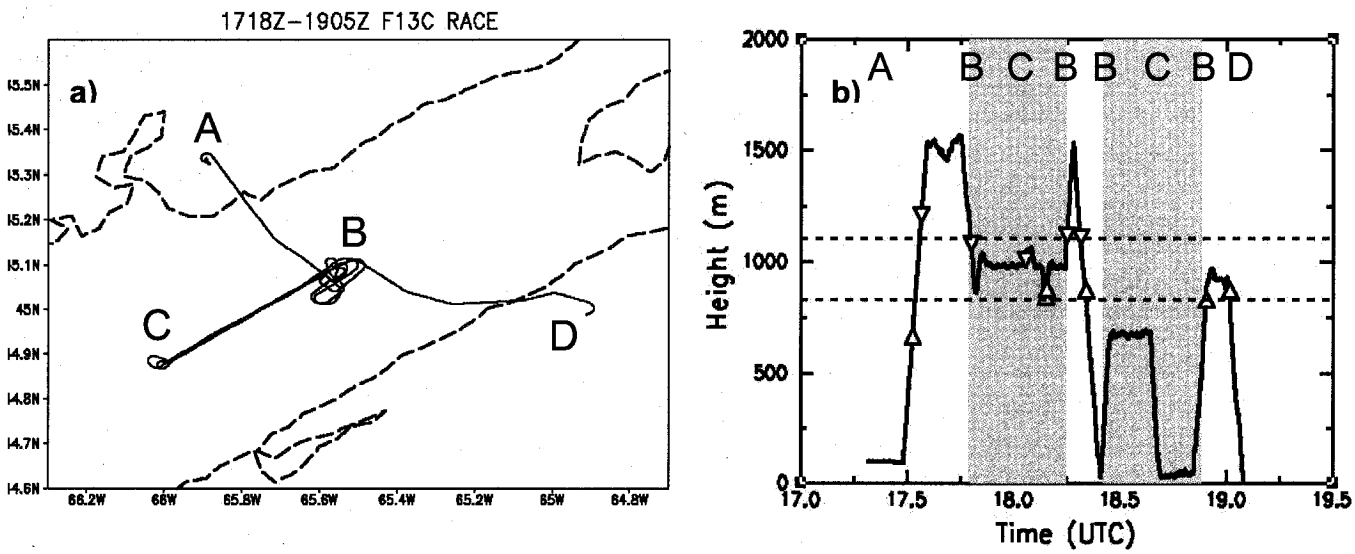

Figure 2.4: (a) Horizontal flight pattern. (b) Time series of aircraft altitude showing the vertical levels of the measurements. The shaded areas highlight the level flight segment BC. The cloud base and the cloud top are shown with triangle pointing up and down, respectively. The average cloud base (829 m) and cloud top (1108 m) heights are show in dashed lines.

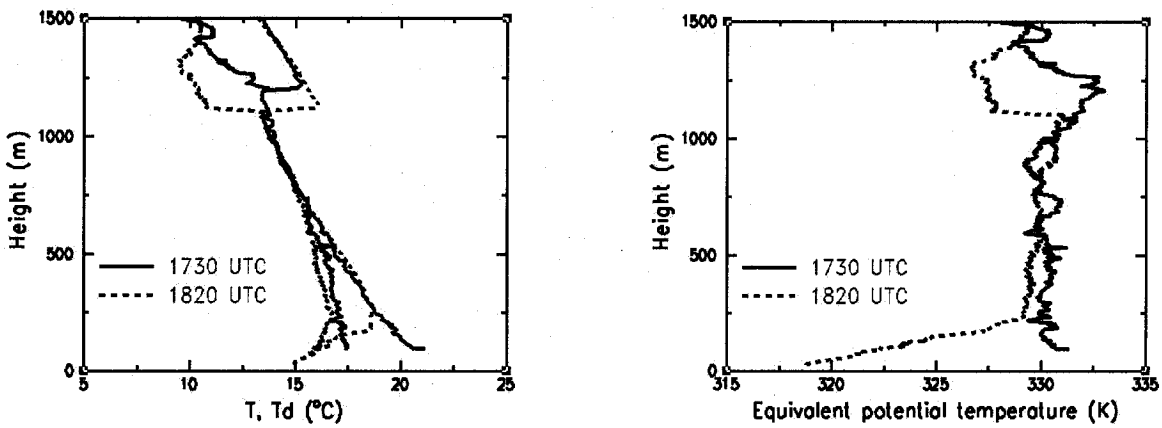

Figure 2.5: Vertical thermodynamic structure (air temperature, dew-point temperature and equivalent potential temperature) measured at 1730 UTC (solid line) and 1820 UTC (dashed line).

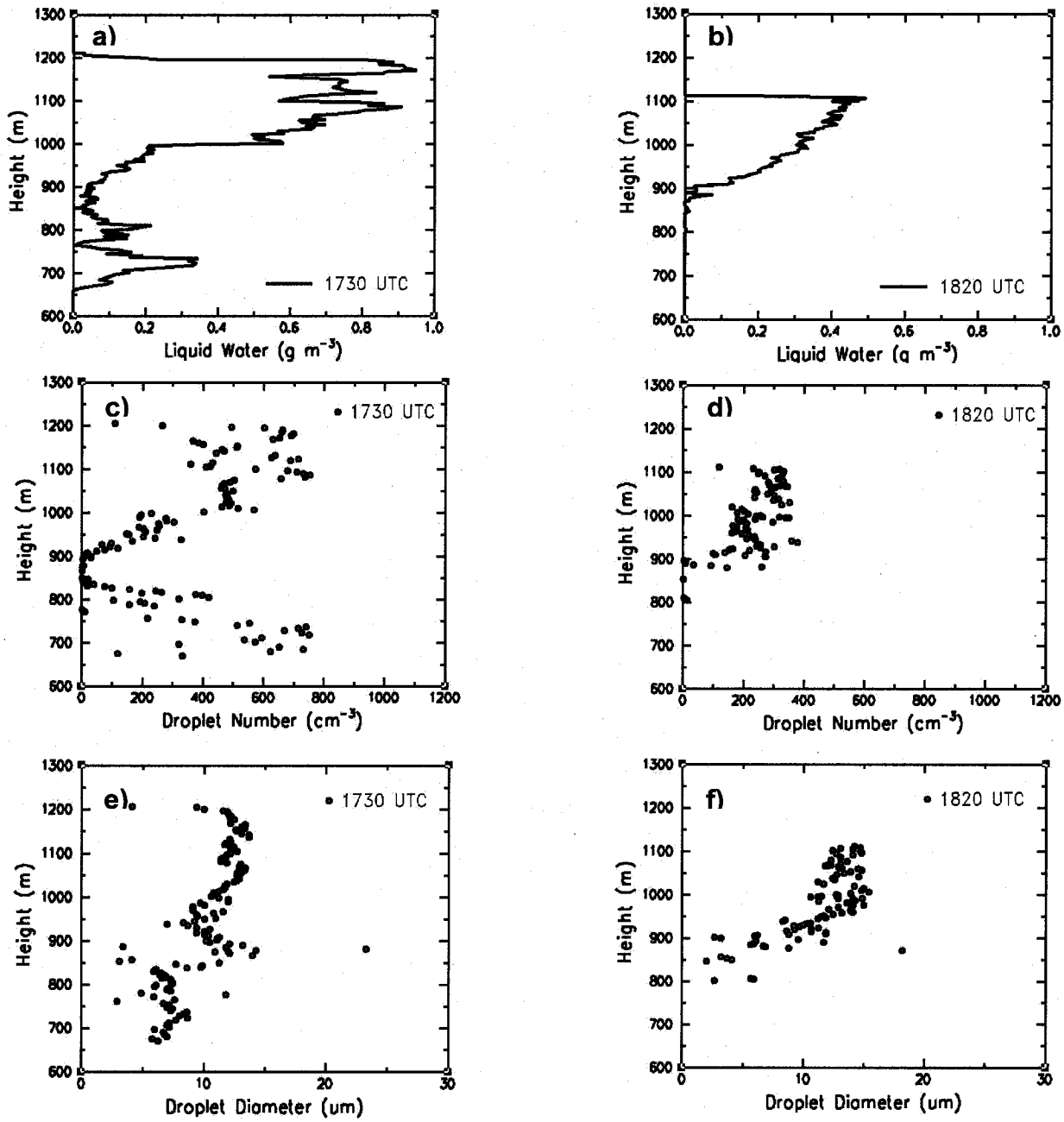

Figure 2.6: Variation of LWC, droplet concentration and mean volume diameter with height on the ascent at 1730 UTC (left column) and on the descent at 1820 UTC (right column). LWC is from King probe and droplet number and volume mean diameter are FSSP data, each point being derived from a one-second averaged spectrum.

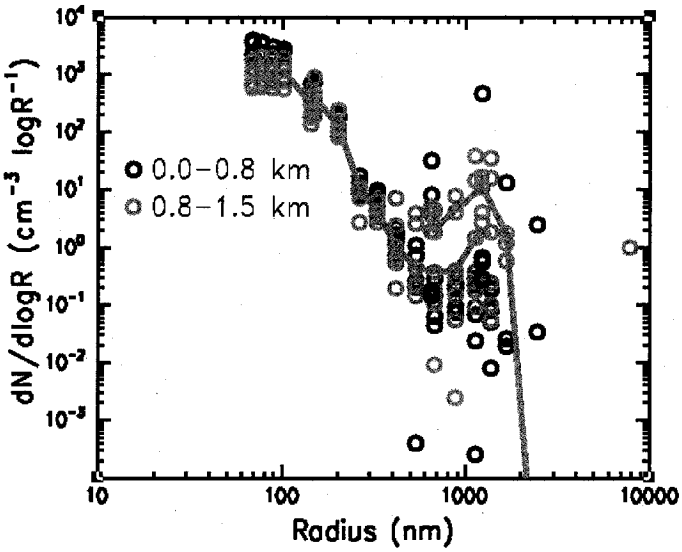

Figure 2.7: Aerosol size spectra (cm^{-3}) collected by PCASP and FSSP (values at RH < 85 % considered only) averaged over every 100 m altitude from the ground to 1500 m (color legend explained in the figure). The line indicates the spectrum at 1 km altitude.

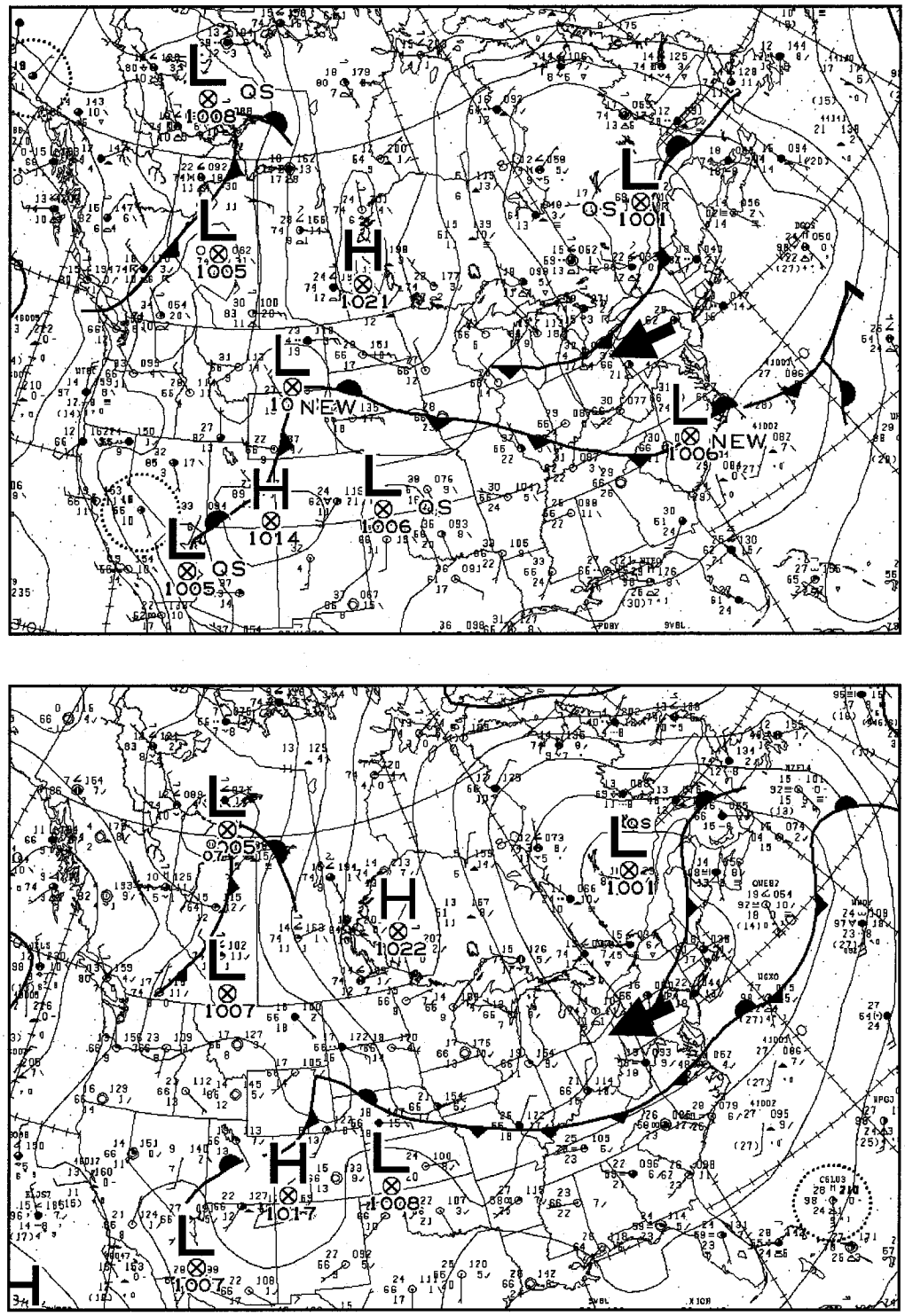

Figure 2.8: CMC surface analysis at 0000 and 1200 UTC, 11 Jul 2001. The location of the surface fronts is indicated. The arrows show the location of Lake Erie.

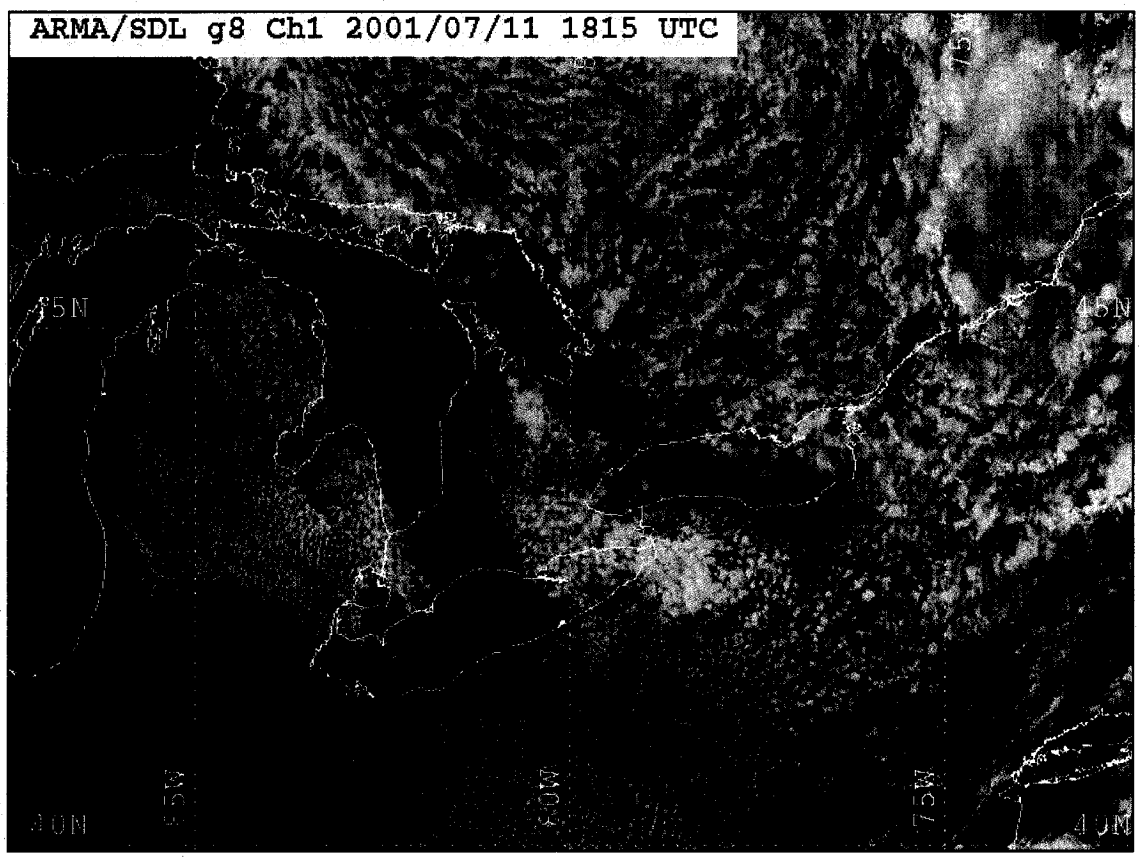

Figure 2.9: Satellite image at 1815 UTC over the Great Lakes, Lake Erie to the south and Lake Ontario to the east. The low-level cloudiness south of the Lake Erie is subject of this study.

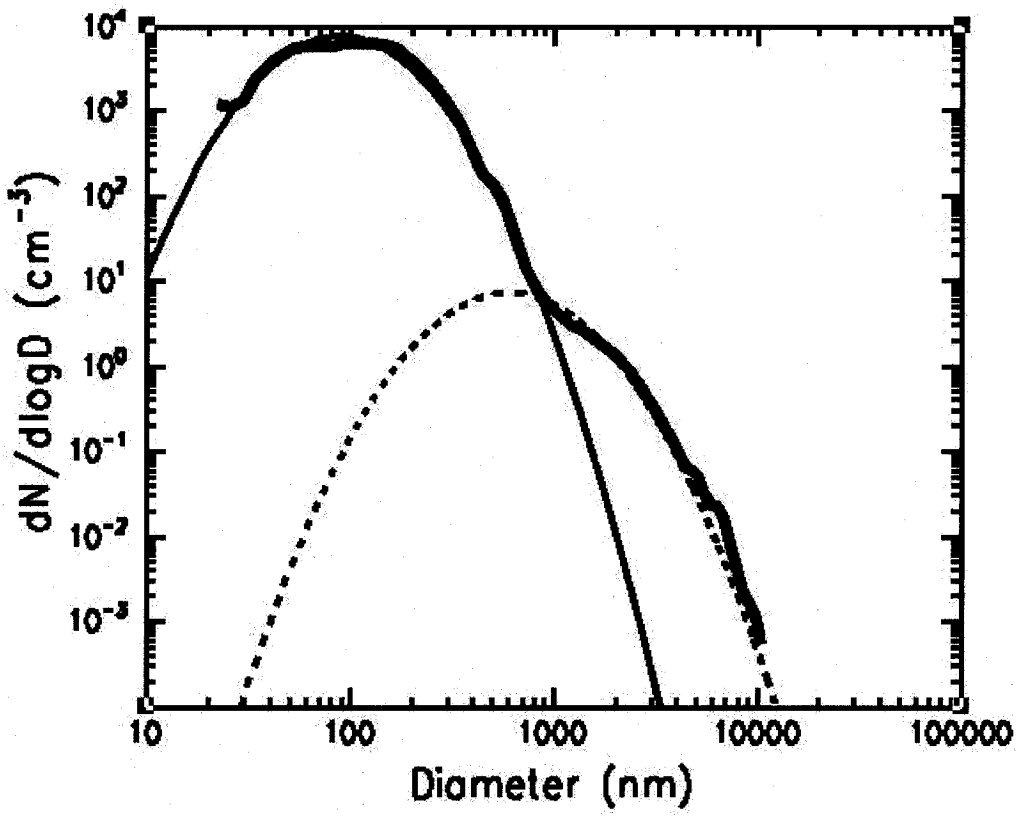

Figure 2.10: Aerosol size distribution collected in the Great Lakes region (grey line). Superimposed are lognormal fits to the observed distribution (solid and dashed black lines) with parameters listed in Table 2.2.

Chapter III

Model improvements and modeling strategy

3.1 Model description

MC2 is a three-dimensional, fully elastic, non-hydrostatic, limited-area model based on the Navier-Stokes equations (Benoit et al., 1997). The model has been used to study a wide range of phenomena from small-scale convection to large-scale synoptic events (e.g., Robert, 1993; Benoit et al., 1997; Nagarajan et al., 2001). It is formulated in a terrain-following Gal-Chen vertical coordinate and, to ensure numerical efficiency and stability over a wide range of scales, it adopts a semi-Lagrangian advection scheme and semi-implicit time-differencing scheme (Robert et al., 1985; Tanguay et al., 1990). A comprehensive physics package, described in Mailhot et al. (1998), includes the following main components: radiation processes, planetary boundary layer processes based on turbulent kinetic energy (Benoit, 1989), implicit vertical diffusion, and condensation processes. The radiation component consists of solar and terrestrial radiation schemes that are fully interactive with clouds (Garand and Mailhot, 1990). Clouds and precipitation are generated by a convective scheme and a stratiform (explicit) scheme. Milbrandt and Yau (2005) have recently extended the suite of cloud schemes in the model by adding the bulk double-moment microphysical scheme of Cohard and Pintry (2000).

Since aerosols affect clouds through their impact on the droplet concentrations, the newly implemented double-moment microphysics has been adopted in the present study. The scheme relies on the assumption that the condensed water can be partitioned between relatively small

cloud droplets and large hydrometeors, also loosely referred to also as raindrops although these large drops may not necessarily be associated with precipitation at the ground. The size boundary between cloud droplets and large drops is specified as being near 80 μm in diameter. Those two regions in the drop spectrum are characterized by different influences of the collection kernel. The cloud droplet and large hydrometeor spectra are described by a generalized gamma distribution:

$$n_i(D) = N_i \frac{\alpha_i}{\Gamma(\nu_i)} \lambda_i^{\alpha_i \nu_i} D^{\alpha_i \nu_i - 1} \exp\left\{-(\lambda_i D)^{\alpha_i}\right\} \tag{3.1}$$

where the index $i \in [c,r]$ stands for cloud or rain, respectively. Like other bulk approaches, this one is based on moments of the drop size distribution, namely the zeroth, N_i, and the third moment,

$$Q_i = (1/\rho_a) \int_0^\infty (\pi/6) \rho_w D^3 n_i(D) dD . \tag{3.2}$$

As these two moments are determined from equation (3.1), the slope parameter of the drop size distribution λ_i, which in a two-moment scheme is a variable, can be deduced from

$$\lambda_i = \left\{ \frac{\pi}{6} \rho_w \frac{\Gamma(\nu_i + 3/\alpha_i)}{\Gamma(\nu_i)} \frac{N_i}{\rho_a Q_i} \right\}^{1/3} , \tag{3.3}$$

whereas the remaining parameters α_i and ν_i, related to the spectral breadth of the distribution, are held fixed ($\alpha_c = 3$, $\nu_c = 2$, $\alpha_r = 1$, $\nu_r = 2$). The value of the breadth parameter[1] for raindrops, ν_r, has been revised by Milbrandt and Yau (2005) who proposed a diagnostic expression as a function of the raindrop mass-mean diameter, D_{mr}, in the following form:

$$\nu_r - 1 = c_{1r} \tanh[c_{2r}(D_{mr} - c_{3r})] + c_{4r} , \tag{3.4}$$

where the values of the constants are $c_{1r} = 19$, $c_{2r} = 0.6$ mm^{-1}, $c_{3r} = 1.8$ mm, and $c_{4r} = 17$ and $D_{mr} = \left(\frac{\rho Q_r}{\pi/6 \, \rho_w N_r} \right)^{\frac{1}{3}}$. This increase of ν_r with D_{mr} depicts the narrowing of the raindrop spectrum due to sedimentation and prevents the occurrence of unrealistically large raindrop mean sizes due to differential (size-sorting) sedimentation in a two-moment scheme. This effect, which was found to be important in precipitating clouds (Milbrandt and Yau, 2005), has been adopted in the current study. Prognostic equations for the concentration N_i and the mixing ratio Q_i of cloud droplets and raindrops are solved, thus giving four prognostic variables in total.

The microphysical processes represented in the double-moment parameterization are standard for warm rain schemes (e.g., Ziegler, 1985; Seifert and Beheng, 2001). Droplet activation follows the activity spectrum approach (Cohard et al., 1998) first suggested by Twomey (1959). Reversible condensation/evaporation is a result of implicit adjustment to water saturation although strictly speaking explicit condensation rate could in principle be calculated by solving the diffusional-growth equation for gamma droplet spectrum. Drop coalescence process is represented by the stochastic-collection equation, which can be solved approximately for a clearly bimodal spectrum (cloud droplets and large drops). The coalescence is split into several terms: autoconversion, which transfers cloud droplet to the large hydrometeor category, accretion of cloud droplet by large hydrometeors, and self-collection acting on the two drop populations. Autoconversion follows the formulation of Berry and Reinhardt (1974). The accretion and self-collection terms are integrated analytically using Long's (1974) collection kernel. Large-hydrometeor self-collection includes the effects of raindrop collisional break-up in

[1] Milbrandt and Yau (2004) use the symbol α (and refer to it as "shape parameter") which is equivalent to our $\nu - 1$

a crude way. The sedimentation term allows for differential (size-sorting) effect on raindrops, where large particles, by virtue of their large terminal fall speed, appear preferentially at lower levels. This effect is accounted for in two-moment schemes because sedimentation fluxes of N_r and Q_r are computed. Finally, the evaporation of drops falling in an undersaturated environment ($s_w < 0$) is obtained by performing an analytical integration of the diffusion-growth equation over the whole drop spectrum, taking into account a ventilation effect due to raindrop fall. For a complete list of the continuity equations and description of the microphysical source and sink terms, the reader is referred to the original paper.

Cohard and Pinty (2000) parameterization has been tested in several modeling studies, such as a 2-D version of a non-hydrostatic mesoscale model, for the cases of a precipitating orographic cloud and a heavily precipitating tropical rainband (Cohard and Pinty, 2000b). The authors demonstrated realistic drop growth and realistic development of large raindrops compared to observations and to results obtained with a bin-resolving model. The parameterization has also been tested in the framework of a 3-D non-hydrostatic mesoscale model (Pinty et al., 2001). The simulations for that study were done at very high resolution (1 km) for a real case of warm orographic precipitation. The study demonstrated the sensitivity of the amount, intensity, and location of precipitation to the CCN activation spectrum and showed that an accurate simulation of precipitation with a standing forcing, such as fine scale orography, needs to incorporate details about the CCN spectrum.

3.2 Model modifications

Studies of the marine boundary layer show increasing evidence that the aerosol, and particularly those particles that serve as CCN, not only impact clouds but that clouds in turn

exert a measurable influence on the abundance and characteristics of CCN. The impact of clouds on CCN can take place via different mechanisms. First, nucleation scavenging in clouds reduces the number and the mass concentrations of the dry aerosol. Second, cloud droplet collisions followed by coalescences reduce the CCN concentration. Thus, upon the droplet's evaporation the released particles will have smaller concentrations and larger sizes than the CCN on which they originally formed. Cloud droplet-cloud droplet collisions, however, are inefficient in non-drizzling clouds; hence other processing mechanisms need to be considered in such clouds. Dissolution of trace gases in clouds followed by aqueous-phase chemical reactions is another mechanism for cloud processing which increases the amount of solute dissolved in cloud water (e.g., Penkett et al., 1979; Hegg and Hobbs, 1982; Chameides, 1984, Liu et al., 1993). Provided that on complete evaporation each droplet produces a single particle (Mitra et al., 1992), aqueous chemistry will enhance the particles mass concentration without impacting the particle number concentration, the result being that CCN are on average larger and thus more easily activated.

a) System of equations

To account for the aerosol processes, continuity equations were added to the model equations for the dry and activated aerosol and for the chemical species. Three categories of dry aerosol are introduced (subscript 'A'): one background and two regenerated modes resulting from cloud-to-particle and large hydrometeor-to-particle conversion, respectively. Aerosol activated in clouds is represented by four categories: three categories in cloud corresponding to each mode of the dry particle spectrum (subscript 'AC') and one CCN category in large drops (subscript 'AR') to account for transfer of solute from the activated categories in cloud by drop collision-coalescence. The terms 'activated aerosol' and 'CCN' are used interchangeably in this

manuscript, always referring to the actually activated aerosol, although CCN is often used to refer to the aerosol that can potentially be activated. The chemical species for which continuity equations have been introduced include four species: total (gas phase + dissolved) trace-gas concentrations of SO_2 and NH_3, total concentration of H_2O_2 acting as oxidant, and total concentration of S(VI) in cloud water from oxidation. This brings the total number of continuity equations for aerosol and chemical species to 18: $4i+2$ equations for the scalars describing $i=3$ modes of dry and activated aerosol ($4i$ equations for the mass and the number concentration in each dry and activated aerosol mode and 2 equation for the total (sum of all modes) aerosol in large drops), and 4 equations describing the chemical species (Table 3.3). Note that the equation for the number concentration of activated CCN in large drops is identical to the equation for number concentration of large drops. Integration of this number of extra equations is a manageable task using the message-passing interface. The continuity equations, described in terms of concentrations and/or mixing ratios, are written in symbolic form as follows:

$$\frac{\partial Q_{A,1}}{\partial t} = \sum \left.\frac{\partial Q_{A,1}}{\partial t}\right|_{NMT} - \xi_1^Q ; \tag{3.5}$$

$$\frac{\partial N_{A,1}}{\partial t} = \sum \left.\frac{\partial N_{A,1}}{\partial t}\right|_{NMT} - \xi_1^N ; \tag{3.6}$$

$$\frac{\partial Q_{A,2}}{\partial t} = \sum \left.\frac{\partial Q_{A,2}}{\partial t}\right|_{NMT} - \xi_2^Q + \sum_{i=1}^{3} \delta_i^Q + \delta_{S(VI)}^Q ; \tag{3.7}$$

$$\frac{\partial N_{A,2}}{\partial t} = \sum \left.\frac{\partial N_{A,2}}{\partial t}\right|_{NMT} - \xi_2^N + \sum_{i=1}^{3} \delta_i^N ; \tag{3.8}$$

$$\frac{\partial Q_{A,3}}{\partial t} = \sum \left.\frac{\partial Q_{A,3}}{\partial t}\right|_{NMT} - \xi_3^Q + \eta^Q ; \tag{3.9}$$

$$\frac{\partial N_{A,3}}{\partial t} = \sum \frac{\partial N_{A,3}}{\partial t}\bigg|_{NMT} - \xi_3^N + \eta^N ; \tag{3.10}$$

$$\frac{\partial Q_{AC,i}}{\partial t} = \sum \frac{\partial Q_{AC,i}}{\partial t}\bigg|_{NMT} + \xi_i^Q - \nu_i^Q - \mu_i^Q - \delta_i^Q , \; i = 1,3 ; \tag{3.11}$$

$$\frac{\partial N_{AC,i}}{\partial t} = \sum \frac{\partial N_{AC,i}}{\partial t}\bigg|_{NMT} + \xi_i^N - \nu_i^N - \mu_i^N - \delta_i^N , \; i = 1,3 ; \tag{3.12}$$

$$\frac{\partial Q_{AR}}{\partial t} = \sum \frac{\partial Q_{AR}}{\partial t}\bigg|_{NMT} + \sum_{i=1}^{3} \nu_i^Q + \sum_{i=1}^{3} \mu_i^Q + \nu_{S(VI)}^Q + \mu_{S(VI)}^Q - \eta^Q - \phi^Q ; \tag{3.13}$$

$$\frac{\partial N_{AR}}{\partial t} = \sum \frac{\partial N_{AR}}{\partial t}\bigg|_{NMT} + \sum_{i=1}^{3} \mu_i^N - \chi^N - \eta^N - \phi^N \tag{3.14}$$

$$\frac{\partial Q_{SO_2}}{\partial t} = \sum \frac{\partial Q_{SO_2}}{\partial t}\bigg|_{NMT} - \varepsilon_{S(VI)}^Q - \pi_{S(VI)}^Q ; \tag{3.15}$$

$$\frac{\partial Q_{NH_3}}{\partial t} = \sum \frac{\partial Q_{NH_3}}{\partial t}\bigg|_{NMT} - \alpha_{NH_3}^Q ; \tag{3.16}$$

$$\frac{\partial Q_{H_2O_2}}{\partial t} = \sum \frac{\partial Q_{H_2O_2}}{\partial t}\bigg|_{NMT} - \pi_{S(VI)}^Q ; \tag{3.17}$$

$$\frac{\partial Q_{S(VI)}}{\partial t} = \sum \frac{\partial Q_{S(VI)}}{\partial t}\bigg|_{NMT} + \varepsilon_{S(VI)}^Q + \pi_{S(VI)}^Q - \nu_{S(VI)}^Q - \mu_{S(VI)}^Q - \delta_{S(VI)}^Q ; \tag{3.18}$$

The subscript NMT refers to non-microphysical tendencies (advection, turbulence and numerics). The meanings of the other symbols are given in Table 3.1 and are explained in the sections below.

b) Nucleation

Nucleation scavenging of aerosol is central to the current investigation since it provides a mechanism by which clouds are affected by the aerosol. The representation of droplet activation in the double-moment microphysical scheme adopted in the present study follows the activity-spectrum approach (Cohard et al., 1998). The critical analysis that follows is aimed at examining the suitability of this parameterization for the purposes of the present study. This parameterization follows Twomey's (Twomey, 1959) analytical approach proposing a power-law dependence of the total CCN number, N_{CCN}, at a given percent supersaturation with respect to water, s_w, in the form $N_{CCN} = Cs_w^k$ (CCN activity spectrum). Cohard et al. (1998) takes this approach a step further by developing a more realistic four-parameter relationship between CCN number and supersaturation. This was achieved by fitting the relationship to results from a size-resolving (bin) nucleation model. The cumulative CCN number is given by the following expression:

$$N_{CCN} = Cs_{w,\max}^k F\left(\mu, \frac{k}{2}, \frac{k}{2}+1, -\beta s_{w,\max}^2\right) \tag{3.19}$$

for a maximum supersaturation $s_{w,\max}$ expressed in percent. The values of the coefficients were tabulated for two predetermined aerosol types, either continental or maritime, following lognormal distribution and are given in Table 3.2. This activation parameterization is suitable for cloud studies. It is shown to improve the estimate of CCN number by limiting the activated CCN number at high supersaturations. However, being developed for pre-determined non-varying lognormal aerosol (continental or maritime), this parameterization cannot account for the changes in the aerosol spectrum during the cloud lifecycle. Thus a parameterization for varying aerosol is better suited for the purposes of this study. Below I present an alternative approach for predicting the activated CCN number for varying aerosol spectrum.

Abdul-Razzak and Ghan (1998, 2000) activation parameterization is developed for multiple aerosol modes, each composed of internal mixture of material and each competing with each other for water. The aerosol is represented by multi-modal lognormal distribution (Eqn. 2.1) with total number concentration $N_{A,i}$, geometric mean radius $a_{m,i}$, and geometric standard deviation $\sigma_{A,i}$ of aerosol mode i. The total mass mixing ratio, $Q_{A,i}$, can be derived from the other parameters of the distribution. The CCN number and mass activated is the number and the mass concentration of the aerosol larger than the size of the smallest activated aerosol. Thus the integration of the lognormal aerosol distribution, with the lower integration limit being the size of the smallest activated particle, leads to (Von der Emde and Wacker, 1993):

$$N_{CCN,i} = \frac{N_{A,i}}{2}[1 - erf(u_i)] \tag{3.20}$$

$$Q_{CCN,i} = \frac{Q_{A,i}}{2}\left[1 - erf(u_i - \frac{3\sqrt{2}}{2}\ln\sigma_{A,i})\right], \tag{3.21}$$

where

$$u_i = \frac{\ln(a_{crit,i} / a_{m,i})}{\sqrt{2}\ln\sigma_i}, \tag{3.22}$$

and $a_{crit,i}$ is the dry radius of the smallest activated aerosol. Since the critical saturation ratio $S_{m,i}$ for activating particles with radius equal to the mode radius $a_{m,i}$ is given by

$$S_{m,i} = \frac{2}{\sqrt{B}}\left(\frac{A}{3a_{m,i}}\right)^{\frac{3}{2}} \tag{3.23}$$

and the maximum saturation ratio $S_{\max}$ of an air parcel rising adiabatically at uniform speed, equal to the critical saturation ratio of the smallest activated aerosol particle $a_{crit,i}$, is given by

$$S_{\max} = \frac{2}{\sqrt{B}}\left(\frac{A}{3a_{crit,i}}\right)^{\frac{3}{2}}, \tag{3.24}$$

(3.22) becomes

$$u_i \equiv \frac{2\ln(S_{m,i}/S_{\max})}{3\sqrt{2}\ln\sigma_i}. \tag{3.25}$$

Thus the problem of determining the CCN number and the CCN mass activated reduces to that of finding an expression for $S_{\max}$. The maximum saturation ratio $S_{\max}$ can be evaluated approximately from the saturation ratio balance equation with $\frac{dS}{dt} = 0$. The approach followed by Abdul-Razzak and Ghan (1998) is to obtain two approximate expressions for $S_{\max}$, one for relatively "small" values of $S_{m,i}$ (i.e., $a_{m,i} >> a_{crit,i}$) and one for relatively "large" values of $S_{m,i}$ (i.e., $a_{m,i} \sim a_{crit,i}$). Expressions for $S_{\max}$ corresponding to the two regimes are derived after neglecting curvature, solute, and gas kinetic effects in the droplet growth equation. The two expressions are combined to form a single expression for $S_{\max}$ for all values of $S_{m,i}$ as follows:

$$S_{\max} = 1\Bigg/\left\{\sum_{i=1}^{3}\frac{1}{S_{m,i}^2}\left[f_i\left(\frac{\zeta}{\eta_i}\right)^{\frac{3}{2}} + g_i\left(\frac{S_{m,i}^2}{\eta_i + 3\zeta}\right)^{\frac{3}{4}}\right]\right\}^{\frac{1}{2}}. \tag{3.26}$$

By employing dimensionless adjustment coefficients, evaluated using results of detailed numerical simulations of the aerosol nucleation process,

$$f_i = 0.5\exp(2.5\ln^2\sigma_i) \text{ and} \tag{3.27}$$

$$g_i = 1 + 0.25\ln\sigma_i, \tag{3.28}$$

errors due to simplifying assumptions are largely eliminated. The dimensionless terms are given by

$$\zeta = \frac{2A}{3}\left(\frac{\alpha V}{G}\right)^{\frac{1}{2}} \tag{3.29}$$

and

$$\eta_i = \frac{(\alpha V / G)^{\frac{3}{2}}}{2\pi\rho_w \gamma N_{A,i}}, \tag{3.30}$$

where A accounts for surface tension effects in the Köhler equilibrium equation, V is the updraft velocity, G accounts for diffusion of heat and moisture to the particles, and α and γ are coefficients in the saturation ratio balance equation.

This approach yields a parameterization of CCN activation with only four dimensionless parameters (Eqn. 3.27-3.30) on which the CCN number depends. It accounts for the effect of the dynamic factors on the activation process and is expressed directly in terms of parameters of the aerosol distribution. Besides the CCN number, the parameterization determines the maximum saturation ratio, the mass of the activated aerosol, and the size of the smallest activated aerosol. From these quantities one can determine the impact of nucleation scavenging on the mass and the number concentration of the dry aerosol.

Applying nucleation within a model grid box follows the approach of Ghan et al. (1997), in which nucleation is applied either when a cloud forms within a layer ("new cloud") or when air flows from clean air into the cloud ("preexisting cloud"). The nucleation rate, therefore, can be expressed as

$$\xi_i^N = \frac{N_{CCN_i}}{\Delta t} \qquad \text{"new cloud"} \tag{3.31}$$

$$\xi_i^N = -\nabla \cdot N_{CCN_i}\vec{V} \qquad \text{"preexisting cloud"} \tag{3.32}$$

where $\vec{V} = (u, v, w)$ is the three-dimensional velocity vector. I neglect droplet formation on the sides and top of clouds but account for transport of air into cloud base. Thus, the nucleation rate for "preexisting cloud" reduces to $-\frac{N_{CCN_i} w_b}{\Delta z}$, where Δz is model layer thickness, w is vertical velocity, and the subscript b denotes cloud base. This treatment of the nucleation process, which practically neglects droplet nucleation within cloud interior (within clouds, droplets are transported by vertical mixing), contrasts that of Cohard et al. (1998), which diagnoses the CCN number throughout the cloud vertical extent. This approach is motivated by the observation that, in stratiform clouds, droplet nucleation takes place predominantly at cloud base (Rogers and Yau, 1996), while in deep convective clouds, accelerating updrafts can cause supersaturations and droplet nucleation in the cloud interior as well.

c) Solute transfer

Another major modification for the purposes of this study is inclusion of an algorithm that keeps track of solute within drops following CCN activation (equations 3.12, 3.13, and 3.14). The approach adopted here follows the idea that collisions and coalescences among the various drop size categories cause a redistribution of the scavenged aerosol in such a manner that the main aerosol mass, typically contained in the large drops, is always associated with the main water mass, as described by Flossmann et al. (1985). Thus solute is transferred from cloud to large drops via the processes of accretion and self-collection at a rate commensurate with the degree of depletion of cloud water, that is, the mass fraction of the transferred solute is equal to the mass fraction of the transferred cloud water. Thus, the collection kernel for drops determines the mass fraction of solute transferred to large drops. In practice, this assumption implies (1) that the distribution with radius of the solute in cloud water follows the cloud droplet distribution and

(2) a constant-with-radius ratio of the mass of solute to the mass of water. The solute conversion rates can be written as follows:

$$\nu_i^Q = \frac{RCAUTR}{Q_C} Q_{AC,i}; \tag{3.33}$$

$$\nu_i^N = \frac{CCSCOC}{N_C} N_{AC,i}; \tag{3.34}$$

$$\mu_i^Q = \frac{RCACCR}{Q_C} Q_{AC,i}; \tag{3.35}$$

$$\mu_i^N = \frac{CCACCR}{N_C} N_{AC,i}; \tag{3.36}$$

$$\chi^N = \frac{CRSCOR}{N_R} N_{AR}; \; i = 1,3, \tag{3.37}$$

where $RCAUTR$ and $CCSCOC$ are respectively the tendencies of cloud mixing ratio and cloud droplet concentration due to self-collection; $CRSCOR$ is the tendency of raindrop concentrations due to self-collection; and $RCACCR$ and $CCACCR$ are respectively the tendencies of cloud mixing ratio and droplet concentration due to accretion between cloud droplets and raindrops (Cohard and Pinty, 2000; original nomenclature used).

d) Particle regeneration

The process of drop-to-particle conversion which takes place during evaporation of clouds follows the principle that one particle is generated for every evaporated drop. This approach is supported by the observation that cloud droplets rarely break up or splinter during the evaporative process. Laboratory experiments of the drop-to-particle conversion process by Mitra et al. (1992) suggest that, in evaporating clouds, each cloud droplet produces a single aerosol particle with mass and composition given by the mass and the composition of the foreign

material present in the drop. A major controversy had arisen in the earlier literature prior to Mitra et al. (1992) regarding the possibility of break-up of particles resulting from crystallization of evaporating drops. (A good discussion on the problem can be found in Mitra et al., 1992.) However, most of the earlier experiments were carried out by means of a setup which did not properly simulate the dynamics of the atmospheric clouds.

The implementation of particle regeneration in the present study is facilitated by the knowledge of $N_{AC,i}$, the potential number of particles in each activated aerosol mode that can be regenerated. Two dry aerosol modes form as a result of particle regeneration, one from cloud-to-particle conversion and another one from large drops-to-particle conversion. Both modes are assumed to follow log-normal distribution with geometric standard deviation $\sigma_{A,i}$ equal to that of the initial background mode. Recall that the spread of the particle spectrum is not a predictive quantity in the current treatment. Thus the particle regeneration tendencies can be written as follows:

$$\delta_i^Q = \frac{Q_{AC,i}}{\Delta t};\ \delta_i^N = \frac{N_{AC,i}}{\Delta t}\ \ i = 1,3; \tag{3.38}$$

$$\eta^Q = \frac{Q_{AR}}{\Delta t};\ \eta^N = \frac{N_{AR}}{\Delta t}. \tag{3.39}$$

The regenerated aerosol modes can activate subsequently in clouds and thus can undergo multiple condensation-evaporation cycles. Particle regeneration following partial drop evaporation is not considered at the present time. This is motivated by the fact that partial drop evaporation in the double-moment parameterization has no effect on drop concentrations N_c and N_r. Although, whenever complete evaporation occurs in a grid box, obviously $N_c = 0$ and $N_r = 0$. Such a sharp transition between "in-cloud" and "out-of-cloud" drop concentration is

believed to be justified if one is not interested in monitoring sub-grid effects (Cohard and Pintry, 2000).

e) Sedimentation of solute with large drops

Solute in large drops sediments with the terminal fall speed of the large drops that depends on drop diameter D. Milbrandt and Yau (2005) improved the representation of sedimentation in Cohard and Pinty (2000) parameterization by employing a more accurate formula for raindrop terminal fall velocity (Ferrier, 1994) given by

$$V_T(D) = \gamma a_R D^{b_R} \exp(-f_R D), \tag{3.41}$$

where $\gamma = (\rho_0 / \rho)^{1/2}$, ρ is air density and ρ_0 is surface air density, and the values of the coefficients are $a_R = 4854$, $b_R = 1$, and $f_R = 1.95$. The sedimentation rate for solute in large drops is given by the vertical flux convergence for falling drops

$$\phi^Q = \frac{1}{\rho}\frac{\partial(Q_{AR} V_{QT})}{\partial z}, \quad \phi^N = \frac{\partial(N_R V_{NT})}{\partial z} \tag{3.42}$$

where V_{QT} and V_{NT} are respectively the mass-weighted and concentration-weighted terminal fall speed and are given by

$$V_{QT} = \frac{\int_0^\infty \frac{\pi}{6}\rho_w D^3 V_R(D) n_R(D) dD}{\int_0^\infty \frac{\pi}{6}\rho_w D^3 n_R(D) dD} = \gamma a_R \frac{\lambda_R^{\nu_R+3}}{(\lambda_R + f_R)^{\nu_R+b_R+3}} \frac{\Gamma(\nu_R + b_R + 3)}{\Gamma(\nu_R + 3)} \text{ and} \tag{3.43}$$

$$V_{NT} = \frac{\int_0^\infty V_R(D) n_R(D) dD}{\int_0^\infty n_R(D) dD} = \gamma a_R \frac{\lambda_R^{\nu_R}}{(\lambda_R + f_R)^{\nu_R+b_R}} \frac{\Gamma(\nu_R + b_R)}{\Gamma(\nu_R)}. \tag{3.44}$$

f) Aqueous chemistry

Another significant modification to the model is associated with the addition of aqueous chemistry. The aqueous chemistry module follows the approach of Tremblay and Leighton (1986). This study developed a bulk aqueous sulfate chemistry module and coupled it to the 3-D cumulus cloud model of Yau (1980). This module was extensively tested in the literature. It formed the basis for a chemistry-cumulus model, which was applied to study chemistry of a rainband (Leighton et al., 1990). The chemistry-cumulus model was found to agree favorably with observations from the Eulerian Model Evaluation Field Study (Leighton et al., 1996), it was used for evaluation of a transport and deposition model (Glazer and Leighton, 1994) and for development of aqueous-sulfate chemistry parameterizations for use in regional climate models and in large-scale models (Song and Leighton, 1998; von Salzen et al., 2000).

The aqueous chemistry module in the present study considers oxidation of soluble S(IV) species (i.e., SO_2, HSO_3^-, SO_3^{2-}) to S(VI) (i.e., H_2SO_4, HSO_4^-, SO_4^{2-}) via O_3 and H_2O_2 acting as oxidants. It is currently believed that these two oxidation mechanisms are the most important pathways for aqueous production of S(VI) (Schwartz, 1984). Other potential oxidants, such as transition metal ions (e.g., Nash, 1979), free radicals (Chameides and Davis, 1982), oxides of nitrogen (e.g., Nash, 1979; Martin et al, 1981; Chang et al., 1981), and oxygen (Penkett et al., 1979), are omitted on grounds of small time scales or inefficiency within the ambient cloud water acidity levels. Species present in the gas phase include SO_2, NH_3, HNO_3, CO_2, O_3, and H_2O_2. As mentioned earlier, continuity equations were introduced only for selected species including the total (gas-phase + dissolved) concentrations of SO_2, NH_3, H_2O_2, and S(VI) from oxidation, while the remaining gas-phase concentrations were kept fixed. Under ambient cloud water acidity levels, the reaction of oxidation by O_3 is not O_3-limited, thus if oxidation by O_3 is considered, a typical background value of 30 ppbv is chosen. Gaseous HNO_3 is the main source

of NO_3^-, however, nitrate chemistry if not a focus of this study and the concentration of HNO_3 was set to zero. Lastly, atmospheric CO_2, which, in the absence of other species, is responsible for lowering the pH of cloud water to 5.6, is present in a relatively stable concentration of 350 ppmv. Gaseous SO_2, NH_3 and H_2O_2 are depleted by uptake on drops and aqueous chemical conversion and replenished by large-scale advection. Gas-phase chemistry is omitted. The solubility of each gas species is determined by the Henry's law constants describing the equilibrium concentrations of gases dissolved in aqueous phase. The Henry's law constants used in this study and the dissociation reactions of SO_2, NH_3, HNO_3 and CO_2 in solution are given in Table 3.4. Values of the Henry's law constants can be found in Schwartz et al. (1982) and Chameides (1984) among others; the values listed in Table 3.4 are from Chameides (1984) unless otherwise specified. The solubility and dissociation reaction constants are temperature dependent and are recalculated during each iteration through the chemistry routine. In addition to the ions present in solution due to dissociation of dissolved gases, other ions will also be present due to dissociation of the original CCN particles on which droplets form. Hence, for CCN particles consisting of ammonium sulfate $(NH_4)_2SO_4$ there will be extra ammonium (NH_4^+) and sulfate (SO_4^{2-}) ions present in solution. SO_4^{2-} ion will subsequently be generated in all droplets as a result of oxidation of *S(IV)*. The concentrations of NH_4^+ and SO_4^{2-} ions in the chemistry calculations are treated independently, allowing for variable ratios between the two. This affects the droplet acidity, the solubility and dissociation of SO_2, and the oxidation of *S(IV)* via the O_3 reaction.

The rate of sulfate production by O_3 and H_2O_2 is given by:

$$\varepsilon^{Q}_{S(VI)} = \left.\frac{dS(VI)}{dt}\right|_{O_3} = \left(k_0[SO_2] + k_1[HSO_3^-] + k_2[SO_3^{2-}]\right)[O_3] \text{ and} \qquad (3.45)$$

$$\pi^{Q}_{S(VI)} = \left.\frac{dS(VI)}{dt}\right|_{H_2O_2} = \frac{k_3[H^+][HSO_3^-]}{1+K[H^+]}[H_2O_2], \tag{3.46}$$

where [] denotes the aqueous species concentrations in M, $K = 13\ \mathrm{M}^{-1}$ at 298 K, and k_0, k_1, and k_2 are the oxidation rate constants of O_3; k_3 is the oxidation rate constant of H_2O_2; these are temperature dependent and are recalculated every timestep through the chemistry routine from the expressions given in Table 3.5. The H^+ ion concentration in cloud water can be obtained from a closure of the electro-neutrality equation provided that $[OH^-] << [H^+]$, $[SO_3^{2-}] << [HSO_3^-]$ and $[CO_3^{2-}] << [HCO_3^-]$, which is a reasonable approximation for acidic solutions. Thus the full electro-neutrality equation reduces to:

$$[H^+] + [NH_4^+] = [HSO_3^-] + 2[SO_4^{2-}] + [NO_3^-] + [HCO_3^-], \tag{3.47}$$

which, after applying the equilibrium rate expressions listed in Table 3.4, can be solved efficiently for $[H^+]$ by iterations.

The aqueous chemistry module is active when the cloud-water mixing ratio exceeds 1×10^{-3} g kg^{-1}. This avoids problems associated with chemistry of non-ideal high ionic strength solutions found typically close to cloud boundaries, as suggested by Bower and Choularton (1993) among others. Above 1×10^{-3} g kg^{-1}, ionic concentrations are generally larger than 0.01 M. Upon entering the chemistry module, an initializing subroutine is first called. This subroutine performs time splitting within the model timestep (30 sec) for the main chemistry routine, which is subsequently entered with a timestep of 2 sec. Test simulations have also been performed with a timestep of 1 sec with an insignificant difference in the results. A smaller timestep may be required for the $SO_2 + O_3$ pathway, however, it has been switched off in the simulations presented here. The numerical scheme for time integration is a centered difference

with an implicit damping term. Chemistry calculations are performed after a3-hour model spin-up to allow the model to generate clouds.

S(VI) produced inside clouds by oxidation can transfer from cloud drops to large drops in a similar manner as solute from nucleation:

$$\nu^{Q}_{S(VI)} = \frac{RCAUTR}{Q_C} Q_{S(VI)};\ \mu^{Q}_{S(VI)} = \frac{RCACCR}{Q_C} Q_{S(VI)}. \tag{3.48}$$

Following cloud-to particle conversion

$$\delta^{Q}_{S(VI)} = \frac{Q_{S(VI)}}{\Delta t} \tag{3.49}$$

and, to account for the formation of $(NH_4)_2 SO_4$ particle, the total (gas-phase + dissolved) NH_3 concentration is reset to the gas-phase concentration at equilibrium (source/sink term $\alpha^{Q}_{NH_3}$). Large drop sedimentation resulting in precipitation at the ground acts as a sink of S(VI) from oxidation residing in large drops.

g) Omissions

The current work has ignored a number of physical and chemical processes affecting the aerosol. Brownian coagulation of aerosol particles as well as convective diffusion scavenging of aerosol particles by raindrops are ignored on grounds of inefficiency within the time scales of interest for this study. Gravitational-hydrodynamic (impaction) scavenging of aerosol particles by raindrops is neglected as it is of secondary importance (Flossmann et al., 1985). Homogeneous nucleation of new particles from the gas phase is neglected. Gas-phase chemistry and fresh gaseous emissions are also ignored. Production of extra soluble material in drops via aqueous chemistry is postponed for a future study. Inclusion of these processes would be of interest in a comprehensive aerosol model but in this study would detract from our examination

of the roles of the processes of primary interest. In that respect the results presented here are to some extent tentative. Nevertheless, they are useful in that they place some bounds on the extent of the effect of droplet collision-coalescence on the aerosol spectrum.

3.3 Modeling strategy

MC2 is a nested grid-point model and derives its lateral boundary conditions from large-scale analysis or from a previous model run. It is capable of one-way nesting to gradually reduce the spatial scales resolved by the models to the desired resolution. Lateral boundary conditions, which are applied at each time step, must be specified at regular time intervals. The boundary conditions at each time step are then obtained by interpolation between the regular times.

a) RACE case modeling strategy

1) NESTING PROCEDURE

One-way double nesting was performed starting from 27 km down to 3 km resolution (nesting factor of 3). The 27-km simulation was 36 hr in length starting at 12 UTC on 31 August 1995 using initial and boundary conditions from the CMC regional analyses. The convective and condensation processes at this resolution were represented by the Khain and Fritsch (1990, 1993) convective parameterization and the Kong and Yau (1997) mixed-phase explicit cloud microphysical parameterization. The 9-km simulation was 30 hr in length starting at 18 UTC on the same day using, every 6 hours, initial and boundary conditions from the 27-km simulation. The same condensation and convective schemes were used at this resolution.

At 3-km resolution, the integration was 21 hr in length starting at 3 UTC on 1 Sep 1995. At this resolution, all clouds are explicit and are represented by the double-moment cloud

microphysical parameterization. The total number of grid points used in the horizontal and the vertical was 450×300×65. The model lid was at 25 km. For simulation of stratiform clouds, the grid spacing in the boundary layer and near the inversion should be as fine as is practically possible given computer memory and integration time constraints. Thus below 2 km the vertical grid spacing was 50 m with total 40 levels, while above 2 km the vertical spacing increases linearly with height to nearly 2500 m for the top-most layer. The time step was 30 sec. The presented results are at the 3-km resolution. The numerical experiments are not intended to be case studies of the event nor do they intend to test if more accurate results can be obtained by simulating real case stratiform clouds with double-moment microphysical scheme. Instead our intent is to provide a physically plausible framework for investigating the intricate interactions of stratiform clouds with the aerosol.

2) MODELING EXPERIMENTS AND AEROSOL INITIAL CONDITIONS

The presented results are divided into three parts: a control experiment, which employs the simple activation parameterization (Eqn. 3.19) and non-varying uni-modal aerosol; sensitivity experiments M1 and M2, which employ the mechanistic activation (Eqn. 3.20-3.21) and varying one-modal and two-modal aerosol (with coarse mode) respectively; and experiments aimed toward the explaining the role of collision-coalescence processing of clouds, which employ the mechanistic activation and varying one-modal aerosol, M1 (multiple cloud cycles; same experiment as before), S1 (one cloud cycle), and S0 (no collision-coalescence).

The observed aerosol spectra initialized the sensitivity experiments (Table 2.1). The first mode was assumed to consist of completely soluble ammonium sulfate ($(NH_4)_2SO_4$) and the second mode of completely soluble sodium chloride ($NaCl$). In the experiments examining CCN processing, homogeneous composition is considered due to the fact that heterogeneous

chemical composition of processed particles with varying degree of mixing adds a significant computational burden.

The model uses the conservative mass mixing ratio and number concentration of aerosol. In the horizontal direction, a uniform aerosol was assumed; in the vertical direction, the measured aerosol spectra were used until 1500 m (highest level in the measurements). Above that level, a uniform aerosol with concentration of 200 cm^{-3} (same mean radius as that at the lower levels) and no coarse mode was assumed.

b) Lake Erie case modeling strategy

1) NESTING PROCEDURE

In the Lake Erie case, the nesting strategy was similar to that in the RACE case. One-way triple nesting was performed from 36-km resolution down to 3-km. At 36 km, the simulation was 24 hr in length starting at 0 UTC on 11 July 2001. The CMC regional analysis data provided initial and boundary condition (36-km resolution; 16 levels).

At 3 km, the integration was 18 hr in length starting at 6 UTC on 11 July 2001. The double-moment microphysics and the mechanistic activation were employed at this resolution. The model grid was designed in a fashion similar to the RACE case. The total number of grid points was 400×380×60; the model lid was at 25 km. The vertical grid spacing was 70 m (38 levels) below 2.5 km and above that level increased linearly with height to nearly 2500 m for the top-most layer. The time step was 30 sec. The presented results are the 3-km resolution.

2) MODELING EXPERIMENTS AND INITIAL CONDITIONS

Three experiments are presented. The first experiment excluded the effects of droplet collision-coalescence and aqueous chemistry on the particle spectrum (S0). The second

experiment included only drop collision-coalescence (S1). Finally, the last experiment included both drop collision-coalescence and aqueous chemistry with H_2O_2 acting as oxidants (SO1).

To initialize the modeling experiments the first mode of the observed aerosol spectrum was taken (Fig. 2.10). A pure, completely soluble, $(NH_4)_2SO_4$ composition of the aerosol was assumed. The assumption of uniform mixture in this case is justified also by the fact that aqueous chemistry adds to the variability of a non-uniform mixture. Similarly to the RACE case, a uniform distribution was assumed in the horizontal; in the vertical, the particle concentration was uniform within the depth of the mixing layer while above the concentrations decrease exponentially with scale height of 2 km to a background concentration of 200 cm^{-3}.

The initial chemistry conditions are assumed for illustrative purposes. The gas concentrations are given in parts per billion by volume (ppbv), however the model uses the conservative mixing ratio units of kg kg^{-1} (air). The initial values of the advected chemical species, SO_2 = 5 ppbv, NH_3 = 1 ppbv, H_2O_2 = 1 ppbv, have been assumed uniform in the mixing layer. As for the aerosol, a uniform-in-horizontal and exponentially decaying-with-height distribution was assumed above the mixing layer. The values remaining species, which remain fixed, are O_3 = 0-30 ppbv, HNO_3 = 0 ppbv, and CO_2 = 350 ppmv.

The chemistry input mimics the initial conditions used by Bower and Choularton (1993) (for their run 1) and Feingold et al. (1998), except for the concentration of O_3 which in the present study was set to zero. High concentrations of SO_2, as well as adequate amounts of H_2O_2 acting as oxidant ensure strong aqueous-phase oxidation of SO_2. The availability of 1 ppbv of NH_3 and the lack of HNO_3 helps to neutralize some of the acidity and aids the solubility and dissociation of SO_2 and its conversion to S(VI). At the level of acidity present the conversion will be dominated by the H_2O_2 reaction (Bower et al., 1991). The initial values of

gas-phase concentrations are in agreement with observations and other model studies (Bower and Choularton, 1993; Mcdonald et al., 1995; Feingold et al., 1998; Zhang et al., 1999; Feingold and Kreidenweis, 2000).

Table 3.1: Description of the microphysical and aqueous chemistry source and sink terms in Eqn. 3.5-3.18.

Symbol	Sinks	Sources	Processes
ξ_i^Q	$Q_{A,i}$	$Q_{AC,i}$	Nucleation
ξ_i^N	$N_{A,i}$	$N_{AC,i}$	
ν_i^Q	$Q_{AC,i}$	Q_{AR}	Autoconversion
$\nu_{S(VI)}^Q$	$Q_{S(VI)}$	Q_{AR}	
ν_i^N	$N_{AC,i}$	-	Cloud self-collection
μ_i^Q	$Q_{AC,i}$	Q_{AR}	Accretion
μ_i^N	$N_{AC,i}$	N_{AR}	
$\mu_{S(VI)}^Q$	$Q_{S(VI)}$	Q_{AR}	
δ_i^Q	$Q_{AC,i}$	$Q_{A,2}$	Cloud-to-particle conversion
δ_i^N	$N_{AC,i}$	$N_{A,2}$	
$\delta_{S(VI)}^Q$	$Q_{S(VI)}$	$Q_{A,2}$	
χ^N	N_{AR}	-	Rain self-collection
ϕ^Q	Q_{AR}	Q_{AR}	Rain sedimentation
ϕ^N	N_{AR}	N_{AR}	
η^Q	Q_{AR}	$Q_{A,3}$	Rain-to-particle conversion
η^N	N_{AR}	$N_{A,3}$	
$\pi_{S(VI)}^Q$	Q_{SO_2}, $Q_{H_2O_2}$	$Q_{S(VI)}$	$S(IV)$ to $S(VI)$ oxidation by H_2O_2
$\varepsilon_{S(VI)}^Q$	Q_{SO_2}	$Q_{S(VI)}$	$S(IV)$ to $S(VI)$ oxidation by O_3
$\alpha_{NH_3}^Q$	Q_{NH_3}		Formation of $(NH_4)_2SO_4$ in solution*

* Following cloud-to-particle conversion, the total (gas-phase + dissolved) NH_3 concentration is reset to the gas-phase concentration at equilibrium to account for the released $(NH_4)_2SO_4$ particle.

Table 3.2: Parameters of the lognormal spectra and coefficients in the expression for cumulative CCN number (equation 3.5) in Cohard et al. (1998).

Aerosol type	Chemical composition	$(N_A;\ a_m;\ \sigma_A)$ (cm^{-3}; nm; no unit)	C	k	μ	β
Continental	$(NH_4)_2SO_4$	(842; 21.8; 3.19)	3270	1.56	0.70	136
Maritime	$NaCl$	(67; 133; 1.62)	1.93×10^8	4.16	2.76	1370

Table 3.3: Summary of aerosol and chemical species considered in the model.

Species	Number of scalars	Comments
Dry aerosol	6	Scalars for aerosol mass and number concentration of one background mode and two processed modes; assumed to be log-normally distributed with fixed σ_a
Activated CCN	8	Scalars for the mass and number concentration of activated CCN in cloud and for activated CCN in rain
Trace gases	3	Scalars for SO_2, NH_3, H_2O_2; O_3 and HNO_3 kept fixed
Chemical species	1	Scalar for S(VI) in cloud water; aqueous components of gas species and activated CCN in cloud water are calculated assuming equilibrium and reversible process
Total	18	

Table 3.4: Solubility and dissociation equilibrium constants used for the cloud chemistry.

Equilibrium reactions	Equilibrium constant* at 298 K, K_{298}, M or M atm^{-1}	$-\frac{\Delta H}{R}$ at 298 K, K	Reference
$SO_2(g)+H_2O(aq)\leftrightarrow SO_2{\cdot}H_2O$	1.23 M atm^{-1}	3120 K	*Chameides (1984)*
$SO_2{\cdot}H_2O_2\leftrightarrow H^+ + HSO_3^-$	1.7×10^{-2} M	2090 K	*Chameides (1984)*
$HSO_3^- \leftrightarrow H^+ + SO_3^{2-}$	6×10^{-8} M	1120 K	*Chameides (1984)*
$HNO_3(g)\leftrightarrow HNO_3(aq)$	2.1×10^5 M atm^{-1}		*Seinfeld and Pandis (1998)*
	2×10^5 M atm^{-1}		*Schwartz and White (1981)*
$HNO_3(aq)\leftrightarrow H^+ + NO_3^-$	15.4 M		*Seinfeld and Pandis (1998)*
$NH_3(g)+H_2O(aq)\leftrightarrow NH_3{\cdot}H_2O$	58 M atm^{-1}	4085 K	*Chameides (1984)*
$NH_3{\cdot}H_2O\leftrightarrow NH_4^+ + OH^-$	1.7×10^{-5} M	−4325 K	*Chameides (1984)*
$CO_2(g)+H_2O(aq)\leftrightarrow CO_2{\cdot}H_2O$	3.11×10^{-2} M atm^{-1}	2423 K	*Chameides (1984)*
$CO_2{\cdot}H_2O\leftrightarrow H^+ + HCO_3^-$	4.3×10^{-7} M	−913 K	*Chameides (1984)*
$HCO_3^- \leftrightarrow H^+ + CO_3^{2-}$	4.8×10^{-11} M		*Robinson and Stokes (1959)*
$O_3(g)+H_2O(aq)\leftrightarrow O_3{\cdot}H_2O$	1.15×10^{-2} M atm^{-1}	2560 K	*Chameides (1984)*
$H_2O_2(g)\leftrightarrow H_2O_2(aq)$	9.7×10^4 M atm^{-1}	6600 K	*Chameides (1984)*
$H_2O\leftrightarrow H^+ + OH^-$	1×10^{-14} M^2	6716 K	*Chameides (1984)*

* The temperature dependence of the equilibrium constants is represented by $K(T) = K_{298} \exp\left[-\frac{\Delta H_{298}}{R}\left(\frac{1}{T}-\frac{1}{298}\right)\right]$.

Table 3.5: Aqueous-phase reactions and rate coefficients* used for the chemistry.

Aqueous-phase reactions	Rate coefficient*, k_{298}, M s^{-1}	$-\frac{E}{R}$, K	Reference
$S(IV)+O_3 \rightarrow S(VI)+H_2O$	$k_0 = 2.4 \times 10^4$ M^{-1} s^{-1}		*Hoffmann and Calvert (1985)*
	$k_1 = 3.7 \times 10^5$ M^{-1} s^{-1}	−5533	*Hoffmann and Calvert (1985)*
	$k_2 = 1.5 \times 10^9$ M^{-1} s^{-1}	−5280	*Hoffmann and Calvert (1985)*
$S(IV)+H_2O_2 \rightarrow S(VI)+O_2$	$k_3 = 7.5 \times 10^7$ M^{-1} s^{-1}	−4751	*Hoffmann and Calvert (1985)*

*The temperature dependence of the rate coefficients is represented by $k = k_{298} \exp\left[-\frac{E}{R}\left(\frac{1}{T}-\frac{1}{298}\right)\right]$.

Chapter IV

Sensitivity of Marine Stratus to Aerosol

The simulated stratus cloud thermodynamic and microphysical properties in experiments CTRL, M1, and M2 are compared with the aircraft observations collected during RACE campaign. For the purpose of the comparison, the aircraft observations are averaged over 50-sec intervals corresponding approximately to a 3-km flight path (Twin Otter operates at an airspeed of 50-70 m s^{-1}). A single verification time of 1800 UTC was chosen for the model output justified by the fact that the stratus cloud changed little within the 110-min duration of the flight (1720-1910 UTC) (Mark Couture, MSC, personal communications). The model values are spatially interpolated from the model grid onto the 3-D flight track.

The large-scale precipitation system, which preceded the marine strtaus formation, is also examined in experiments CTRL, M1 and M2.

4.1 Control Experiment

a) Thermodynamic and microphysical properties (CTRL)

Fig. 4.1a and 4.1b shows a comparison of model vertical soundings with two aircraft soundings, one taken along leg AB of the flight track (over land) at around 1730

UTC and the other taken at point B of the flight track (in the middle of the Bay) at around 1820 UTC. Note that the times of the two soundings depart approximately equally from the model verification time of 1800 UTC. Despite the uncertainties associated with the verification method the model soundings compare reasonably well to the aircraft soundings. In the cloud layer the average difference between the two is within the instrument error of ± 0.5 °C. The characteristic capping inversion is observed in the two soundings. The height of the inversion is closely reproduced, especially over land; over water, the simulated inversion height was 200 m lower than the observed one and a second overlaying inversion layer was simulated. The inversion strengths in the model are comparable to the observed inversion strengths (around 2–3 °C) over land and in the Bay. The inversion thickness in the model was overestimated: 100 m over land and 200 m over water compared to a few meters in the observations. This discrepancy between the simulated and observed inversion height and thickness is due at least partially to the inadequate vertical resolution in the model, which was 50 m in the boundary layer (BL height was about 1500 m). In the layer below the cloud over land, the model temperature and dew point temperature were in reasonable agreement with the observed values with the temperature following roughly the dry-adiabatic lapse rate. Over water, the below-cloud layer was characterized by a strong sea-surface inversion with strength of about 3–4 °C and thickness of 200 m. The sea-surface inversion thickness in the model was smaller (by about 50 m); in addition, the sea-surface temperature was slightly warmer (by about 1-2 °C). This produced a too warm below-cloud layer. The sea-surface temperature in the model is from analyses and was kept fixed.

The flight-track variations of temperature and RH were also reasonably predicted by the model (Fig. 4.2). The model temperature followed the observed temperature within the instrument error of ± 0.5 °C, except close to the surface. For example, note the temperature variations around 1820 UTC and between 1840-1850 UTC. The model reproduced the locations of the saturated and drier regions in the observations. Naturally there are some discrepancies between the model and the observations. Over the Bay the below-cloud layer in the model was generally drier than observed (see RH variation between 1715-1730 UTC, around 1800 UTC, and between 1820-1840 UTC). It can also be seen that in the layer above the cloud the model was much drier than the observations with RH as low as 50 % (see the RH signals between 1735-1745 UTC and 1815 UTC).

The simulated LWC agreed remarkably well with the observed LWC (Fig. 4.3 a). As in the observations, the model showed larger values of LWC over land, reaching 0.5 g m^{-3}, and smaller values over the Bay with a maximum of 0.3 g m^{-3}. The only discrepancy between the modeled and the observed LWC (the LWC signal around 1830-1840 UTC) is at the most southwestern point of the flight track (point C; see Fig. 2.4) and is related to the larger horizontal extent of the cloud in the model than in reality.

While the LWC showed excellent agreement between the model and the observations, the droplet concentration in experiment CTRL was greatly under-predicted (Fig. 4.3b) with values as low as 10–20 cm^{-3} compared to 300–500 cm^{-3} measured by FSSP counter. This translates to a mean volume radius of around 20 μm compared to 7 μm in the observations.

A comparison of the updraft velocity in the vicinity of the cloud (Fig. 4.3c) is insightful because the updraft controls the supersaturation and thus droplet concentration.

Comparison of grid-mean vertical velocity in the model with aircraft observed values requires considering only observations over level-flight periods as large aircraft vertical velocities can introduce significant errors in the measurements of small wind gusts (Mark Couture, MSC, personal communications). The model updraft velocity was of the order of a 10-20 cm s^{-1} while the observed values were about 0.5 to 1 m s^{-1} (Fig. 4.3c). Clearly, the model underestimated the updraft velocity on the scale of the model-grid spacing. Since the updraft controls the supersaturation and droplet concentration, the underestimation of the droplet concentration by the model can, at least in part, be explained by the underestimation of the updraft velocity. One, however, should keep in mind that the model vertical velocities represent volume averages (over the model grid box) while the aircraft-measured vertical velocities represent line averages (over flown distance). Thus the larger volume being represented in the model might also be, in part, a reason for the underestimation.

b) Cloud spatial distribution (CTRL)

The simulated cloud base and cloud top heights are shown in Fig. 4.3d. Although the observations provide only a few data points their variation was small, especially over the Bay, giving a good basis for comparison with the model. The track-average cloud top in the model (1091 m) compared reasonably to the observed cloud top (1108 m), while the track-average cloud base (672 m) was 157 m too low than the observed cloud base (829 m). This led to over prediction of the track-average cloud thickness by 140 m (Fig. 4.3d). The variation along the flight track of the cloud base and height in the model reveals a cloud with approximately the same thickness over land and over water, which is in contrast to the aircraft observations (also supported by the satellite image) revealing

thicker cloud over land than over the Bay (Fig. 4.3d). The present results obtained with a two-moment microphysics are consistent with the earlier study of Guan et al. (2000) obtained with one-moment microphysics. My study however improved the simulation of cloud-top height.

The model needs to be able to produce a reasonable representation of the unbroken stratus deck. Fig. 4.4a shows the horizontal distribution of LWC and droplet concentration in the model at an altitude of 1050 m, which represents roughly the mean conditions in cloud. The cloud features captured by the model, which are evident on the satellite image (see Fig. 2.3), include the horizontal extent of the cloud from the coast of New Brunswick over the Bay, the clear region in the northeastern part of the Bay and the cloudiness over Nova Scotia. The cloud features evident on the satellite image but not present in the simulation include the organization of the cloud field over New Brunswick and Nova Scotia in bands oriented approximately north south. Note the lack of detail in the spatial distribution of droplet concentration, which was almost uniform horizontally.

Fig. 4.4b and 4.4c show the vertical distribution of cloud LWC, large hydrometeor volume-mean radius, droplet concentration, and large hydrometeor concentration along track ABC (see Fig. 2.4). The horizontal loops performed by the aircraft while taking the vertical profile at point B can also be seen in Fig. 4.4 by the almost repetitive pattern in the cloud field around point B. Note that point B of the flight track was close to the edge of the cloud, which explains the thinning of the cloud in this part of the domain.

The vertical profiles over water in the model reveal close-to-adiabatic profile of LWC (segment BC; Fig. 4.4b), which is characteristic for stratus clouds, and uniform-

with-height profile of droplet concentration (segment BC; Fig. 4.4c), also characteristic of stratus clouds. Both are in agreement with the observed profiles of these quantities over Bay of Fundy (Fig. 2.6b and 2.6d). The simulated profile of droplet concentration over land was also uniform (segment AB; Fig. 4.4c), which contrasts the observations showing two distinct maxima of droplet concentration (Fig. 2.6c). As we shall see in the subsequent experiments, the mechanistic activation can account for this spatial variability in droplet concentration. Large drops sizes and concentrations (also shown in Fig. 4.4b and 4.4c respectively) were present in insignificant concentrations (< 0.1 dm^{-3}) to be associated with precipitation.

Note some amount of water was also present in the large hydrometeor category. Below cloud (altitude 400 m), drizzle-size drops (100 μm in radius) are observed in concentration of less than 10 dm^{-3}. However, these drops evaporate before reaching the ground and cannot be associated with precipitation.

The obtained results are consistent with an earlier study by Guan et al. (2000) that simulated the same case using one-moment bulk microphysical parameterization. In Guan et al. (2000; their Fig. 5a), the simulated cloud-top height was on average 100 m too low compared to the observations (1100 m) and cloud-base height was on average 20 m higher than the observations (830 m) thus producing a too thin cloud. This study shows better agreement with the observations for the cloud thickness. This was a result of improving the simulation of cloud-top height, much closer to that observed, though the cloud base here remains too low relative to the observed value. Ways of improving the simulation of cloud-base height are discussed in the sensitivity experiments presented in the following section.

c) Large-scale precipitation (CTRL)

The cold frontal system swept across the area of Bay of Fundy between 6 and 15 UTC. At 9 UTC the precipitation reached its maximum intensity, 1-2 mm hr^{-1} (Fig. 4.5a; maximum daily accumulation 1-2 mm). Southerly winds prevailed ahead of the system; westerly winds prevailed behind the system (also shown in Fig. 4.5a). Cross section through the system reveals its vertical extent (Fig. 4.5b). The vertical velocity in the upstream part of the system shows moderate updrafts; precipitation-induced downdrafts dominate in the downstream part of the system (also shown in Fig 4.5b). Towards the end of the examined period, the precipitation gradually reduced and the cloud lowered substantially.

4.2 Mechanistic activation with one-modal aerosol

a) Thermodynamic and microphysical properties (M1)

Similar analysis was performed for experiment M1 as for experiment CTRL. Comparable agreement with the observations was found in the two experiments for the thermodynamics properties as well as for LWC (Fig. 4.6a). A noticeable improvement from experiment CTRL is observed, not surprisingly, in the simulation of droplet concentration (Fig. 4.6b). An excellent agreement with the observations was found for the maximum droplet concentration, 400 cm^{-3}, while the track-average value was slightly underestimated, 150 cm^{-3} versus observed value of 300 cm^{-3}. As a result the corresponding droplet volume-mean radius, around 10 μm, was also much closer to observed. Thus introducing mechanistic activation to a first order lead to improving the prediction of droplet concentration.

b) Cloud spatial distribution (M1)

A significant improvement, relative to experiment CTRL, was found for the simulation of cloud base height; the simulation of cloud top height improved to a lesser degree (Fig. 4.6c). The simulated track-averages of cloud base height, 827 m, and of cloud top height, 1135 m, gave excellent agreement with the observed values (829 m and 1108 m, respectively). This resulted in improvement of the simulated cloud thickness (308 m compared to observed thickness of 279 m). The variability of the cloud thickness over land and over water is also better simulated. The model captured the observed differences in cloud thickness over land and over water: thinner cloud was simulated over water (higher cloud base) and thicker cloud over land (lower cloud base). Thus experiment M1 gives much better agreement of the cloud thickness with the observations relative to experiment CTRL and Guan's study, mainly due to improvement in the simulated cloud-base height. Recall, experiment CTRL produced a cloud with approximately the same thickness over land and over Bay of Fundy.

Fig. 4.7a shows the horizontal distribution of cloud LWC and droplet concentration in experiment M1 at an altitude of 1050 m. Similarly to experiment CTRL, the position and the horizontal extent of the cloud was in reasonable agreement with those on the satellite image. In this experiment, however, the cloudiness over Nova Scotia is more extensive than in experiment CTRL thus is more representative of the cloud as seen by satellite. The banded structure of the cloud, as seen by satellite, in this experiment like in experiment CTRL is lacking.

The spatial distribution of LWC resembled that in experiment CTRL (Fig. 4.7b). The maximum LWC was reached in the upper half of the cloud layer, which agreed with the observations. The spatial distribution of the cloud droplet concentration showed greater variability in horizontal (Fig 4.7a) and in vertical. In vertical, the observed two maxima of the droplet concentration over land (Fig. 2.6c) are captured by the mechanistic activation (Fig. 4.7c), while experiment CTRL produced a uniform profile. Thus the introduced by the mechanistic activation greater spatial variability in the droplet concentration field better represented the observed variability. Droplet concentration over water was roughly uniform with height, which resembled experiment CTRL and was in agreement with the characteristic uniform-with-height profile found in the observations.

The water content in the large hydrometeor category in this experiment, similarly to experiment CTRL, was insignificant to be associated with precipitation (precipitation rates did not exceed 0.01 mm hr^{-1}). Drizzle-size drops, however, falling in an under-saturated environment, if evaporate completely, could serve as giant CCN. As can be seen, below cloud (400 m altitude) drizzle drops (>100 μm in radius) were present in concentration of less than 1 dm^{-3}; smaller drops were present in concentrations of the order of 10 dm^{-3}. It is noteworthy that due to the small concentrations evaporating drizzle-drops can be expected to be only a minor source of giant CCN.

c) Large-scale precipitation (M1)

Introducing mechanistic activation affected the large-scale precipitation preceding the marine stratus (Fig. 4.8). The mechanistic activation produced weaker precipitation rates in the less vigorous (upstream) part of the system, largest differences being of the order of 0.1-1 mm hr^{-1} (daily accumulations differences <1 mm; Fig. 4.8a). This was

consistent with larger CWP upstream (Fig. 4.8b) and higher droplet concentration overall (Fig. 4.8c). The higher droplet concentration suppressed the initiation of rain upstream but not in the more vigorous (downstream) part of the system.

4.3 Mechanistic CCN activation with two-modal aerosol

Similar analysis was performed for experiment M2. The addition of second (coarse) mode in the particle spectrum had a pronounced effect on both the cloud microphysical properties and the cloud spatial structure.

a) Microphysical properties (M2)

The coarse mode in the particle spectrum affected to a lesser extent LWC (Fig. 4.9a) but had dramatic impact on droplet concentration (Fig. 4.9b). Droplet concentration is substantially reduced (< 50 cm^{-3}) from experiment M1. By virtue of its large size the coarse mode activates at lower supersaturations than the first mode. The resultant effect is reduction of supersaturation, which prevents the activation of the smaller-in-size but more numerous first mode.

b) Cloud spatial distribution (M2)

The effect of the coarse mode on the cloud vertical structure, relative to experiment M1, was lowering by 100 m the track-mean cloud base (712 m) and by about 90 m the track-mean cloud top (1047 m); the latter one was result mainly of lower cloud top over the water portion of the track (Fig. 4.9c). Although these changes correspond to two grid points in vertical (model vertical resolution was 50 m in the cloud layer), such

effects suggest aerosol-cloud-dynamics feedbacks as suggested by Feingold at al. (1996b) and Jiang et al. (2002) for lightly drizzling stratocumuli. Evaporative cooling of drizzle drops at cloud base can destabilize the sub-cloud layer (just below cloud base) and lead to more vigorous development of clouds, thus increasing LWP (Feingold at al., 1996b). Reduced drizzle on the other hand may in some circumstances lead to the opposite effect (Jiang et al., 2002).

The spatial distributions of LWC and droplet concentration in horizontal and in vertical resemble that in experiment M1 except for droplet concentration the values are much smaller (Fig. 4.10).

c) Large-scale precipitation (M2)

The addition of the coarse mode affected the large-scale precipitation fields (Fig. 4.11). In the less vigorous (upstream) part of the system, the precipitation rates were stronger (change 0.01-1 mm hr^{-1} or < 1mm change in daily accumulation; Fig. 4.11a). This was consistent with smaller cloud LWP upstream (change 0.1-1 mm; Fig. 4.11c) and lower droplet concentrations overall (change 10-100 cm^{-3}; Fig. 4.11b). The less vigorous (downstream) part of the system remained unaffected by the coarse mode.

d) Comparison with experiment CTRL

Interestingly enough, the two-modal particle spectrum in experiment M2 produced similar results, for both the stratus cloud and the precipitating system, to those obtained with the simple activation. Although detailed examination of the underlying reasons is outside the scope of this work, this result is not surprising given that the

aerosol spectrum in the simple activation parameterization was, roughly speaking, average of the two-modal spectrum. The fact that both experiments CTRL and M2 had profound implication on the droplet concentration relative to experiment M1 suggests that representing the modality or the spread of the particle spectrum is important to correctly predict droplet concentration.

4.4 Discussion

a) Simple versus mechanistic activation

The results obtained with the simple and the mechanistic activation parameterizations produced an order of magnitude difference in droplet concentration in the simulation of a case of marine stratus. It is therefore necessary to examine closely the differences between the two parameterizations. The following three factors come into play. The mechanistic activation consists of a forcing term in the aerosol continuity equation. Therefore, both mass and number of particles are preserved. The simple activation assumes a non-varying aerosol and an infinite source of CCN and thus is not mass conserving. This difference manifests itself in the regions of strong updrafts where the simple activation produces much higher numbers of activated particles. Second, the mechanistic approach generates new droplets only at cloud base whereas the simple activation estimates the number of activated CCN at every cloud level. As a result, the more vigorous parts of the cloud, on average, would generate higher CCN number with the simple approach. This would also produce a different vertical distribution of droplet concentration. Third, the simple parameterization uses an initial spectrum with lower number concentration and smaller mean radius compared to the mechanistic

parameterization (respectively 842 cm^{-3}, 21.8 nm, $\sigma_A = 3.19$ versus 1200 cm^{-3}, 50 nm, $\sigma_A = 1.7$; values at cloud base). Therefore, given other factors are equal, the more polluted initial spectrum should activate higher CCN number than the less polluted one. Our results demonstrate that the differences in the initial aerosol spectra determine the magnitude of droplet concentration in the stratus cloud. The representation of new droplet formation in the interior of the cloud determines the vertical distribution of droplet concentration in the stratus cloud.

Despite the fact that the droplet concentrations produced by the mechanistic activation agreed more closely with the observations than the simple activation, the concentrations still represented only about half of the observed values. To explain the underestimation one needs to consider the factors regulating the CCN number. In a non-precipitating cloud, in which drop collision-coalescence is a minor sink of drops, the number of the activated CCN regulates the droplet number. The CCN number, in turn, is governed by the supersaturation that increases as a result of ascent of the air and decreases as a result of condensation. The magnitude of the updraft predicted by a numerical model is, however, grid-size dependent in the sense that the grid size determines the scales resolved by the model. Thus the grid spacing and the grid-resolved updraft velocity represent limitation to the correct prediction of droplet concentration.

Indeed, the under-prediction of droplet concentration with mechanistic activation was associated with under-prediction of the updraft velocity by the model (respectively ~0.1 m s^{-1} and ~ 1 m s^{-1} for model and observations). This is a particular problem for shallow strata and stratocumuli. These cloud types are governed by small-scale (few meters) fluctuations of the vertical velocity due to turbulence, which clearly cannot be

captured by the mesoscale model grid. The problem can be resolved by parameterizing the sub-grid variability of the vertical velocity, for example, by using the approach of Golaz et al. (2002) developed for BL clouds. Golaz et al. (2002) discussed the use of joint probability density functions to describe sub-grid variability of vertical velocity, temperature, and humidity in BL clouds.

The different initial aerosol spectra in the simulations with the mechanistic and the simple activation schemes led to differences in the distribution of the frontal precipitation. Pinty et al. (2001) reported similar sensitivity of the precipitation pattern and intensity to the CCN spectrum for a case of orographic precipitation. A quantitative comparison with Pinty et al. (2001) study is not possible because of the different forcing mechanisms and the different aerosol loadings. However, a qualitative comparison reveals similar mechanisms. For example, Pinty et al. (2001) reported a decrease in the precipitation amount and intensity in the upstream edge of the orographic bands and disappearance of the less intense bands following an increase of the aerosol load from twice (equivalent concentration 134 cm^{-3}) to six times (equivalent concentration 402 cm^{-3}) the base case particle concentration. (The remaining parameters of the aerosol distribution were kept fixed.) The reduction of the precipitation in the rainbands was associated with more extensive and thicker clouds.

b) Effect of giant CCN

The reduction by the coarse mode of the marine stratus cloud base height and to a lesser degree of cloud top height suggests a response involving an aerosol – cloud – dynamics interaction. Such a response appears to be more complex than the accepted

hypothesis associated with the second indirect effect. The possibility of drizzle-induced destabilization of the sub-cloud layer (by evaporative cooling of drizzle drops), which can lead to more vigorous development of clouds (Feingold et al., 1996b), remains to be confirmed in a more detailed study.

The complex response of the precipitating system to the presence of the coarse mode has potential implications for short-term weather forecasting. Particularly, the fact that the upstream part of the system was sensitive to the coarse mode but the downstream part was not suggests sensitivity of the spatial distribution of precipitation to details of the aerosol spectrum (modality or, equivalently, spectral breadth). Previous studies have only suggested sensitivity of the amount of precipitation to the aerosol loading (e.g., Pinty et al., 2001).

The mechanism via which the coarse mode affects the number of the activated CCN, the droplet concentration, and the initiation of large drops, depends on three factors: the abundance of the fine mode, the mean radius of the coarse mode, and the magnitude of the updraft (Ghan et al., 1998; O'Dowd et al., 1998). Two separate regimes exist: for high concentrations of the fine mode (1000 cm^{-3}) and weak updrafts (< 0.5 m s^{-1}) the coarse mode tends to reduce the total number of activated particles; for moderate concentrations (100-300 cm^{-3}) and strong updrafts (> 0.5 m s^{-1}), on the contrary, activation of the coarse mode tends to increase the total number activated by adding to the activated fine particles. The weak updraft velocity limits the increase of the supersaturation; thus activating the coarse mode lowers the supersaturation and prevents the fine mode from activating. For strong updraft velocities the increase of the supersaturation is not limited. Furthermore, a coarse mode with relatively small mean

radius (0.1 μm; film-drop mode) increased the total number of activated CCN under most conditions while a coarse mode with relatively large mean radius (1 μm; jet-drop mode) decreased the total activated CCN number under almost all conditions.

The present study is characterized by conditions of high concentrations of the fine mode, large mean radius of the coarse mode, and a weak updraft velocity (0.1-0.2 m s^{-1}). These conditions led to a reduction, by the coarse mode, of the droplet concentration for the marine stratus cloud. Similar reduction of the droplet concentration was observed for the precipitating system, which resulted in enhanced rain intensities in the upstream part of the system.

The presence of coarse-mode aerosols reduces the cloud droplet concentration because the large particles grow at expense of the smaller particles. However, inherent to the mechanistic activation parameterization of Abdul-Razzak and Ghan (1998) is the assumption that large particles have sufficient time to reach their equilibrium size according to Koehler theory. More recent studies suggested problems with the equilibrium assumption (Nenes et al, 2001; Phiney et al., 2003) and pointed out the importance of considering kinetic limitations to the droplet condensational growth. Basically, the Abdul-Razzak and Ghan (1998) parameterization underpredicts the number of cloud droplets in the presence of coarse aerosol (Phiney et al, 2003). This underprediction is significant for particle concentration in the accumulation mode higher than 1000 cm^{-3}. For particle concentrations lower than or of the order of 1000 cm^{-3}, such as the conditions of the present study, the underprediction is small. Investigating the effect of the equilibrium assumption on droplet concentration certainly should be the subject of a more detailed future study.

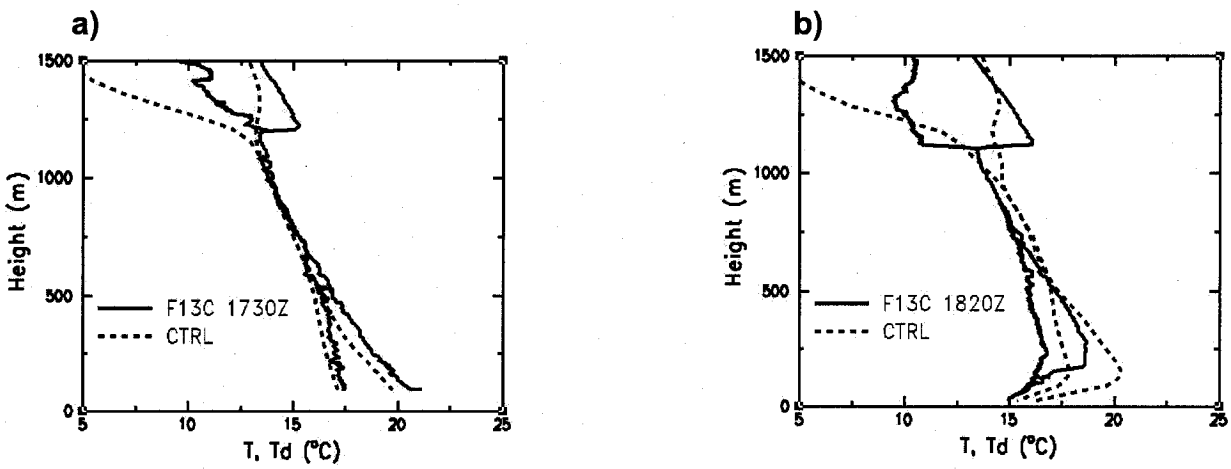

Figure 4.1: Vertical profile of temperature and dew point temperature from aircraft measurements (solid lines) and in experiment CTRL (dashed lines). The profiles are taken: a) over land (observation time ~ 1730 UTC) and b) in Bay of Fundy (observation time ~ 1820 UTC). Model values are valid at 18 UTC.

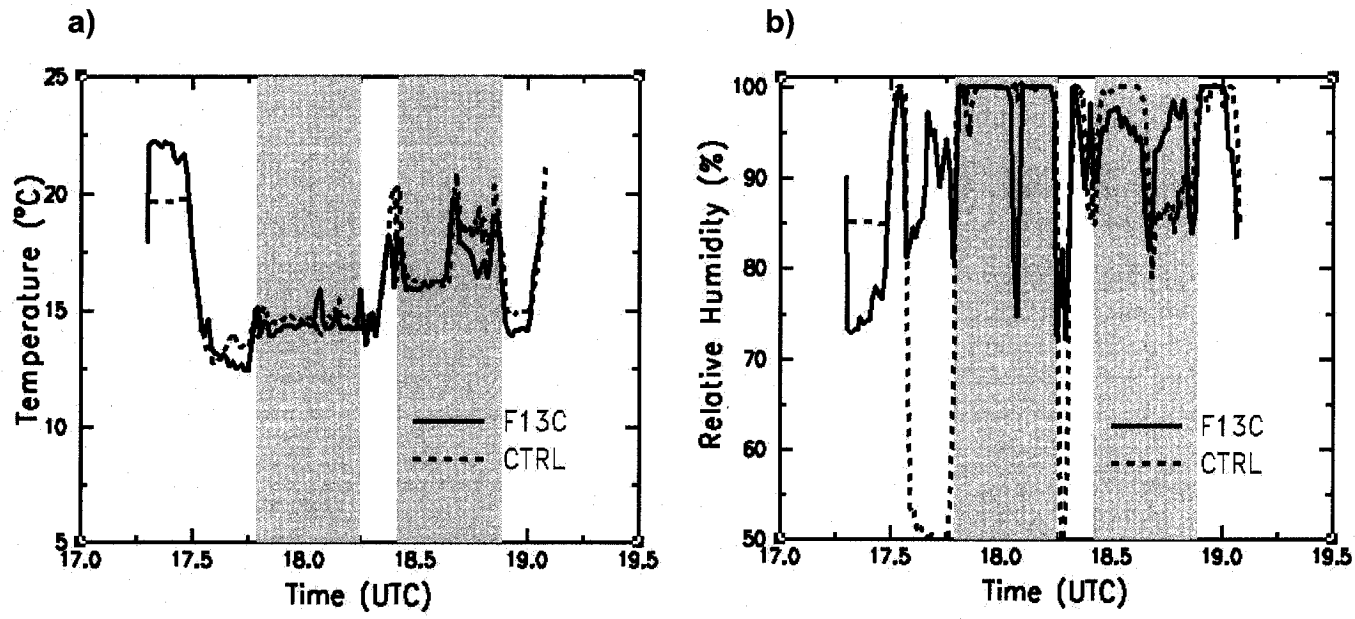

Figure 4.2: Along-track comparison of various fields from observations (solid lines) and in experiment CTRL (dashed lines): a) air temperature (°C) and b) relative humidity (%).Time along the horizontal axis indicates flight time. Model values are valid at 18 UTC. Shaded areas highlight the level flight segment BC.

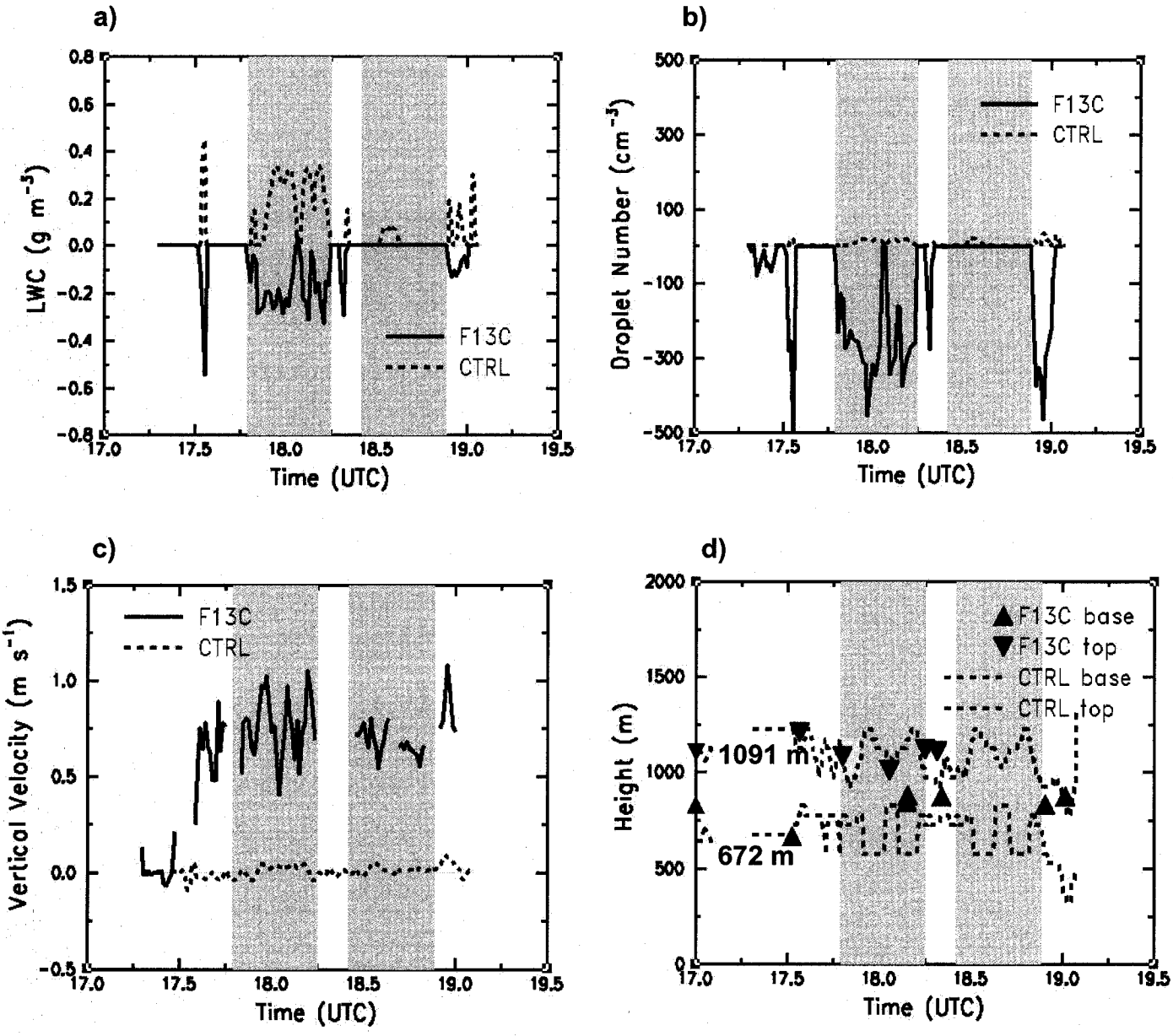

Figure 4.3: Comparison of various fields from experiment CTRL (dashed) and from observations (solid) along the aircraft track: a) LWC (g m^{-3}); b) droplet concentration (cm^{-3}); c) vertical velocity (m s^{-1}); and c) cloud-base and cloud-top heights (m). For a) and b) the observed values are multiplied by −1. Time along the horizontal axis indicates flight time. Model values are valid at 18 UTC. Shaded areas highlight the level flight segment BC.

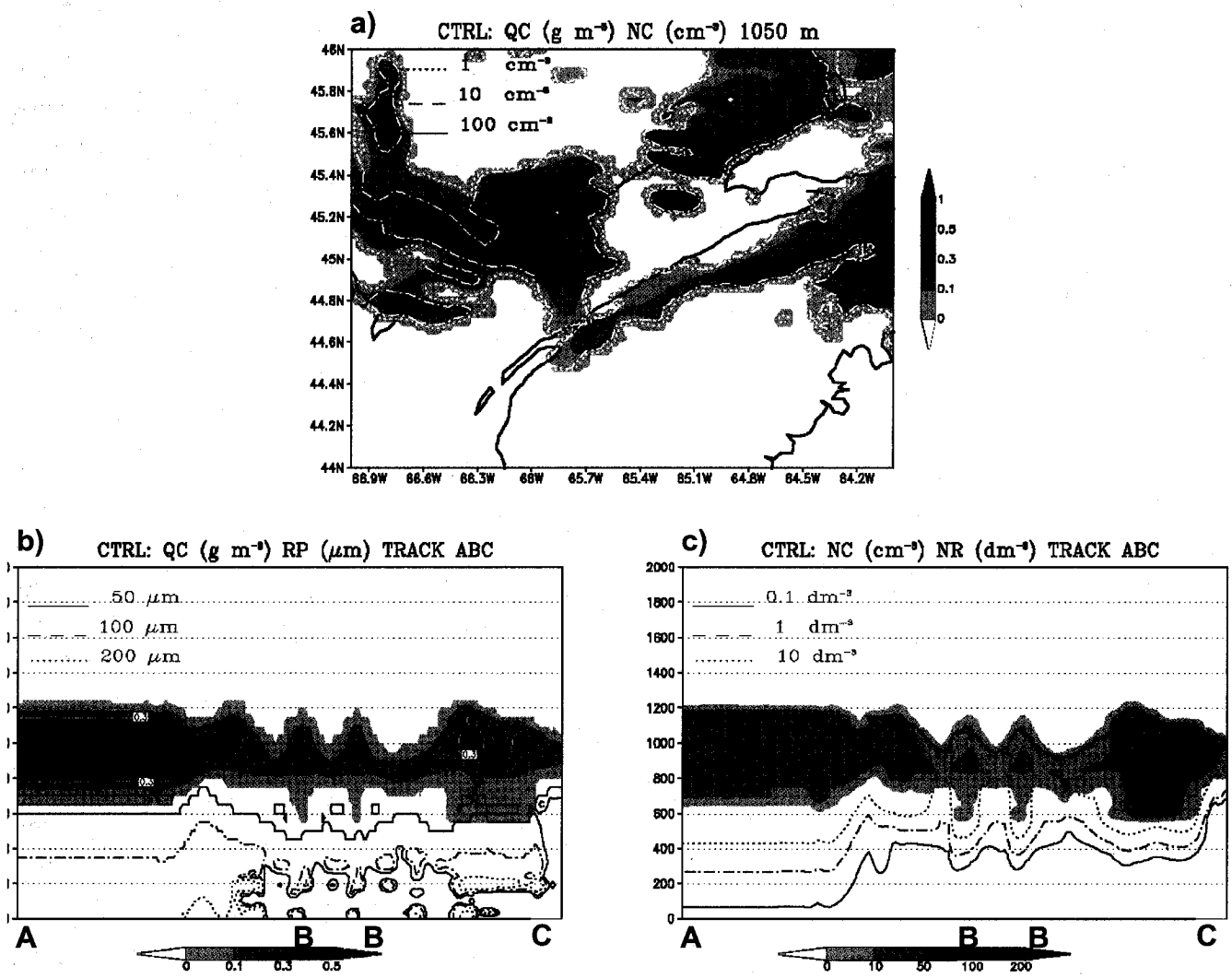

Figure 4.4: Spatial distribution of various cloud field in experiment CTRL. a) Horizontal distribution of LWC (shading; g m^{-3}) and droplet concentration (contours; cm^{-3}) at altitude 1050 m. Vertical distribution of b) LWC (shading; g m^{-3}) and raindrop radius (contours; μm) and c) cloud concentration (shading; cm^{-3}) and raindrop concentration (contours; dm^{-3}). The vertical cross section is taken along track ABC. Panels are valid at 18 UTC.

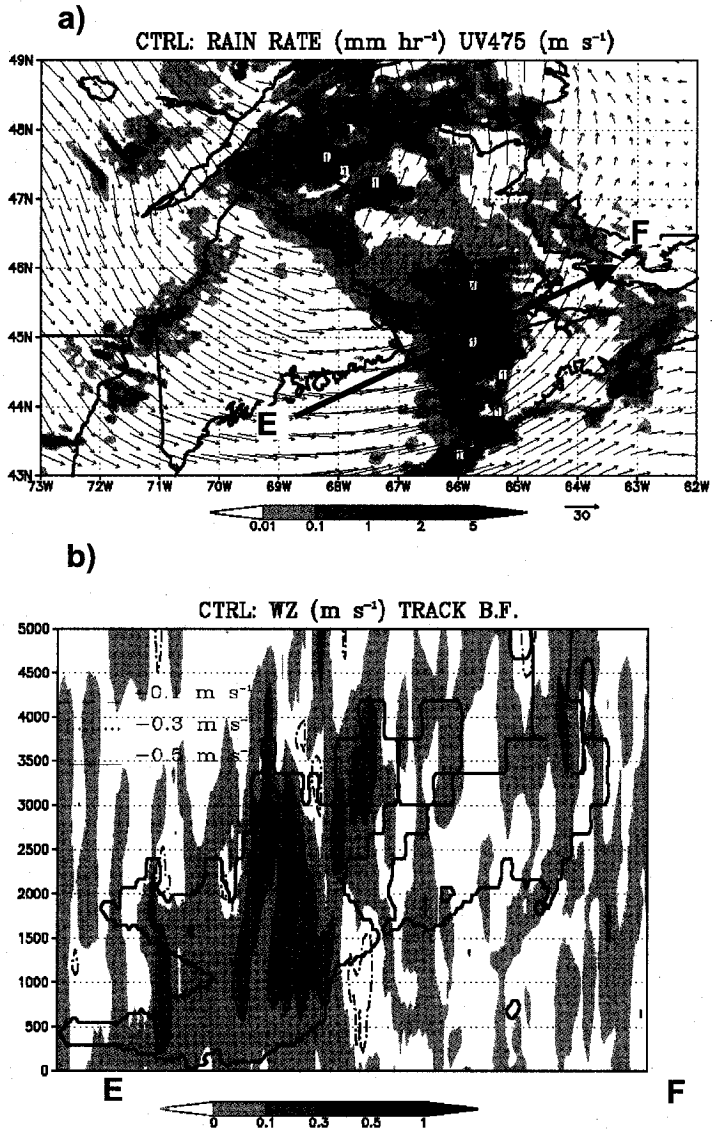

Figure 4.5: Various fields in experiment CTRL: a) horizontal distribution of rain rate (mm hr^{-1}) and horizontal winds; the line EF indicates the vertical cross section in b); b) vertical cross-section of vertical velocity (m s^{-1}; positive values in shading negative in contours) along line EF; solid contour shows the cloud boundary. Panels are valid at 9 UTC.

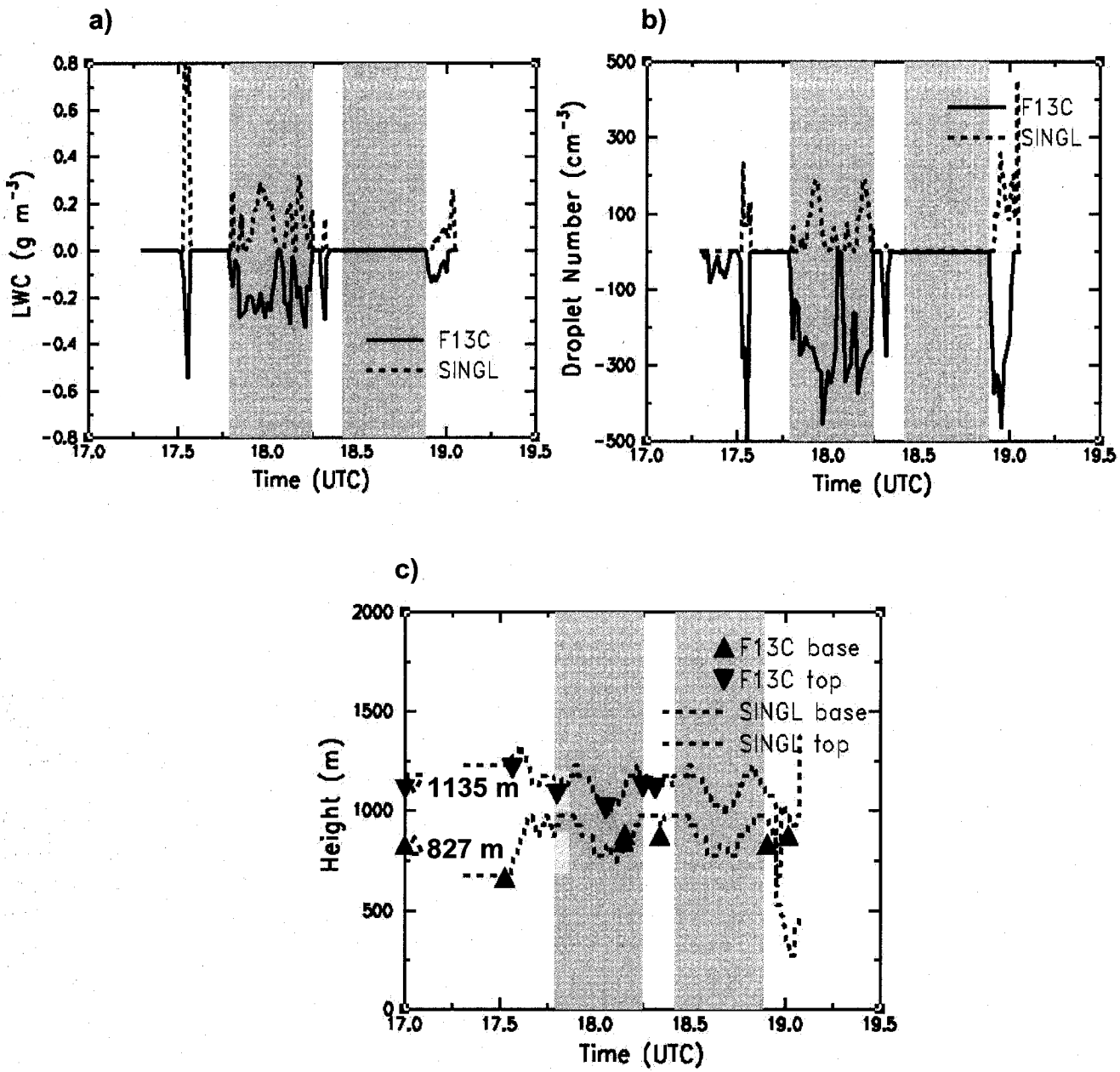

Figure 4.6: Same as: a) Fig.4.3a; b) Fig. 4.3b; c) Fig. 4.3d but for experiment M1.

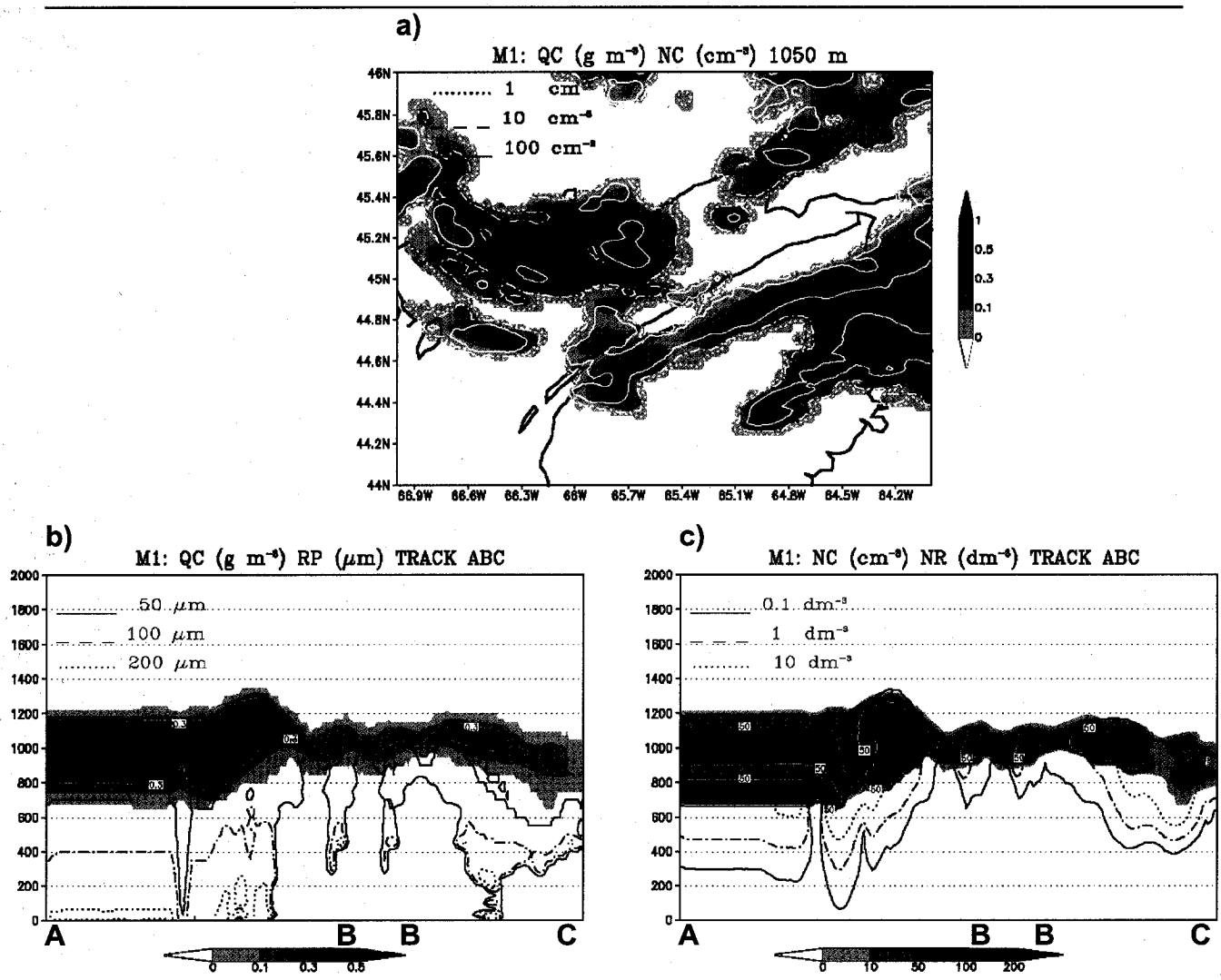

Figure 4.7: Same as Fig. 4.4 but for experiment M1.

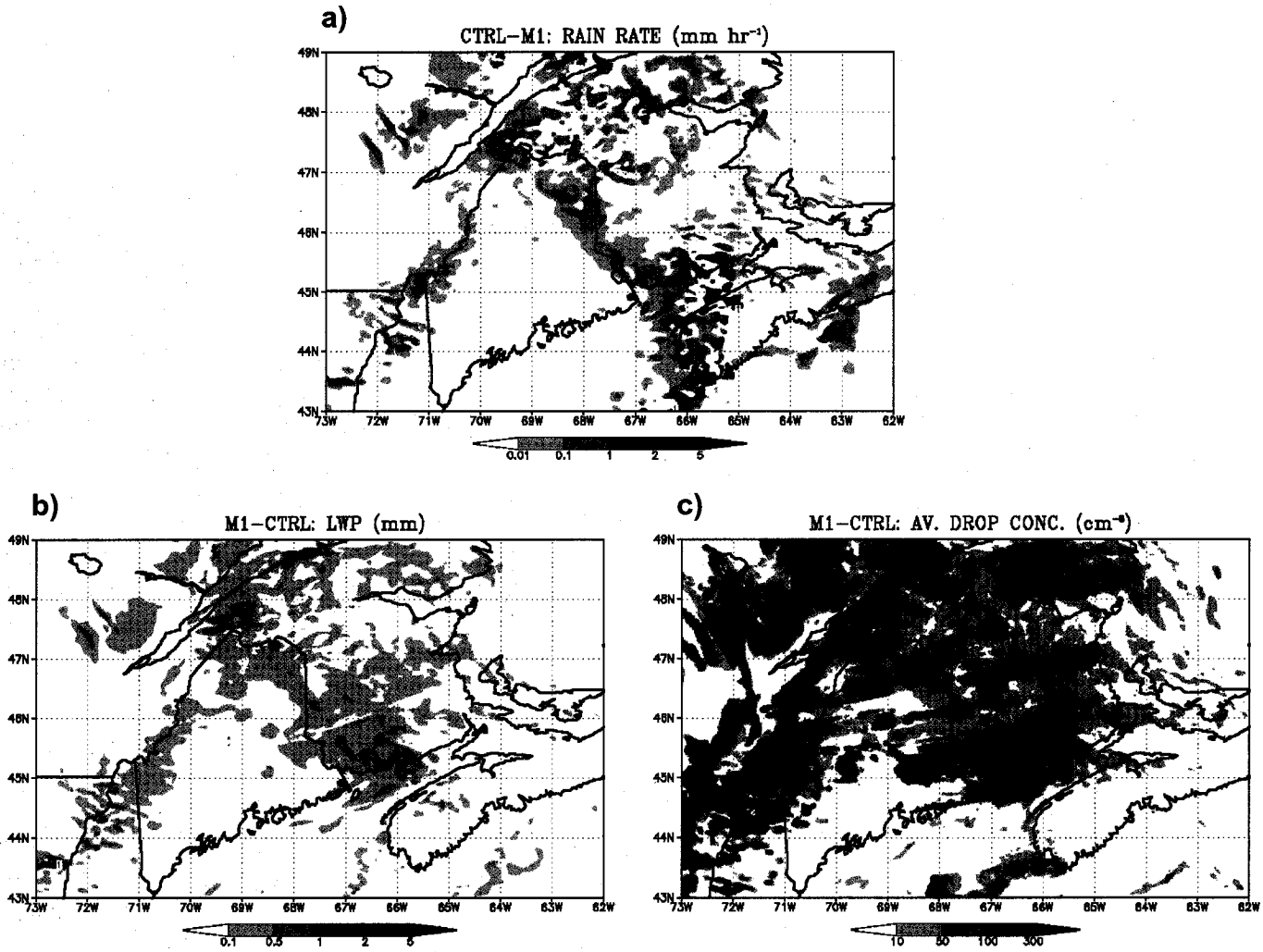

Figure 4.8: Various fields in experiment M1: a) change of rain rate (mm hr^{-1}) relative to experiment CTRL; b) change in LWP (mm) relative to experiment CTRL; and c) change in column-average droplet concentration (cm^{-3}) relative to experiment CTRL. Panels are valid at 9 UTC.

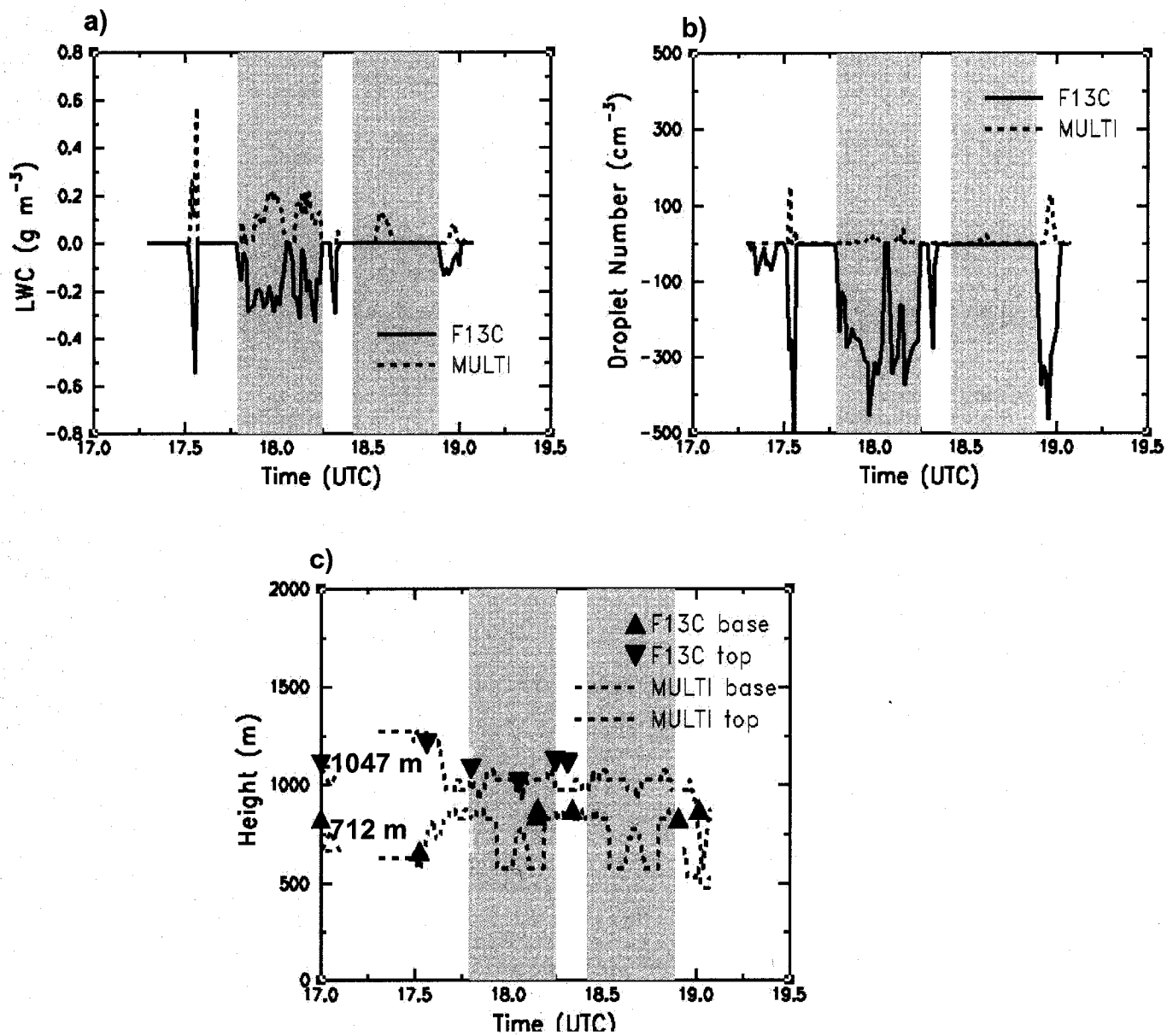

Figure 4.9: Same as: a) Fig.4.3a; b) Fig. 4.3b; and c) Fig. 4.3d but for experiment M2.

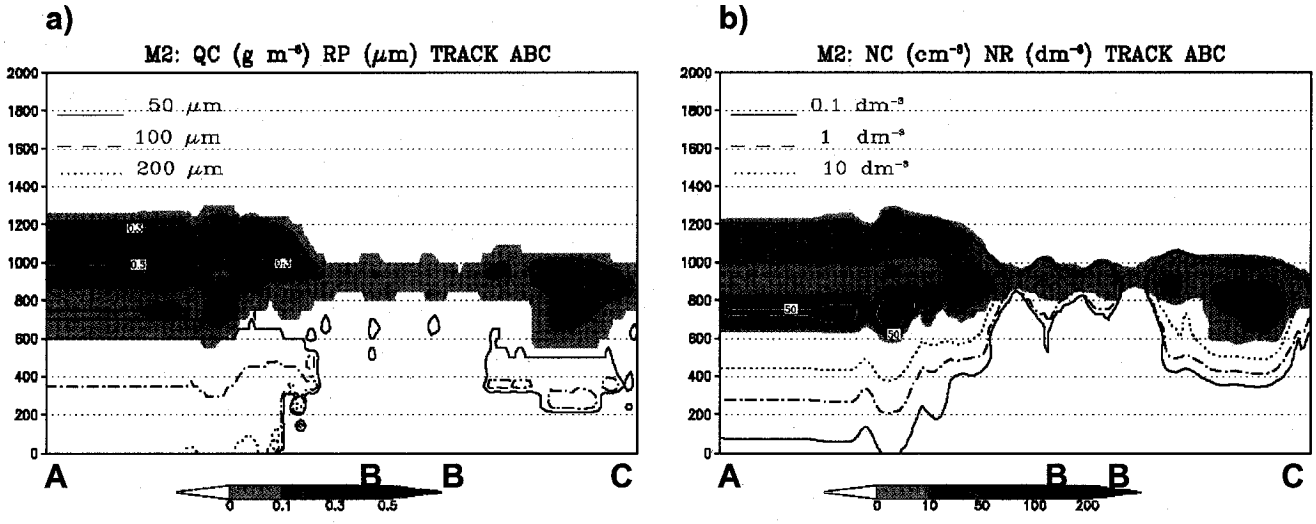

Figure 4.10: Same as: a) Fig. 4.4b; and b) Fig. 4.4c but for experiment M2.

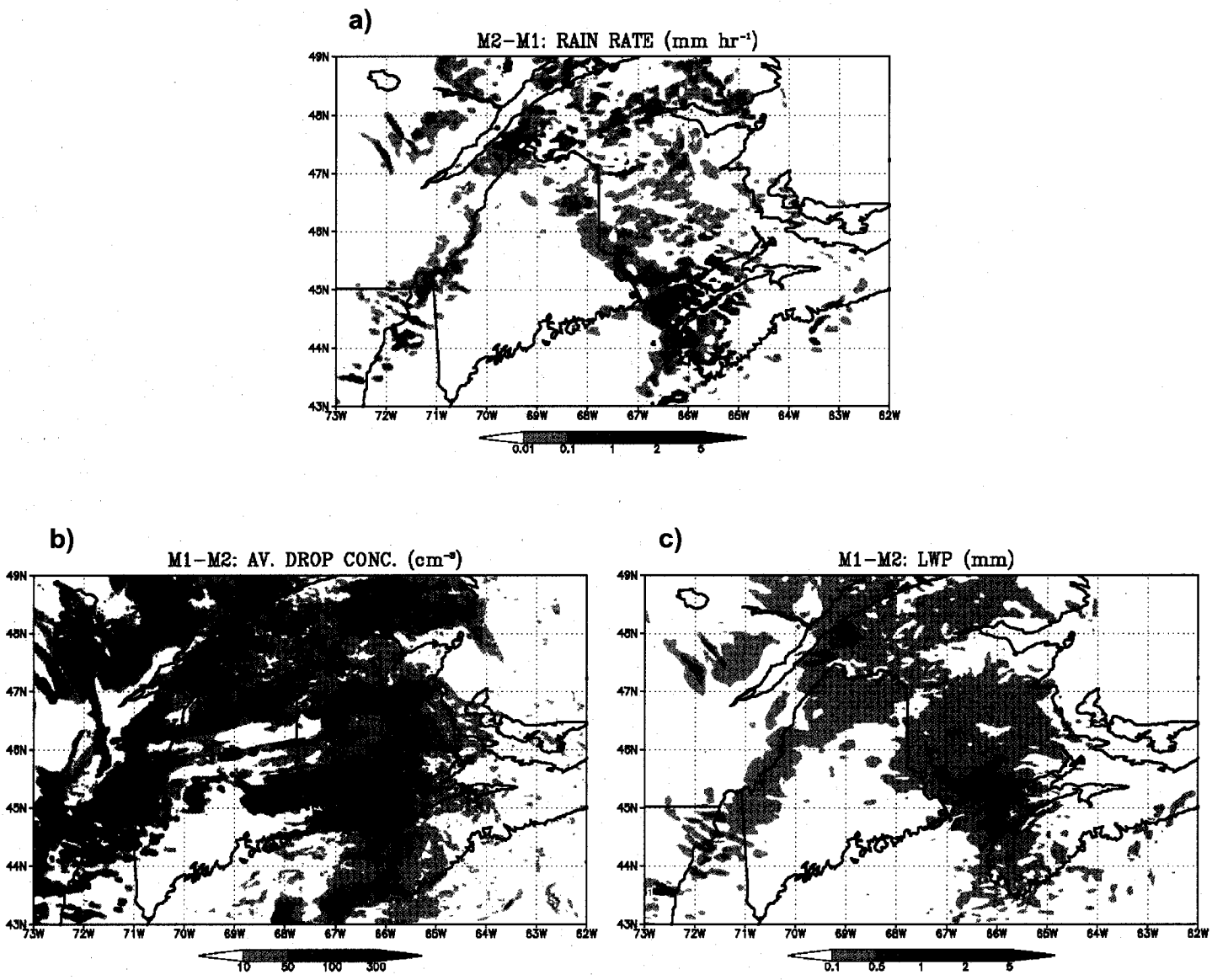

Figure 4.11: Various fields in experiment M2: a) change of rain rate (mm hr^{-1}) relative to experiment M1; b) change in LWP (mm) relative to experiment M1; and c) change in column-average droplet concentration (cm^{-3}) relative to experiment M1. Panels are valid at 9 UTC.

Chapter V

Collision-Coalescence Processing of Aerosol

In a cloud in which no collision-coalescence between drops (interaction between drops) takes place, the number of activated particles is equal to the number of particles emerging after the cloud dissipates. Therefore, the particle distribution remains unchanged. If droplet interactions occur, the activated particles have, after a cloud dissipates, larger radii and their number diminish. This shall be termed cloud processing.

Processing of aerosol by collision and coalescence of drops in the precipitating system is examined with three aims in mind: 1) to establish bounds on the degree of modification of the aerosol spectrum by collision and coalescence of drops; 2) to determine the areas of maximum modification; and 3) to determine the impact on the droplet concentration and precipitation. The analysis is restricted to the experiment with mechanistic activation parameterization and one-modal aerosol (M1) and to two additional experiments, including one processing cycle (S1) and excluding processing (S0). Experiments M1 and S1 were used to determine the extent of processing due to respectively multiple and single nucleation-evaporation processing cycles. Experiment S0 was used to determine the unprocessed spectrum, relative to which the extent of processing in experiments M1 and S1 can be determined. In experiments S0 and S1, since

the regenerated particles do not enter subsequent cloud cycles obviously the clouds are identical.

5.1 Experiments examining collision-coalescence processing

a) Experiment excluding collision-coalescence (S0)

The regenerated aerosol is analyzed after 6, 9 and 12 hours of processing (0900-1500 UTC; Fig. 5.1). It represents the activated particle spectrum that, in this experiment, remains unmodified by drop collision-coalescence. It is characterized by mean radii of up to 60-70 nm and concentrations of up to 300 cm^{-3} at the higher levels; at the lower levels close to the surface larger mean radii are also observed.

Spatially, the regenerated aerosol can be seen in cloud surroundings as well as in cloud interstitial air and with the development of the system it spreads over a substantial area. The main interest if this work is in the processed particles residing outside clouds since these particles can be measured in field experiments and their properties be verified. Nevertheless the processed particles residing in the cloud-interstitial air may be important source of CCN in clouds since they represent an additional source of CCN to that from the background aerosol. As it will be shown in the next section, activation of the regenerated particles can impact the cloud droplet concentration and precipitation in the frontal system. Note, below the cloud lower boundary in the leading edge of the system the signal from the regenerated aerosol is weaker and patchy.

Nucleation in clouds substantially modifies the background aerosol. The particle mean radius of the background aerosol reduces by 10-30 % in cloudy regions (Fig. 5.2).

Thus it can be expected that in cloud-interstitial air the activation of the regenerated aerosol have impact on droplet concentration in the cloud.

The weak signal from the regenerated aerosol below the cloud can be explained, at least partially, by precipitation removal of solute residing in rainwater. In the precipitation-induced downdraft region in the leading edge of the system (similar to Fig. 4.5b) fewer particles get regenerated. To fully explain the diminishing signature of regeneration in the leading edge of the frontal cloud, however, one needs to consider the complex frontal circulation (similar to Fig. 4.5a). The horizontal winds in the rear part of the system are predominantly west southwesterly, while the winds in the leading edge of the system are due north. Note, the analysis was performed along a cross section parallel roughly the winds in the rear part of the system (instead of following a trajectory of an air parcel). Thus some of the particles regenerated in the downdraft might be advected away, thus diminishing the effect of processing in the leading edge of the system. A clearer way of performing the analysis could be perhaps following air parcel trajectories. But for the purposes of the current investigation the simpler analysis was considered satisfactory.

b) Experiment including one cloud cycle (S1)

Processing of activated CCN by drop collision-coalescence in clouds results in two regenerated modes. The first mode forms through drop-to-particle conversion of cloud droplets and the second mode forms through drop-to-particle conversion of large drops. The two modes grow in size through the process of self-collection of cloud droplet and large drop, respectively. The second mode grows further by solute transfer from the cloud droplet to the large drop category through the processes of auto-conversion and

accretion. The first mode is equivalent to the regenerated mode in experiment S0 while the second mode is absent in experiment S0.

After 6, 9 and 12 hours of processing, the drop collision-coalescence increased the particle mean radius of the first regenerated mode of up to few nm (3-5 % change) although increases larger than 5 nm (10 % change) are also not uncommon (Fig. 5.3). The corresponding decreases in particle concentration (also shown in Fig. 5.3) are up to 100-300 cm^{-3} (10-60 % change). The signal of processing from this mode is predominantly seen in the upper part of the cloud and above the cloud. Basically for the same reasons described in the previous section, the signal of processing ahead and below cloud is weak and patchy.

The second regenerated mode, released upon evaporation of large drops, is characterized by a wide range of mean radii (Fig. 5.4). Particles with mean radii of 100-500 nm are resent in concentrations up to 1-5 dm^{-3} and are seen predominantly above the cloud. Particles with mean radii exceeding 1 μm (giant CCN) are present in concentrations smaller than 1 dm^{-3} and are seen predominantly below the cloud. It is noteworthy that particle concentration in this mode is too low to represent a significant source of atmospheric aerosol.

The larger growth of the first regenerated mode in the upper part of the cloud is explained by efficient collision and coalescence of cloud droplets. Transfer of solute due to collection of cloud droplets by large drops explains the larger growth of the second regenerated mode below the cloud.

The presented results imply that the impact of collision-coalescence processing over the course of 6 to 12 hours of processing upon particle radius is highly variable but

nevertheless significant. The obtained increase of the particle mean radius makes the particles better CCN by virtue of their larger size and their significant concentration.

c) Experiment including multiple cloud cycles (M1)

Activation of the regenerated modes in subsequent cloud cycles can be expected to enhance the effect of processing on the particle mean size. In this experiment, in order to evaluate the particle growth due to drop collision-coalescence the analysis needs to be restricted to clear regions only. This is because, in the cloudy regions, activation of the regenerated modes reduces the particle mean radius and can counteracts the increase of the particle mean radius due to multiple processing. For example, in experiment S1, 10-30 % larger values of the particle mean radius and number concentration are observed in cloudy regions (Fig. 5.5). In the cloud surroundings, however, no active sink of aerosol exists. In these regions, the increases in the particle mean radius by multiple cycling can be evaluated.

The analysis shows that the impact of multiple nucleation-evaporation cycles on the particle mean radius is most pronounced above the cloud upper boundary and below the cloud lower boundary, the increase being up to several nm (5 % change) for the first regenerated mode and up to 1 μm (30 % change) for the second regenerated mode (Fig. 5.6). This suggests that multiple nucleation-evaporation cycles lead to measurable increase of the particle mean size.

d) Impact of cloud processing on droplet concentration and precipitation (M2)

The activation of the processed aerosol in experiment M2 in addition to the activation of the background aerosol exerted measurable effect of the precipitating system through the effect on droplet concentration. Activation of the regenerated modes leads to increases of droplet concentration by up to 100 cm^{-3} and associated increases of LWC by up to 0.5 g m^{-3} (Fig. 5.7a). The resultant reduction of the precipitation intensity was by up to 0.1 mm hr^{-1} (equivalent reduction in the daily accumulation was by < 0.1 mm) and was observed only in the less vigorous (upstream) part of the system (Fig. 5.7b). The area of maximum precipitation (downstream) remained unaffected by the processing. Thus a spatially non-uniform signal is observed. The precipitation in the more vigorous part of the system was less susceptible to changes in the aerosol due to cloud processing while the precipitation in the less vigorous part of the system was more susceptible to the aerosol changes.

5.2 Discussion

Experiments aimed towards explaining the role of collision-coalescence in clouds revealed: the magnitude of the impact, the areas of maximum impact, and the subsequent effects on droplet concentration and precipitation.

a) Impact on particle size

The magnitude of the impact upon particle radius of 9-12 hours of collision-coalescence processing in frontal clouds associated with small amount of precipitation (1-2 mm) is highly variable but nevertheless significant. The conditions considered were those of high CCN concentrations (N_{CCN} = 1200 cm^{-3}, $\bar{r}_{CCN}$ = 0.05 μm, σ_{CCN} =1.7; valid

at cloud base). One cycle of physical processing increased particle mean radius of the first regenerated mode by up to 10 %; multiple cycles lead to an additional increase of less than 5 %.

Previous work had focused predominantly on studying the effect of droplet collision-coalescence in stratocumulus clouds with or without occurrence of drizzle (e.g. Feingold et al., 1996a; Feingold and Kreidenweis, 2000, 2002). For non-drizzling stratocumuli (LWC 0.1-0.5 g m^{-3}) and low particle concentrations (N_{CCN}= 50 cm^{-3}; $\bar{r}_{CCN}$ = 0.08 μm; σ_{CCN} =1.8) the impact of physical processing upon particle mean radius over the course of 1 hour of processing was highly variable from negligible to on the order of 10 % change (Feingold et al., 1996a). For drizzling stratocumuli (LWP= 200 g m^{-2}) and wide range of particle concentrations (N_{CCN}= 50-200 cm^{-3}, $\bar{r}_{CCN}$ = 0.05-0.1 μm, and, σ_{CCN} =1.8-1.5) the combined impact of physical and aqueous-chemistry processing upon particle mean radius was much larger, between 30-90 % (Feingold and Kreidenweis, 2002). Despite the variability of the conditions for processing and processing mechanisms considered by previous studies, our results are not inconsistent with these studies.

b) Area of maximum impact

The areas of the maximum impact upon particle mean radius reveal a rather complex signal of processing in and around the frontal cloud. The circulation across the front, characterized by shift of the horizontal wind and vertical wind shear, leaves a stronger signal above the cloud upper boundary dominated by the first regenerated mode and a weaker signal below the cloud lower boundary dominated by the second regenerated mode. Previous studies of aerosol processing in cumuli, stratocumuli, and

hill-cap clouds typically consider a simple airflow and find the maximum signal directly below the cloud and downwind of the cloud (e.g. Tremblay and Leighton, 1986; Bower and Choularton, 1993; Feingold and Kreidenweis, 2002).

c) Impacts on droplet concentrations and precipitation

The subsequent impact of aerosol processing on droplet concentration and precipitation in the frontal system suggested a spatially non-uniform response. The precipitation in the less vigorous (upstream) part of the system was suppressed by the activation of the regenerated modes while the maximum precipitation (downstream) remained unaffected. The following scenario can be identified in the upstream part of the system: drop collision-coalescence increases the particle mean radius; the processed particles grow beyond the critical size for activation and increase the number of cloud droplets; the water in the cloud is distributed amongst more numerous but smaller drops thus suppressing the conversion to rain. In this scenario, the increase in the particle size due to physical processing is *not* sufficient to generate a significant number of giant CCN and initiate stronger collection. In the more vigorous part of the system, the increase in droplet concentration is not sufficient to shut down the rain conversion process. Previous studies examined the impact of aerosol processing on droplet concentration in drizzling stratocumuli (Feingold and Kreidenweis, 2000, 2002). These studies concluded that both enhancement and suppression of droplet concentration by cloud processing might occur depending on the input CCN spectrum and the updraft velocities in the cloud. Enhancement of droplet concentration occurred at lower updraft velocities (< 1 m s^{-1}), with the enhancement being more pronounced for CCN spectra with small mean radii, and reduction of droplets concentration occurred at large updraft velocities (> 1 m s^{-1})

(Feingold and Kreidenweis, 2000). The enhancement of droplet concentration obtained in the present study is consistent with the previous findings for low updraft velocities and small mean radii of the processed CCN spectrum. Furthermore, the previous studies concluded that the processed aerosol may or may not affect drizzle depending on the initial CCN spectrum being processed (Feingold and Kredenweis, 2002). The processed aerosol did not affect drizzle for an initial CCN spectrum of relatively low concentrations (< 100 cm^{-3}) when the collection process was quite efficient. The processed aerosol affected drizzle for an initial CCN spectrum of intermediate concentrations (> 150 cm^{-3}); drizzle enhancement is observed at relatively small mean radii (0.05 μm) and drizzle suppression at relatively large mean radii (0.1 μm). Our results support these findings for intermediate CCN concentrations but a more definitive comparison is difficult to make due to differences in the cloud systems considered.

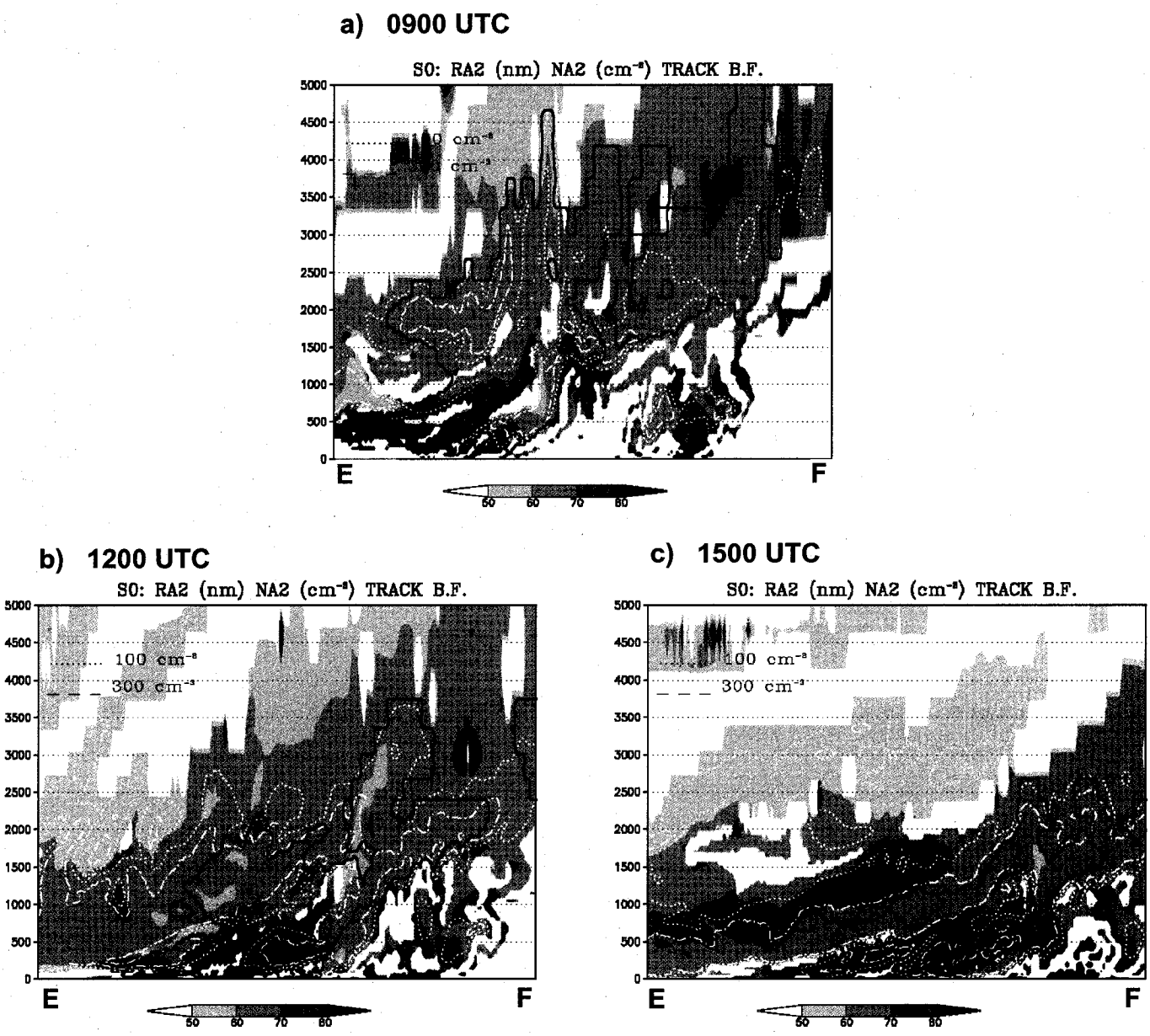

Figure 5.1: Geometric mean radius (nm) (in terms of number) in shading and total number concentration (cm^{-3}) in contours of first processed mode in experiment S0. Panels are valid at: a) 0900 UTC, b) 1200 UTC, and c) 1500 UTC. Solid contour shows the cloud boundary. The cross section is taken along line EF.

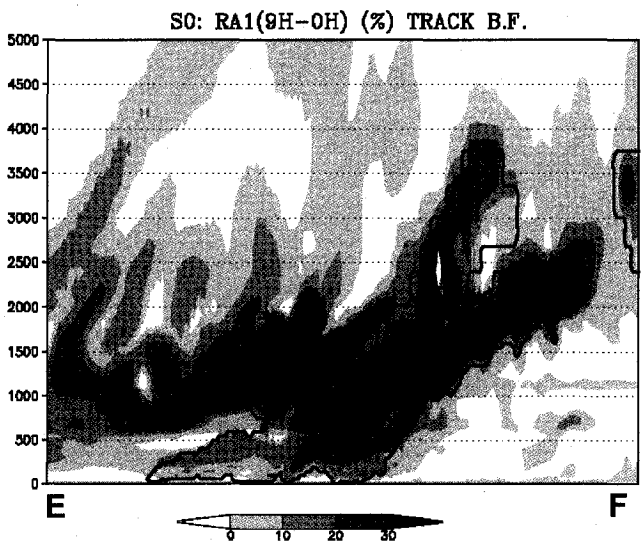

Figure 5.2: Reduction (%) in the geometric mean radius (in terms of number) in shading of the background aerosol mode in experiment S0. Panel is valid at 1200 UTC. Solid contour shows the cloud boundary. The cross section is taken along line EF.

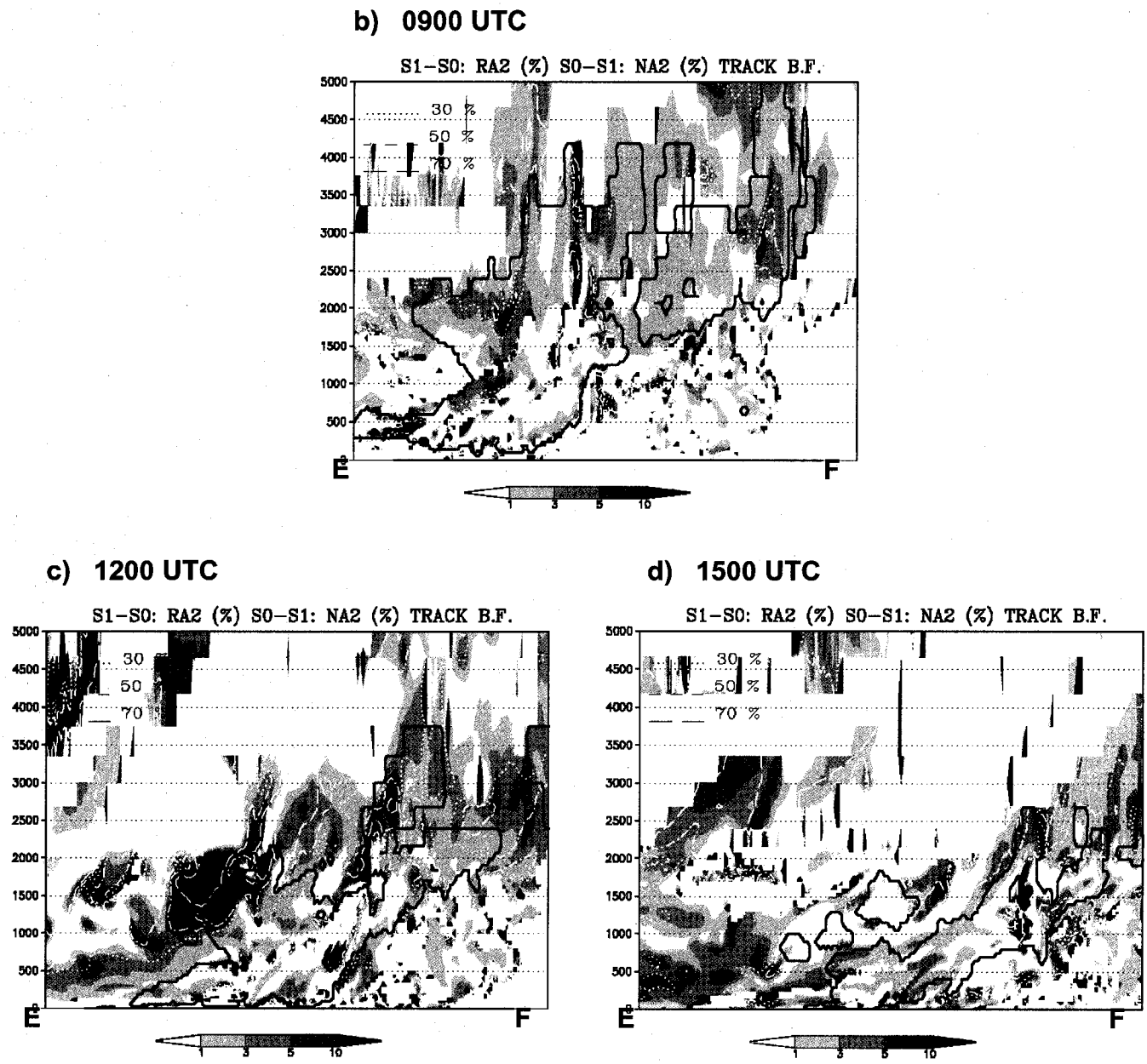

Figure 5.3: Change (%) in geometric mean radius (in terms of number; in shading) in experiment S1 relative to S0 and in total number concentration (in contours) in experiment S0 relative to S1 of the first regenerated mode. Panels are valid at: a) 0900 UTC; b) 1200 UTC; and c) 1500 UTC. Solid contour shows the cloud boundary. The cross section is taken along line EF.

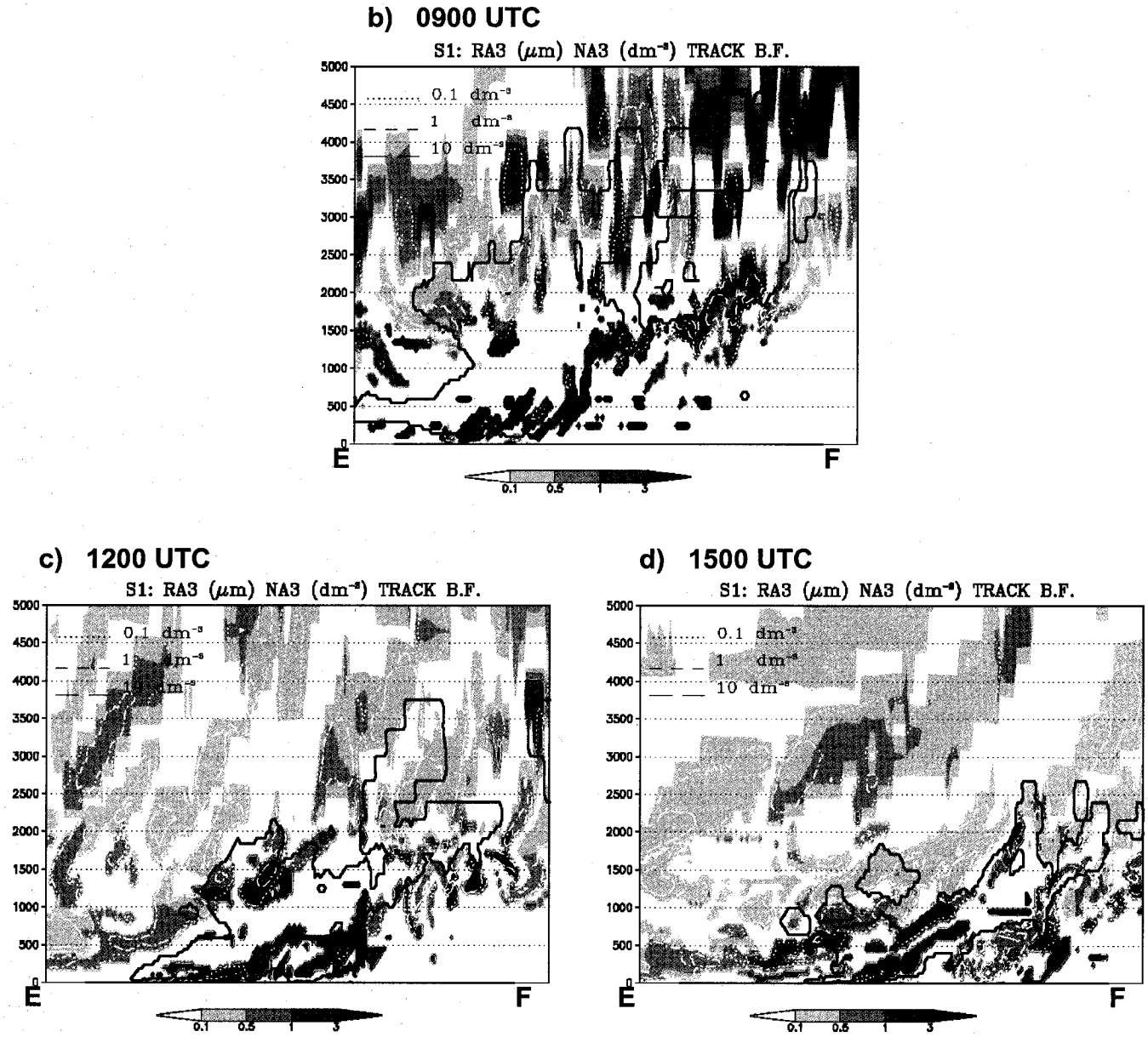

Figure 5.4: Geometric mean radius (in terms of number; μm; in shading) and total number concentration (dm^{-3}; in contours) of the second regenerated modes in experiment S1. Panels are at: a) 0900 UTC, b) 1200 UTC, and c) 1500 UTC. Solid line shows the cloud boundary. The cross section is taken along line EF.

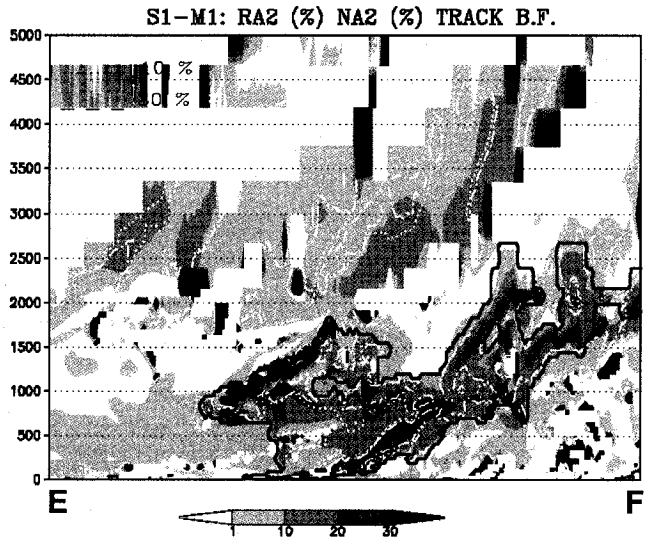

Figure 5.5: Changes (%) of geometric mean radius (in terms of number) in shading and number concentration in contours of the first regenerated mode in experiment S1 relative to M1. Panel is valid at 1500 UTC. Solid contour shows the cloud boundary. The cross section is taken along line EF.

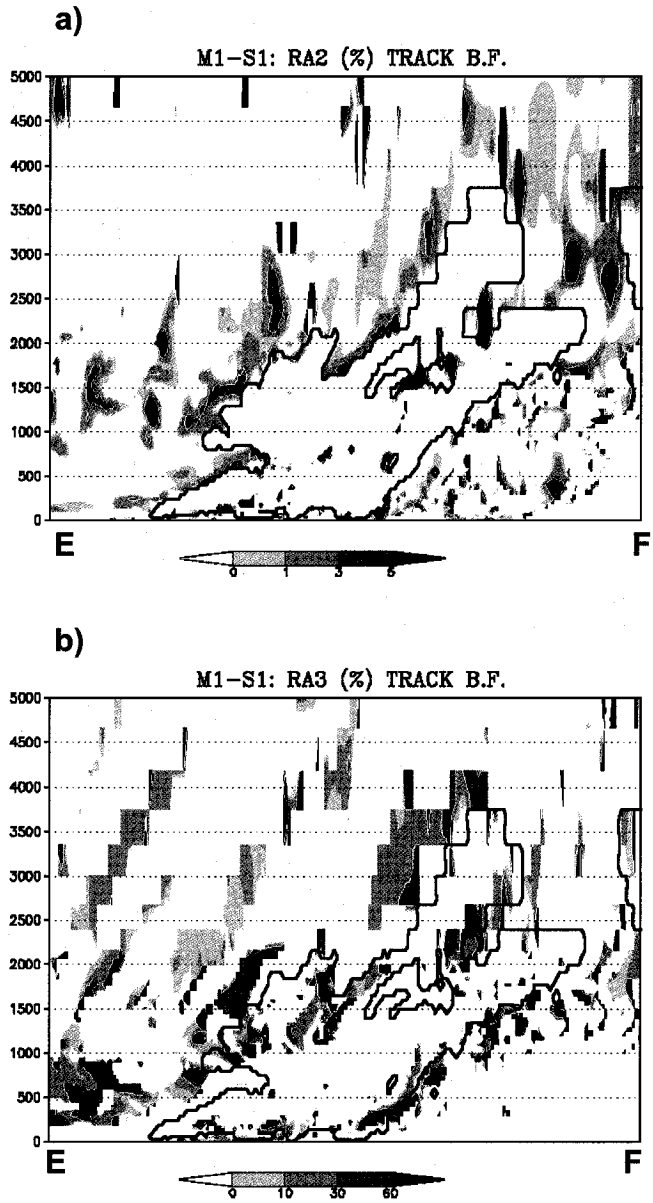

Figure 5.6: Changes (%) in geometric mean radius (in terms of number) of a) first and b) second regenerated modes in experiment M1 relative to S1. Panels are valid at 1200 UTC. Solid contour shows the cloud boundary. The cross section is taken along line EF.

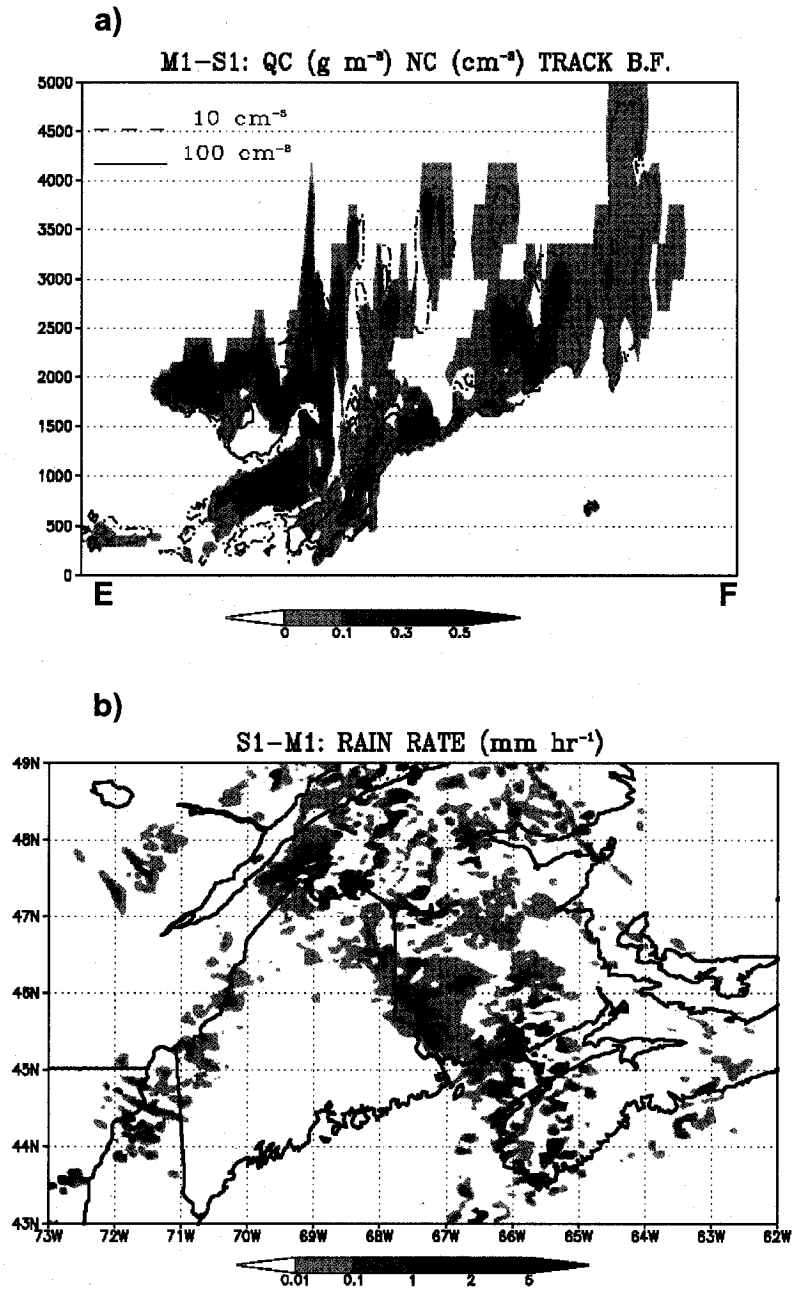

Figure 5.7: a) Changes in cloud LWC (g m^{-3}; in shading) and droplet concentration (cm^{-3}; in contours) in experiment M1 relative to S1. The cross section is taken along line EF. b) Changes in precipitation rate (mm hr^{-1}; in shading) in experiment S1 relative to M1. Panels are valid at 0900 UTC.

Chapter VI

Aqueous-Chemistry Processing of Aerosol

In the subsequent analysis the combined effect on the particle spectrum of collision-coalescence and aqueous-chemistry processing in non-drizzling stratocumulus cloud is examined. The aims are two-fold: 1) to evaluate the relative contributions of the two processing mechanisms and determine the areas of maximum impact; and 2) to evaluate the role of the collection efficiency on the extent of collision-coalescence processing. The latter is achieved through comparison of the stratocumulus case with the frontal case (Chapter V) exhibiting respectively negligible and significant drop collection.

The analysis is limited to experiments with mechanistic activation and one-modal aerosol. The first experiment (S0) excludes processing. Only activation, condensation and evaporation impact the particle spectrum in this experiment. Under such conditions, there should be no processing of CCN so that the ideal scheme would exactly regenerate the initial CCN spectrum that entered the cloud. The second experiment (S1) includes collision-coalescence processing. The last experiment (SO1) includes collision-coalescence and aqueous-chemistry processing with H_2O_2 acting as oxidant. The experiments including processing consider one nucleation-evaporation cycle. Obviously, all experiments have identical clouds.

6.1 Experiments examining collision-coalescence and aqueous-chemistry processing

a) Experiment excluding collision-coalescence (S0)

1) STRATOCUMULUS CLOUD DISTRIBUTION

The stratocumulus cloud begins to form at around 1500 UTC downwind (to the south) of Lake Erie over western New York State, by 1800 UTC the cloud covered almost the entire southern coast of Lake Erie; this time period can be considered cloud incipient stage. The cloud persists over the next 6 hours, which can be considered cloud mature stage. At 2400 UTC, an isolated cloud cell produced light drizzle. During the cloud incipient stage Lake Erie remains, for most part, cloud free.

Figure 6.1a shows the cloud LWP at 1800 UTC (12 hr integration). At 1800 UTC, the spatial distribution of cloud LWP resembles qualitatively the cloud on the satellite image (1815 UTC; see Fig. 2.9). In particular, the horizontal extent of the cloud off (south of) Lake Erie is qualitatively similar; the cloud-free region over Lake Erie as well as the extensive cloudiness over southern Ontario (to the northeast) is also very similar. During the examined period the low-level horizontal winds over the domain of interest remain approximately steady with a southeasterly direction. Occurrence of stratocumulus cloud with standing forcing (lake-land contrast) in a steady airflow represents a relatively simple synoptic situation in which the effect of processing can be expected downstream of the processing cloud and should be easily identifiable.

A vertical cross section through the cloud following roughly the low level winds, labeled as CD (approximately 506 km in length; see Fig. 6.1a), shows the distribution of

the updraft velocity in the cloud (Fig. 6.1b). Droplet evaporation is likely to occur in downdraft regions, thus strong signal from processing can be expected in these regions.

Figures 6.2 and 6.3 show the evolution of various cloud fields along cross-section CD, noting several characteristic features. The cloud vertical extent is highly variable. On average, the cloud base ranges from 1200 m to 1500 m and the cloud top from 2200 m to 2700 m. The range of cloud LWC is 0.1-0.5 g m^{-3}, representing typical values for stratocumulus cloud decks. The cloud is non-drizzling during most of its lifetime though some amount of water resides in large drops. The mean radii in the large drops reach drizzle size (100 μm) only in very confined areas in the lowest cloud levels. At 2400 UTC, when an isolated cloud cell produces light drizzle, drizzle-size drops can be seen reaching the ground without evaporating. Due to light drizzle, a small amount of solute dissolved in large drops can be expected to be removed from the system by wet deposition. Cloud droplet concentrations and the concentrations of large drops (Fig. 6.3) reach several hundred per cm^{-3} and 100 per dm^{-3}, respectively. In summary, the simulated cloud water amount, drop size, and drop concentration are in the typical range for stratocumulus cloud decks thus providing a realistic framework for investigation of cloud processing of CCN.

2) REGENERATED CCN SPECTRUM

Figure 6.4 shows the distribution of the parameters of the background mode at 21 UTC. With cloud formation, nucleation scavenging, which is the only process affecting the background mode, depletes the background mode in large particles. The total particle concentration is noticeably reduced (40-60 % change). More importantly, the particle mean radius is substantially reduced (10-30 %) due to the preferred activation of the

large-size tail of the particle spectrum. Thus nucleation scavenging in clouds depletes the cloud-interstitial aerosol in number concentration and in mean radius compared to the particles in the cloud surroundings.

Experiment S0, which omits the effect of physical processing on CCN spectrum, regenerates the initial CCN spectrum that enters the cloud (first regenerated mode). Since no conversion of solute to large drops occurs, the second regenerated mode is missing in this experiment. As shown in Figure 6.5, the total number concentration of the first regenerated mode varies between 100-2000 cm^{-3} and the mean radius between 50-80 nm. Since the particles in the large-size tail of the distribution activate at lower supersaturations, the particle mean radius of this mode is larger than that of the initial radius of the background mode (44 nm). Finally, note that during the cloud incipient stage the signal of CCN regeneration in the sub-cloud air is very strong, while during the cloud mature stage, when light drizzle is observed at the ground, the effect of particle regeneration is more modest – at this time the signal of particle regeneration left at the incipient stage is advected downstream.

b) *Experiment including collision-coalescence processing (S1)*

The experiment discussed here includes the effect of drop collision-coalescence on the CCN spectrum. Drop collision-coalescence reduces the total CCN concentration without affecting the total mass, hence upon droplet evaporation the released particles should have smaller total concentration and larger mean size than the unprocessed spectrum. The first and the second regenerated modes, formed respectively as a result of cloud droplet and large drop evaporation, are both affected by this process. The first

mode is affected by cloud self-collection. The second mode is affected by cloud autoconversion, accretion of cloud droplets by large drops, and large-drop self-collection. The autoconversion and accretion processes affect both the mass and the number concentration of cloud droplets and large drops, while self-collection affects only the drop number concentration. It is useful to examine the partitioning of the solute dissolved in water between the two categories of drops (Fig. 6.6). Solute in cloud droplets dominates the total solute with mass density 0.1-5 $\mu g\ m^{-3}$. Solute in large drops is non-negligible but has a much smaller density on the order of less than 0.1 $\mu g\ m^{-3}$. Thus since the bulk mass of solute resides in cloud droplets, the main impact of processing can be expected to be associated with particles regenerated from cloud droplets.

The extent of processing is determined by the differences of the first regenerated mode in experiments S1 and S0 (Fig. 6.7). Decrease in particle concentration is shown by the difference $S0 - S1$ and increase in particle mean radius (in terms of number) is shown by the difference $S1 - S0$. The magnitude of processing of the first regenerated mode typically amounts to a 100-300 cm^{-3} decrease (10-30 % change) of particle concentration accompanied by up to a 3-5 nm increase (3-5 % change) of particle mean radius. The extent of the processing on the second regenerated mode reveals similarly small effects (Fig. 6.8). Although large drop evaporation resulted in fairly large particles, mean radii of 200-700 nm (giant CCN), the particle concentrations of this mode are relatively modest, ~0.1 cm^{-3}, three orders of magnitude smaller than the concentrations of the first regenerated mode (100-1000 cm^{-3}). Thus the second regenerated mode is insignificant source of atmospheric CCN.

The conditions for occurrence of the stratocumulus cloud on the coast of Lake Erie, namely standing forcing (water-land contrast) and steady northwesterly airflow, provide a relatively simple synoptic situation. In such situation, the impact of processing is seen in the sub-cloud air during the cloud's incipient stage and downwind of the cloud during the cloud's mature stage. A careful examination of the spatial distribution of the aerosol spectrum changes during the cloud evolution reveals the contributions of the two regeneration mechanisms. Cloud droplet evaporation is more efficient source of processed particles (first regenerated mode; Fig. 6.7) during the incipient stage of the cloud and relatively inefficient during the cloud mature stage. Large drop evaporation appears to be equally efficient source of processed particles (second regenerated mode; Fig. 6.8) during the entire cloud lifecycle.

The spatial extent of the physical processing varies in the horizontal with the position below cloud and in vertical (Fig. 6.7 and 6.8). In the horizontal, it is collocated, as expected, with the downdraft regions (Fig. 6.1b), which favor droplet evaporation. In the vertical, the higher levels (close to cloud base) are dominated by the first regenerated mode while the lower levels (close to the surface) are dominated by the second regenerated mode.

c) Experiment including collision-coalescence and aqueous-chemistry processing (SO1)

We now consider the combined microphysical and chemical effects, including gas-aqueous phase exchange and $S(IV)$ oxidation reaction, on the CCN spectrum. The total (gas-phase + dissolved) concentrations of trace gas species and pH of cloud water

are shown for a selected time in Figure 6.9. A few points are worth mentioning. The concentrations of SO_2 and NH_3 remain undepleted (at all times) while H_2O_2 concentration is being practically depleted. Of course NH_3 is not directly affected by the oxidation but by dissolution in water to produce $(NH_4)_2SO_4$ from $S(VI)$ upon particle regeneration. NH_3 is the most important alkaline compound commonly found in the atmosphere and has a critical influence on the pH of the cloud drops. The pH of cloud water ranges from 4 to 5.5, which represents a moderately acidic situation. Besides dissolution of the gases, the pH is influenced by dissolution of $(NH_4)_2SO_4$ from particles entering the cloud as CCN. Thus in the current system the $S(VI)$ production rate is determined by the amount of dissolved $S(IV)$ in the system and is limited by the availability of H_2O_2 acting as oxidant.

Providing the water mixing ratio exceeds 1×10^{-6} g g^{-1}, the chemistry module is able to model the scavenging of gases by the cloud in an attempt to attain equilibrium and charge neutrality. It can be shown that for a characteristic atmospheric LWC of 1 g m^{-3} the partition of SO_2 between the liquid and the gas phases changes appreciably over the cloud pH range. For acidic solution SO_2 is present predominantly in the gas phase and for more basic solution mostly in the aqueous phase, while H_2O_2 is partitioned almost equally between the aqueous and gaseous phases, independent of pH. Both NH_3 and HNO_3 are present essentially entirely in solution for the pH range of interest here, while O_3 (if present) and CO_2 primarily remain in the gas phase. Following the scavenging of gases the chemistry module calculates the conversion of $S(IV)$ to $S(VI)$ within clouds.

Of interest for this study is the partitioning of solute dissolved in aqueous phase from oxidation and from nucleation. The concentration of *S(VI)* ranges in the limits 0.1-1 μg m^{-3} (Fig. 6.9c) and thus is second in magnitude after the concentration of solute entering the cloud via nucleation (0.1-5 μg m^{-3}, Fig. 6.6) and greater than the concentration of solute dissolved in large drops (on the order of less than 0.1 μg m^{-3}; Fig. 6.6). Unlike solute from nucleation, which generally reaches its maximum in the lower half of the cloud, the concentration of *S(VI)* from oxidation is relatively uniform with height. Thus the material added by oxidation to that already contained within droplets can be expected to have a non-negligible effect on the particles emerging from the processing cloud.

Although only one chemical scenario has been explored, which effectively sets the extent of the chemical processing, still useful conclusions can be deduced about the impact of the processing via the aqueous chemistry pathway on the particle mean size. The results indicate a substantial increase of the mean size of the first regenerated mode by the addition of soluble material due to oxidation (Fig. 6.10). Increases of particle mean radius due to aqueous chemistry of up to 2-3 nm (3-5 % change) from that due to collision-coalescence are observed. These increases of particles radius are comparable to the increases due to collision-coalescence acting alone. However small these increases may seem, it should be emphasized that they apply only to the large-end tail of the particle spectrum, beyond the critical radius for activation. Upon subsequent activation in clouds these particles, as large as 80-90 nm in radius, would activate at much lower supersaturations. During cloud evolution, more pronounced increases are observed in the cloud incipient stage when the vertical velocities in cloud are relatively stronger and the

supply of fresh oxidant (H_2O_2) due to large-scale advection is plentiful. Otherwise, generally after less than 1 hr development oxidation depletes the oxidant completely. The earlier stages of the simulation might also be applicable to conditions of fresh emission of pollutants and oxidants, a process neglected in this study, where aqueous chemistry would dominate particle growth. Another factor to be considered during the cloud incipient stage is collection, which has not yet been able to reduce drop concentrations significantly. During the cloud mature stage, once significant collection rates are established, the particle growth is dominated by physical processing.

Examining the spatial extents of the modifications of the aerosol spectrum by physical and chemical processing reveals the following. The regions of the largest increases of particle radius by physical processing vary in the horizontal with the position below cloud base. In the vertical, the modifications of the particle spectrum in the sub-cloud layer extend all the way to the ground with the upper levels (just below cloud base) being dominated mostly by modifications of the particles in the first processed mode while the lower levels (close to the ground) being dominated by modifications of the particles in the second processed mode. The modifications of the particle spectrum by chemical processing, generally speaking, cover wider areas in the horizontal. In the vertical, larger increases in particle radius are observed in the sub-cloud air close to cloud base and more modest increases close to the ground. The second processed mode in the present study is not affected by chemical processing.

Initial conditions similar to those in the current chemistry run, excepting the concentration of O_3 which has not been set to zero, have been shown by Bower and Choularton (1993) to produce the largest modifications of the CCN spectrum compared

to other runs with varied chemistry input. The authors showed that these conditions were most suitable to the generation of the largest amount of $S(VI)$. In particular, the large amount of SO_2 (5 ppbv) present initially was available for oxidation by 1 ppbv of H_2O_2. The availability of 1 ppbv of NH_3 helps to neutralize the acidity of the solution and aids the solubility and dissociation of SO_2 and its conversion to $S(VI)$. Although in the present chemistry run the O_3 reaction was disabled, at the level of acidity present, the conversion will be dominated by the H_2O_2 reaction (Bower et al., 1991). Thus other chemistry input, less optimal for generation of large amounts of sulfate, can be expected to produce a smaller degree of modification of the particle spectrum.

The obtained increase in the particle radius resulted from one cloud cycle. Evaluating the combined microphysical and chemical impacts on the particle spectrum, as it is being continuously recycled in the cloud, would be useful in a study examining the effect of processing on droplet concentration and precipitation. For the purposes of this study, however, activation of the processed particles would change the cloud morphology and would complicate the analysis.

6.2 Discussion

a) *Relative contribution of collision-coalescence and aqueous-chemistry processing*

Although the results presented in the current study consider a limited set of conditions that may exist in the atmosphere for physical and chemical processing, the study is useful in that it places bounds on the degree to which a persistent stratocumulus cloud layer impacts the particle spectrum. Both, collision-coalescence and aqueous-

chemistry processing occur simultaneously. The effect of the former, as shown here, is a decrease in CCN concentration without change in CCN mass and the effect of the latter is production of additional soluble material in drops by aqueous-phase sulfur oxidation without change in CCN number. Both mechanisms together result in a bi-modal distribution downwind of the processing cloud. The impact on the particle mean radius of collision-coalescence processing is as substantial as that resulting from aqueous-chemistry processing and amounts to a 3-5 % increase.

The mean radius of the particle mode regenerated from cloud droplet evaporation, resulting from the combined effects of physical and chemical processing, reached on average up to 0.08-0.09 μm although values as large as 0.1 μm were also present. This is in reasonably good agreement with the processed particle radii suggested by field observations. The mean radius of the processed mode in observed aerosol spectra, believed to be created by the addition of sulfate mass from aqueous-phase oxidation, usually resides at a radius of about 0.1-0.2 μm (Hoppel et al., 1990).

Processes omitted in the present study can at least in part, explain the underestimation of the processed particle mean radius by the model. These include but are not limited to: fresh emissions of gas species and oxidants and the bulk representation of aerosol, microphysics, and chemistry. Emission of oxidants can potentially impact the obtained results since depletion of H_2O_2 practically shuts down the processing in less than 1 hr. The adopted bulk method for aerosol, microphysics, and chemistry is based on the underlying assumption of uniform $(NH_4)_2SO_4$ chemical composition of drops. Chemical heterogeneity among drops leads to differential chemical conversion in smaller and larger drops, as suggested by studies resolving the aerosol and droplet spectra. The

pH variability among different-size drops tends to enhance the sulfur oxidation in clouds, via the $SO_2 + O_3$ reaction, relative to the oxidation rates predicted from average cloud water composition (Roelofs, 1993; Collet et al., 1994; Gurciullo and Pandis, 1997). Comparison of bulk and size-resolved sulfate chemistry models (Kreidenweis et al., 2003) indicated that that due to the variability of pH among drops, size-resolved models consistently calculate 2-3 times more oxidation via the $SO_2 + O_3$ pathway. In the present study, the $SO_2 + O_3$ reaction had a minor contribution to the total sulfate production. Thus the factor of three underestimation of the contribution can be expected to induce a minor change in the total sulfate formation. Under other atmospheric conditions, however, pH variability among drops might have larger impact.

In addition, a size-dependent composition of the initial aerosol population can also affect the outcome of processing by causing pH variability in the droplet population. Field measurements of pH variation within natural cloud drop populations reveal that small drops forming on small particles are often more acidic than large drops forming on bigger particles, which tend to have more basic composition (e.g., sea salt), with acidity differences of 1 pH unit or more between the smallest and the largest droplets (e.g., Collet et al., 1994).

Studies resolving the aerosol and droplet spectra indicate differential modification of aerosol size categories. The largest modifications of the aerosol spectrum due to aqueous-phase sulfate production occur in the smallest particle size categories activated in cloud (e.g., Hegg and Larson, 1990; Bower and Choularton, 1993; Krendenweis et al., 2003). This creates a minimum ("Hoppel" gap) in the processed aerosol spectrum (Hoppel et al., 1990; Hoppel et al., 1994). Particles equal to or larger than the smallest

activated particle show the largest increase in particle size due to mass addition. The large tail of the particle spectrum shows essentially negligible change, since the relatively small amount of added sulfate mass does not appreciably modify the size of these large particles (Krendenweis et al., 2003).

b) *Comparison with other studies*

Although prior research has addressed similar issues to those addressed here, comparison is sometimes difficult in that these studies addressed different cloud types and omitted or did not quantify the effect of certain processes. For example, Bower and Choularton (1993) and Flossmann (1994) have investigated the role of processing on hill cap clouds and precipiting cumulus, respectively. The work of Bower and Choularton (1993) focused on chemical processing only, while that of Flossmann (1994) included both chemical processing and collision-coalescence. The latter study, however, did not quantify the effect of collision-coalescence on the aerosol spectrum; quantification would have been difficult due to the occurrence of precipitation. Thus, comparison of the present work with those studies would have been misleading due to different conditions.

Nevertheless, studies that considered stratocumulus clouds and quantified the effects of the two processing mechanisms allow some general comparisons and inferences. In these cases, differences with the present study might arise from the use of different chemical scenarios. (Differences in the details of treatment of microphysics and chemistry with the current study are inevitable.) Feingold et al. (1996) reported that the impact of physical processing on the aerosol spectrum regenerated from a stratocumulus cloud was dominant at large LWC (~ 0.5 g m^{-3}), ranging from negligible to of the order

of 10 % change over the course of 1 hour of processing. The effect of aqueous chemistry in conditions of relatively low concentrations of SO_2 (55 pptv) was non-negligible but was generally smaller (on the order of few percent change). In contrast, the impacts of aqueous chemistry for small LWC (< 0.2 g m^{-3}) were as substantial as those resulting from collision-coalescence processing (on the order of 1-2 %). Hatzianastassiou et al. (1998) arrived at similar conclusions. It is emphasized, however, that the lognormal CCN spectra considered by Feingold et al. (1996) and Hatzianastassiou et al. (1998), with clean maritime air with particle concentration not exceeding 100 cm^{-3} and mean particle radius on the order of or less than 0.05 μm, were quite different than the initial aerosol spectrum used in the present study.

More recently, Feingold and Kreidenweis (2002) explored a chemical scenario with higher SO_2 concentrations (1 ppbv) and a wider range of CCN conditions for physical processing (N_{CCN} = 50-200 cm^{-3}, $\bar{r}_{CCN}$ = 0.05-0.1 μm, and, σ_{CCN} =1.8-1.5) in a heavily drizzling stratocumulus (LWP=200 g m^{-3}). That study is in general agreement with the previous studies indicating small impact of aqueous processing on particle size when aerosol concentration is low (less than 100 cm^{-3}) and collection is efficient. In contrast, simulations with aerosol concentrations greater than 150 cm^{-3} resulted in large increases in aerosol mass and radius (larger than 30 % at time of maximum LWP) due to aqueous chemistry. The largest increases were reported for simulations with a relatively small particle radius of 0.05 μm. In simulations with a larger particle radius of 0.1 μm, the second aerosol mode created by the addition of sulfate mass, which usually resides at a similar radius (Hoppel et al., 1990), was not separated substantially from the original

aerosol mode. The occurrence of drizzle in this study makes comparison with the present study difficult.

Thus the different nature of the cloud types simulated in these studies from the stratocumulus cloud simulated in this work together with the sensitivity to environmental parameters used in these studies make definitive comparison difficult. It is noteworthy, however, that the impact of processing, obtained here with a bulk model at cloud system scales of the order of a few km is in agreement with previous work, conducted with more detailed size-resolving models at the large-eddy scales on the order of few hundred meters.

b) *Role of drop collection efficiency*

As demonstrated earlier, the efficiency of the collection process can substantially influence the outcome of physical processing. Processing via the collision-coalescence pathway in clouds experiencing significant collection induced greater increase in particle mean radius than that in clouds with weaker collection. Inevitably, some amount of solute residing in the large drop category is deposited on the ground with precipitation. This effect, which occurs only in the precipitating case, diminishes the impact of processing by the cloud on the aerosol below cloud. In the upper part of the cloud and above cloud, however, larger increase in particle mean radius was observed associated with stronger collection.

Table 6.1 summarizes the modifications of the two regenerated modes in the two cases (see Fig. 5.6, 5.7, 6.7 and 6.8). In the precipitating case, increases in aerosol mean radius of the first processed mode of 2-5 nm (5-10 %) are common although increases as

high as 7 nm are observed in some areas. In comparison, the stratocumulus case is characterized by more modest increases in the mean radius of up to 2-3 nm (3-5 %). The impact on the second processed mode was similarly stronger in the precipitating case, which produced larger particles (0.5-1 μm) than the stratocumulus case (0.2-0.7 μm). However the concentration of this mode in both cases was too small (<0.1 cm^{-3}) to be considered a significant source of atmospheric aerosol.

The two cloud types produced different spatial patterns of processed aerosol. The results for the stratocumulus case, characterized by standing forcing (lake-surface contrast) and steady horizontal winds, suggest that the regions of maximum impact of processing are below and downwind of the processing cloud. The results for the frontal case, characterized by more complex airflow with vertical wind shear and shift of the horizontal winds, suggest maximum impact of processing in the upper part of the cloud and above the cloud. Below the frontal cloud the signal is weaker, which is explained by removal of solute by precipitation.

Table 6.1: Summary of the parameters of the first and second regenerated modes in experiment S1 for Bay of Fundy and Lake Erie cases and changes relative to experiment S0*.

Case N_a a_m	1st processed mode	Change S1–S0	(%)	2st processed mode	(Change S1–S0, %)
Bay of Fundy					
1500 cm^{-3}	50 – 500 cm^{-3}	(–) 100 – 300 cm^{-3}	(20 – 75 %)	0.001 – 0.01 cm^{-3}	(100 %)
50 nm	60 – 75 nm	(+) 2-5 nm	(5 – 10 %)	0.5 – 1 μm	(100 %)
Lake Erie					
5000 cm^{-3}	100 – 2000 cm^{-3}	(–) 100 – 300 cm^{-3}	(10 – 30 %)	0.01 – 0.1 cm^{-3}	(100 %)
44 nm	50 – 80 nm	(+) 0.5 – 2-3 nm	(<1 % – 3-5 %)	0.2 – 0.7 μm	(100 %)

* A plus (minus) sign indicate increase (decrease) relative to experiment S0.

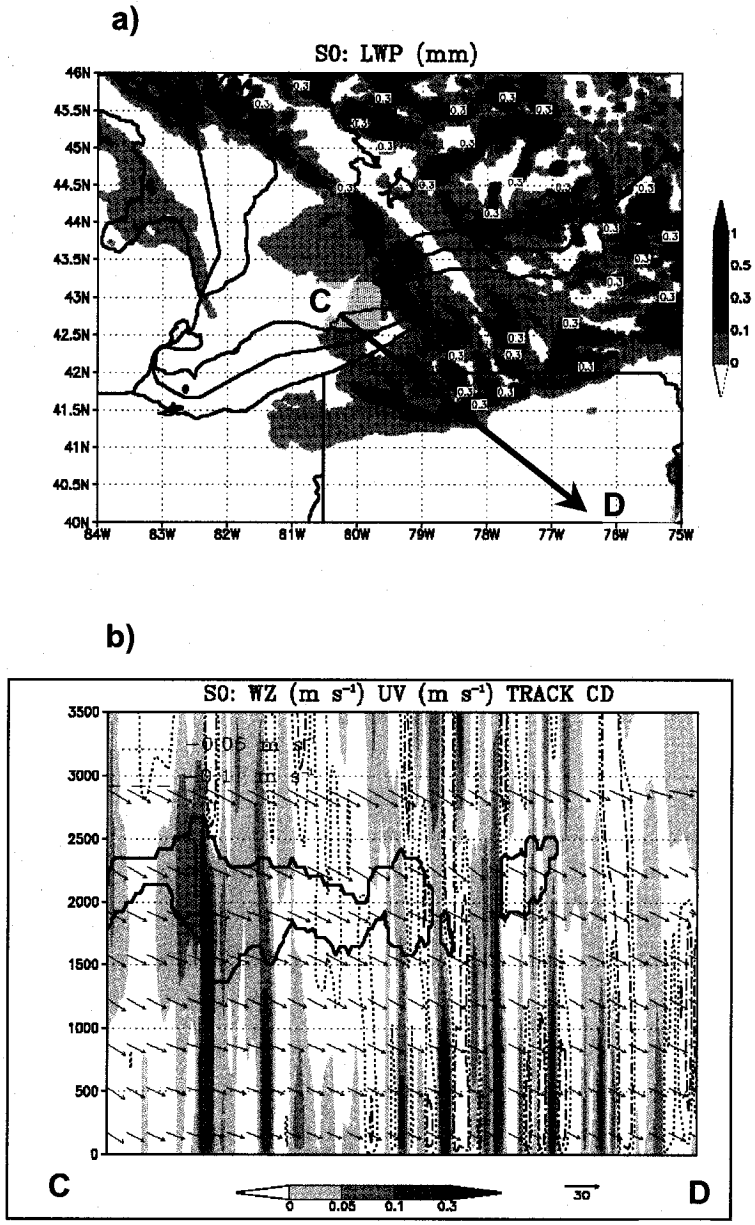

Figure 6.1: Various fields in experiment S0: a) cloud LWP (mm) and horizontal winds (m s^{-1}); line CD indicates the vertical cross-section in b); b) vertical velocity (m s^{-1}) in shading (positive values) and in contours (negative values); the solid contour shows the cloud boundary. Panels are valid at 1800 UTC.

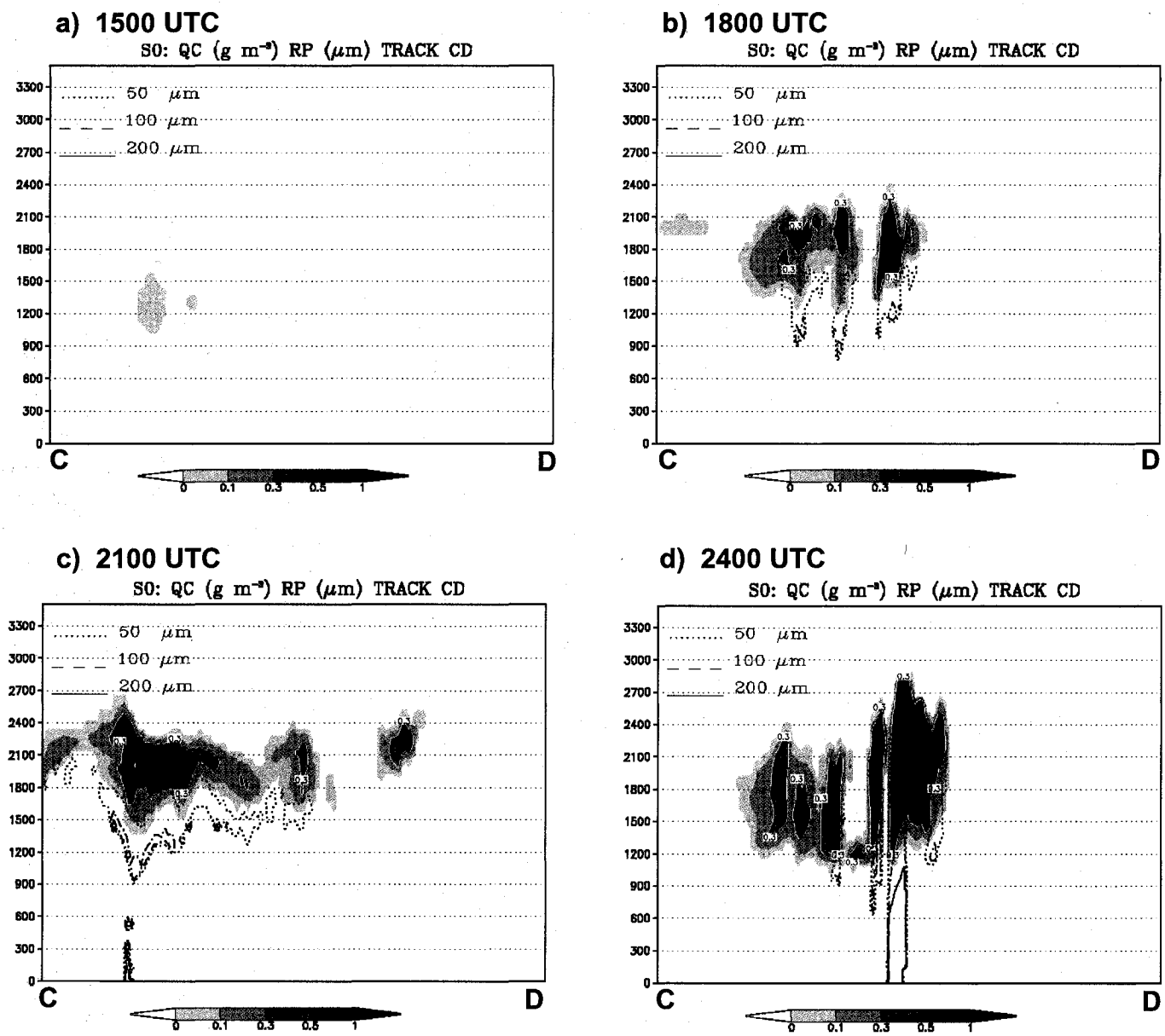

Figure 6.2: Various fields in experiment S0: a) cloud LWP (mm); the arrow indicates cross section CD in the remaining panels; b), c) and d) show cloud LWC (g m^{-3}) in shading and raindrop radius (μm) in contours. Panels are valid at: a) 1500 UTC, b) 1800 UTC; c) 2100 UTC, and d) 2400 UTC.

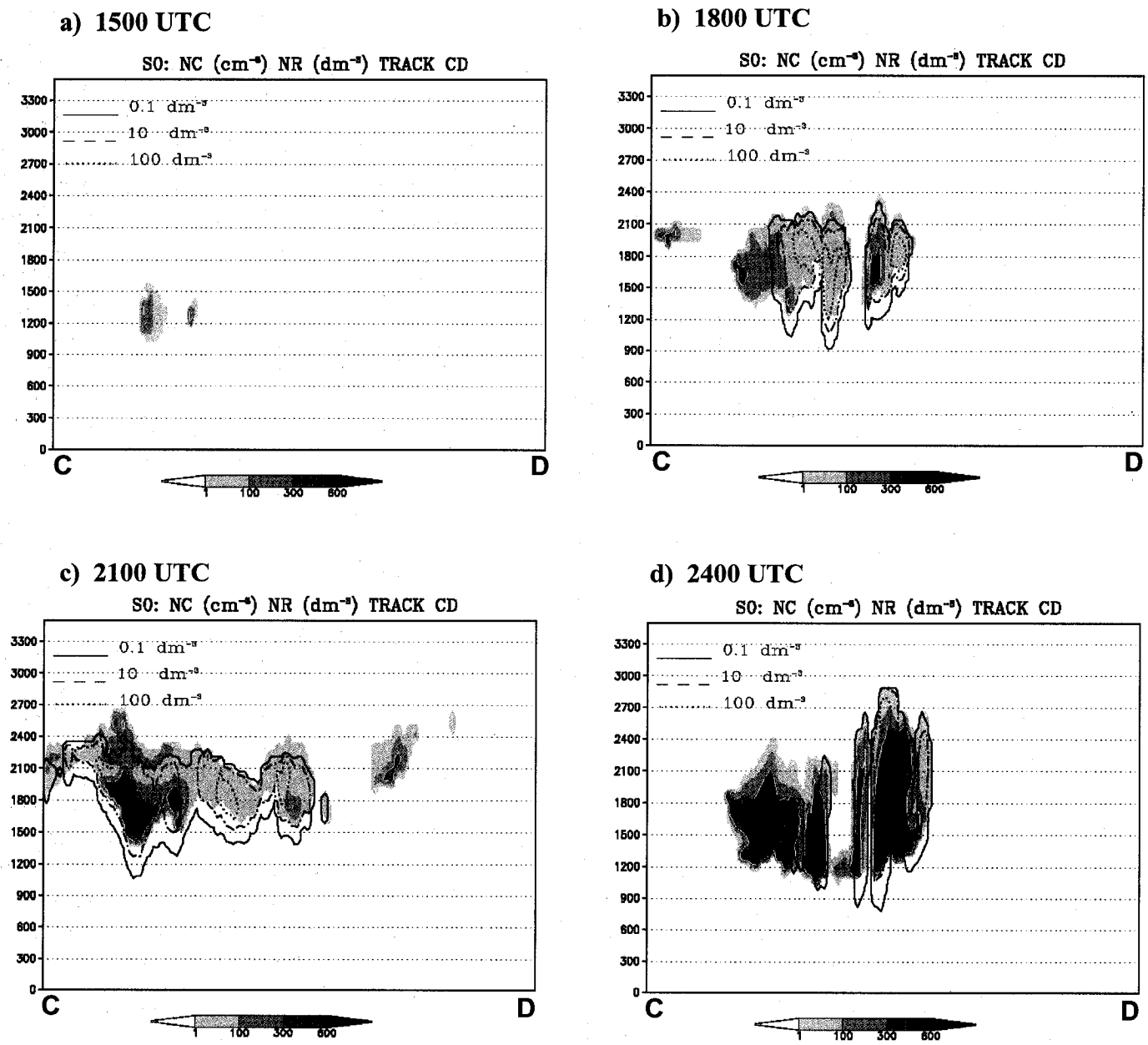

Figure 6.3: Same as Fig. 6.2 but for cloud droplet concentration (cm^{-3}) in shading and raindrop concentrations (dm^{-3}) in contours.

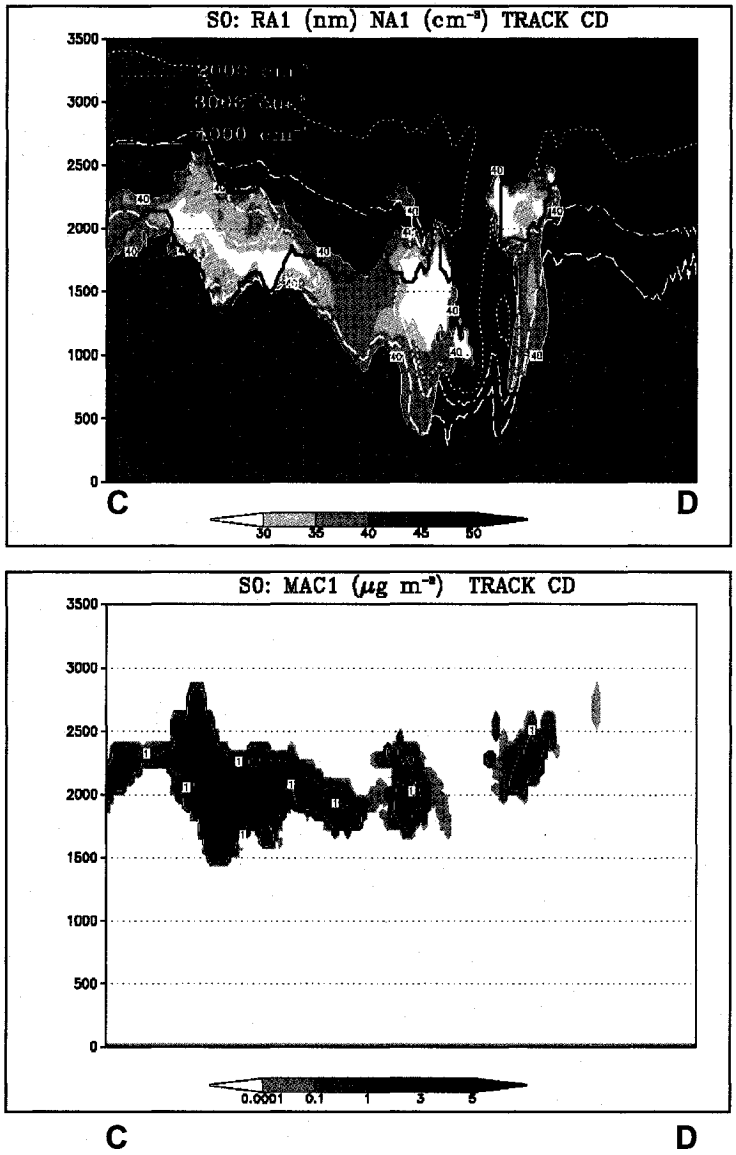

Figure 6.4: Various fields in experiment S0: a) vertical velocity (m s^{-1}; positive values in shading, negative in contours) and horizontal winds (m s^{-1}); b) background aerosol mode geometric mean radius (in terms of number; nm; in shading) and number concentration (cm^{-3}; in contours); and c) solute content in cloud drops (μg m^{-3}). Panels are valid at 2100 UTC. Solid contour shows cloud boundary. The cross-section is taken along line CD.

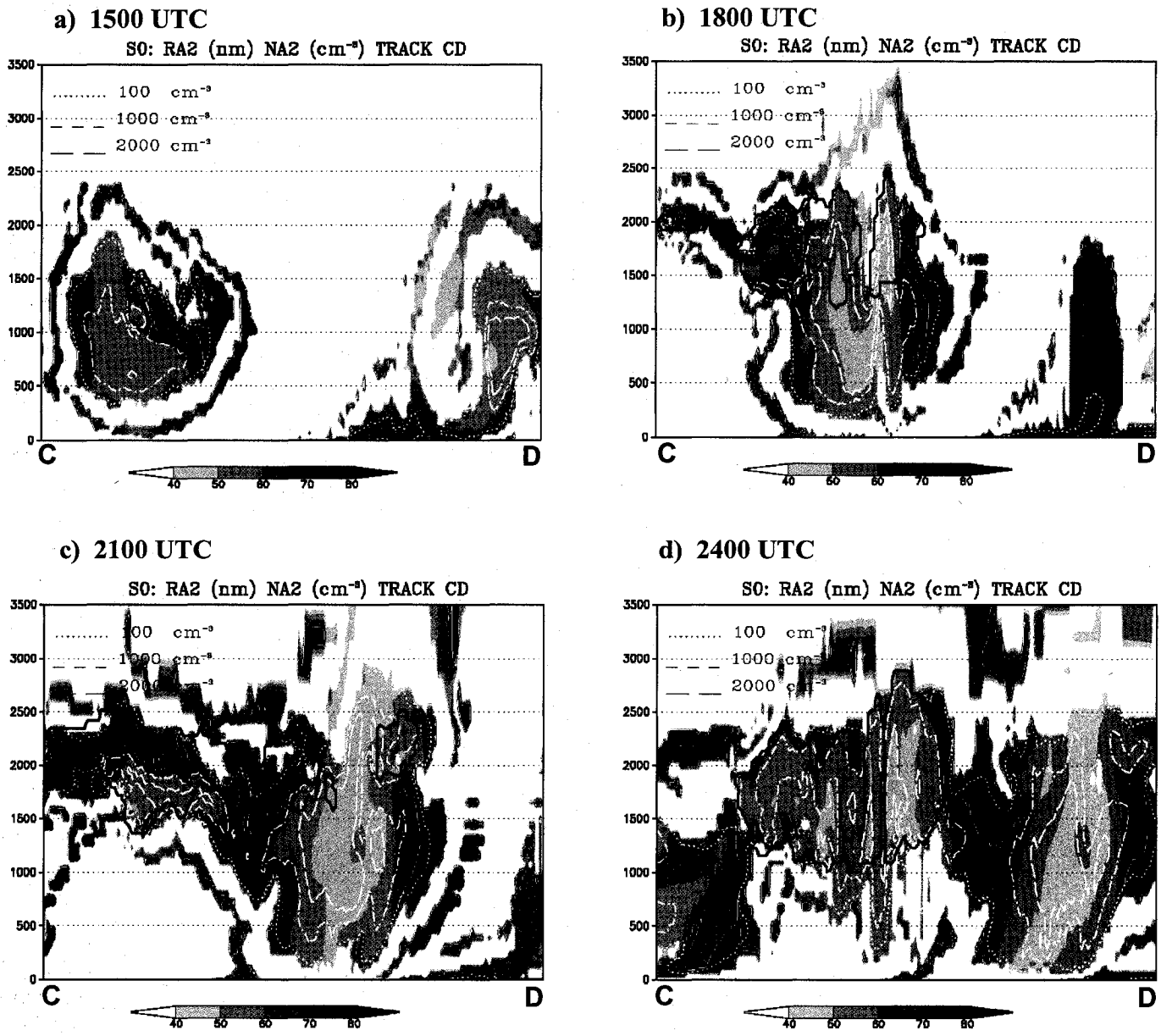

Figure 6.5: Geometric mean radius (in terms of number, nm) (in shading) and number concentration (cm^{-3}) (in contours) of first regenerated mode (without processing). Panels are valid at a) 1500 UTC, b) 1800 UTC, c) 2100 UTC and d) 2400 UTC. The solid contour shows the cloud boundary. The cross-section is taken along line CD.

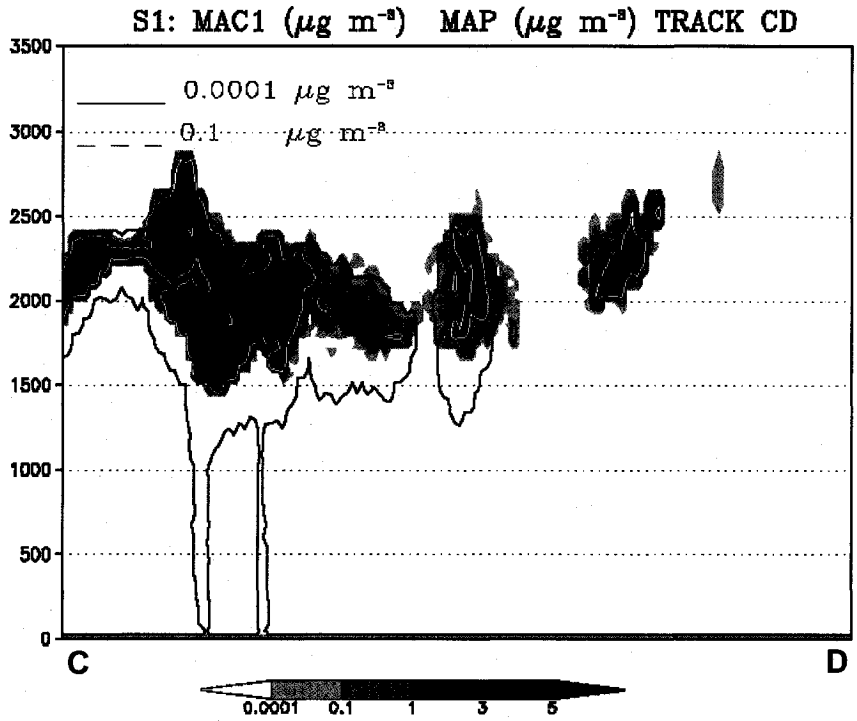

Figure 6.6: Solute content in cloud category (in shading) and in large hydrometeor category (in contours) (μg m^{-3}). The cross-section is taken along line CD.

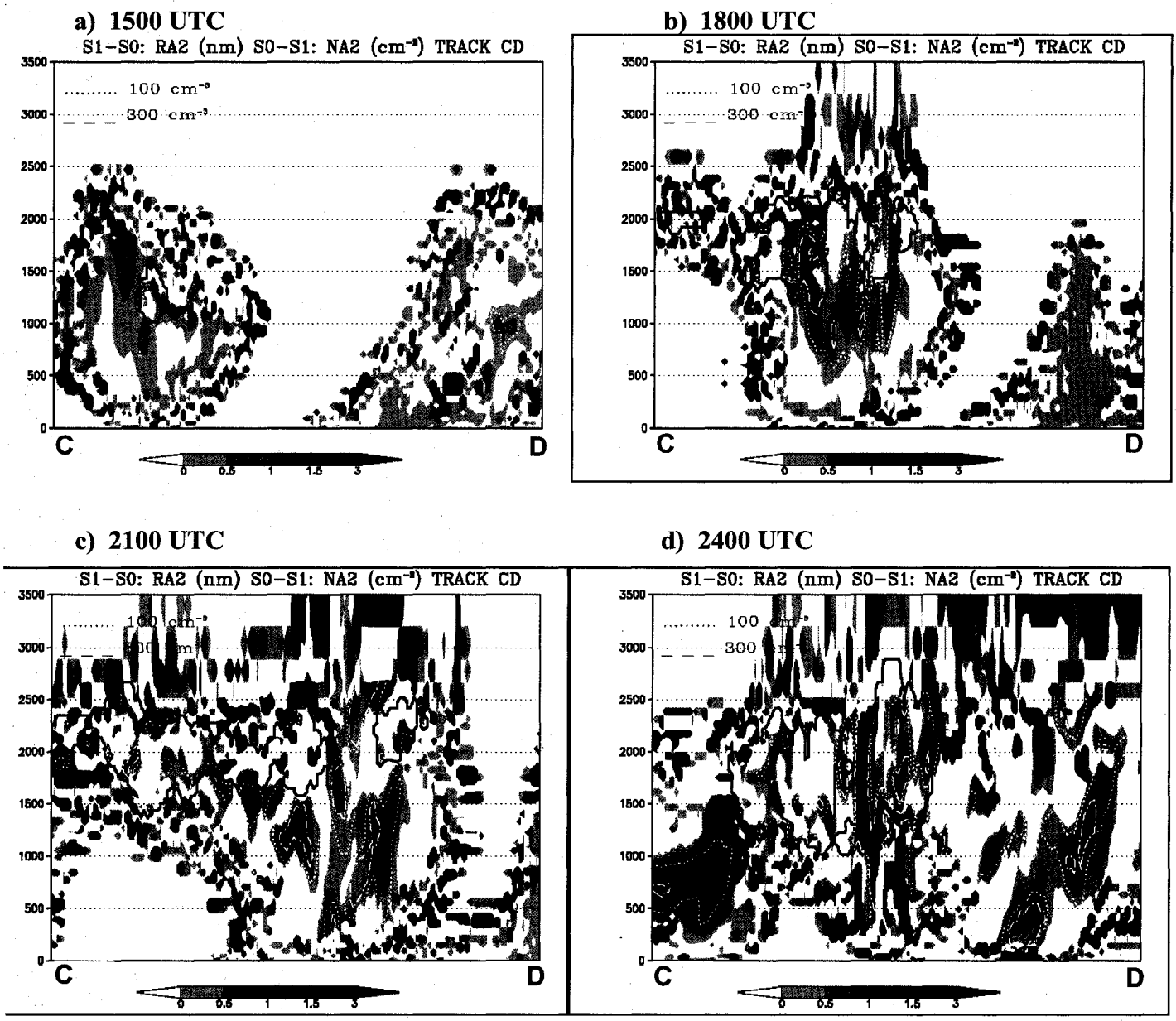

Figure 6.7: Change of the total number concentration (cm^{-3}) of first processed mode in experiment S0 relative to S1. Panels are valid at a) 1500 UTC, b) 1800 UTC, c) 2100 UTC and d) 2400 UTC. The black contour shows the cloud boundary. The cross-section is taken along line CD.

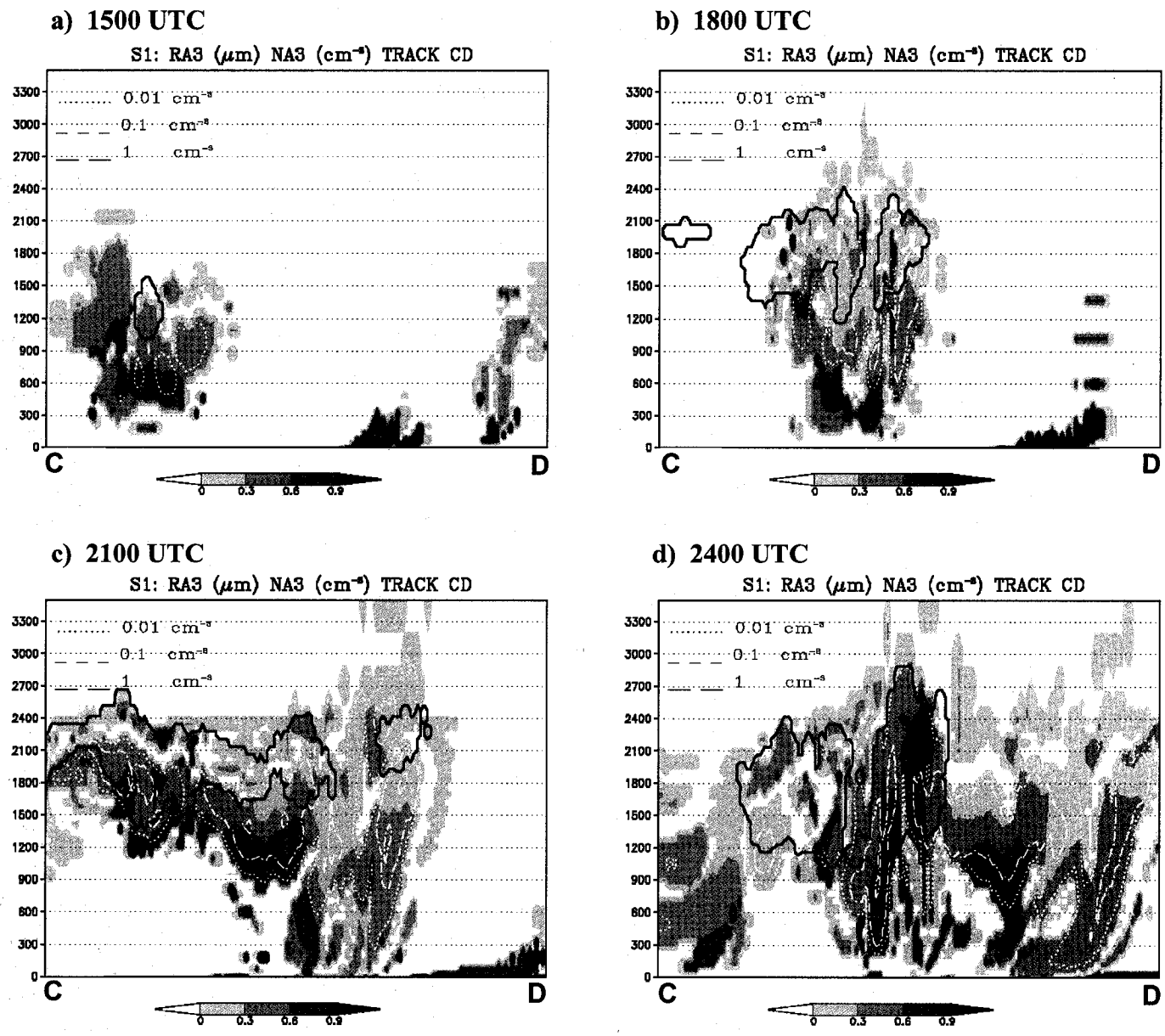

Figure 6.8: Geometric mean radius (in terms of number, μm) in shading and number concentration (cm^{-3}) in contours of second regenerated mode. Panels are valid at a) 1500 UTC, b) 1800 UTC, c) 2100 UTC and d) 2400 UTC. The solid contour shows the cloud boundary. The cross-section is taken along line CD.

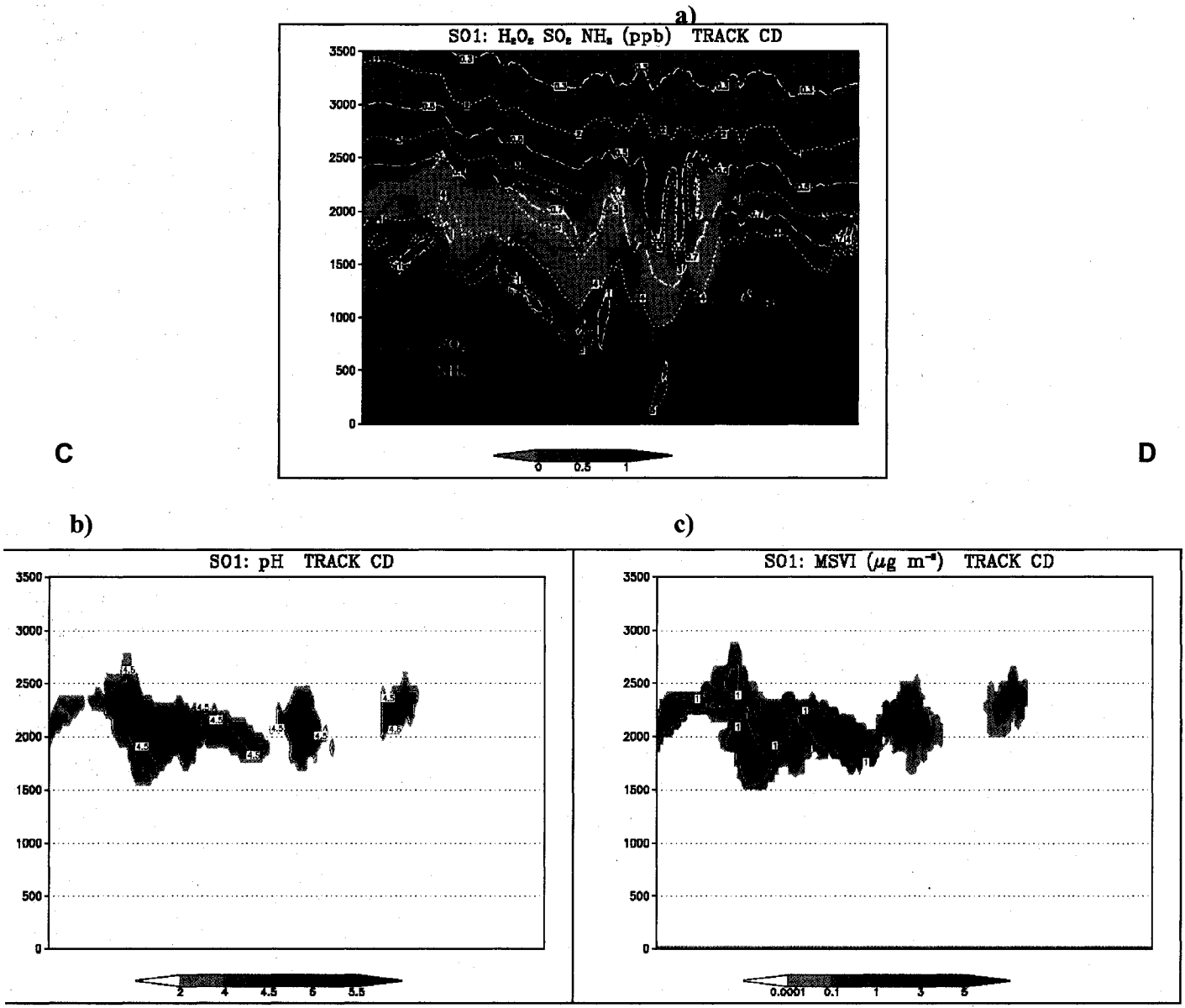

Figure 6.9: Various chemical species in experiment SO1: a) SO_2 (ppbv) b) NH_3 (ppbv) c) H_2O_2 (ppbv) and d) pH units. Panels are valid at 1800 UTC. The cross-section is taken along line CD.

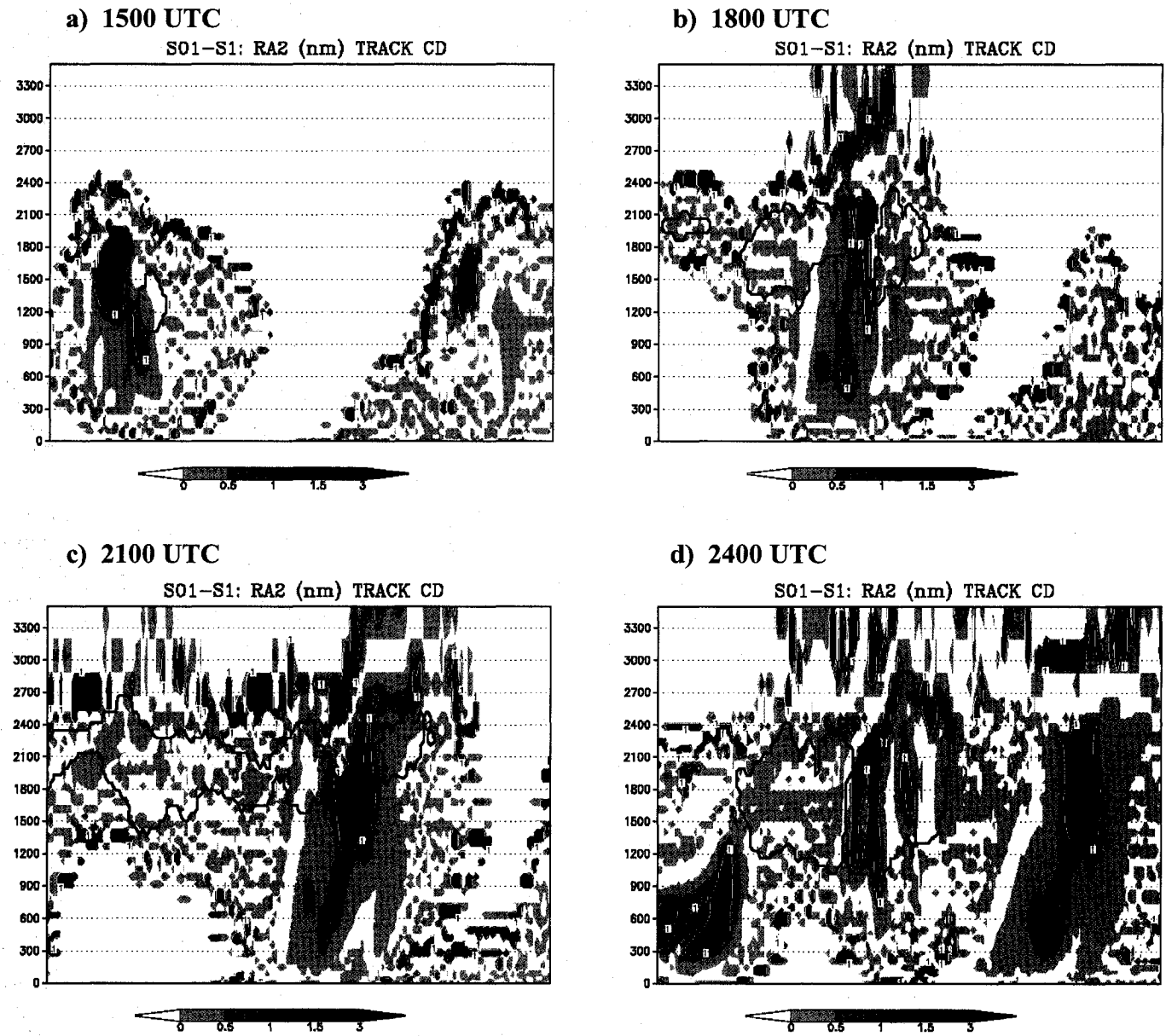

Figure 6.10: Change of the geometric mean radius (in terms of number; nm) of first processed mode in experiment SO1 relative to S1. Panels are valid at a) 1500 UTC, b) 1800 UTC, c) 2100 UTC and d) 2400 UTC. The black contour shows the cloud boundary. The cross-section is taken along line CD.

Chapter VII

Summary and Conclusions

Up to now numerical studies of a coupled aerosol-cloud-chemistry system using mesoscale models have not been attempted. Previous high-resolution studies have only been conducted in an idealized setting or for cloud systems of limited spatial dimensions. Present computational resources enabled us to undertake a high-resolution study exploring the feedbacks between aerosols and clouds using a mesoscale model. The grid spacing used by the model (3 km in the horizontal; 50-70 m in vertical) resolved the cloud system and the modeling domain captured the cloud system during its entire lifetime.

An explicit bulk representation of aerosol – cloud – chemistry feedbacks has been introduced in the model through a system of continuity equations for a multi-modal (background, activated, and regenerated) lognormal aerosol. The aerosol species were represented in terms of properties directly measured by experiment. This allowed us to link directly the cloud properties to the aerosol properties and represent the feedbacks explicitly. The cloud processes were represented by an explicit double-moment microphysical parameterization. The aqueous sulfur chemistry was introduced using a bulk approach and continuity equations for selected chemical species. The philosophy behind this approach is that it provides balance in the detail of representation of dynamics, microphysics, and aerosol. The main advantage is in the separation of the aerosol species, thus modifications of the aerosol spectrum by cloud processes can be accurately determined. The main drawback is the limitation of the two-moment representation of

the aerosol and cloud, which requires the spread of the distribution to remain fixed, and in the bulk approach for chemistry in which the effect of pH variations among drop categories on the oxidation rates is neglected.

The application part of the study includes evaluation of three summertime cases: a marine stratus cloud, a cold frontal system, and a continental stratocumulus cloud. The marine stratus cloud and the frontal system occurred on 1 September 1995 on the eastern coast of Canada near the Bay of Fundy, Nova Scotia. The stratus formed at 18 UTC and the frontal system passed 6 hours earlier. The continental stratocumulus cloud occurred on 11 July 2001 south of Lake Erie. The aerosol effects on cloud and precipitation were evaluated for the marine stratus and the frontal system. The role of aerosol processing in clouds was evaluated for the frontal system and the stratocumulus cloud.

Numerical simulations of the marine stratus and the frontal system were performed with both simple and mechanistic activation parameterizations. The simulations of marine stratus have been verified against extensive aircraft measurements of cloud microphysical and thermodynamic properties taken as a part of the Radiation, Aerosol, and Cloud Experiment. The marine stratus and the frontal system were examined for sensitivity to the presence of giant CCN. The initial aerosol size distributions were taken from the measurements. The aerosol was assumed to have a homogeneous composition.

Simulation of the marine stratus with the simple activation parameterization and a non-varying one-mode aerosol demonstrated reasonable agreement with the observations for the thermodynamic parameters, upon which the stratus cloud depends, and for certain cloud-microphysical parameters. In particular, good agreement was found for air soundings and, on the microphysical side, LWC. Discrepancies, however, were found for the droplet concentration as

well as for the cloud base height, which were both significantly underestimated by the simulation. These discrepancies were overcome to a great extent by a simulation with the mechanistic activation and a varying uni-modal aerosol. In this simulation, the magnitude of the droplet concentration, the vertical distribution of the droplet concentration, and the cloud base height were in excellent agreement with the observations. Prediction of droplet concentration with the mechanistic activation is limited by the non-linear dependence of the number of activated CCN on updraft velocity, which is only described in the model as a grid-average quantity. Simulation of the marine stratus with the mechanistic activation and a varying two-mode aerosol (with giant CCN) demonstrated comparable results to the simulation with simple activation. This was attributed to the similarity of the particle spectrum in these two experiments, both of which included giant CCN. Both simulations produced significantly lower droplet concentration than the simulation with mechanistic activation and a one-mode aerosol. In addition, the cloud base height lowered, which implies aerosol – cloud – dynamics feedbacks. The hypothesis for drizzle-induced cooling of the sub-cloud layer as a primary mechanism of these feedbacks requires a more thorough investigation.

The simulations of the frontal system demonstrated a second-order effect of the giant CCN on precipitation. The upstream (less vigorous) part of the system exhibited enhanced rain intensity. This was due to reduction of droplet concentration by the giant CCN, which was sufficient to suppress the rain intensity in the upstream part but did not affect the maximum precipitation. These results suggest a spatially non-uniform response of the precipitation to the aerosol. This has important implications for short-term precipitation forecasting. Furthermore, the results suggest that it is also important to account for the multi-modality of the aerosol spectrum in regional models simulating the second indirect effect.

The impact on particle mean radius of collision-coalescence processing in the frontal system was highly variable in space. The magnitude of the impact amounted to 10 % for one cloud cycle and 15 % for multiple cycles and is in agreement with previous studies examining cloud processing in drizzling stratocumuli that were obtained at the large eddy scales and that resolved the aerosol and droplet spectra. Changes in the aerosol in and around the cloud due to cloud processing were complex. Due to the frontal circulation the strongest signal was observed above the cloud upper boundary; precipitation removal of solute diminishes the processing signal below the cloud lower boundary.

The impact of collision-coalescence processing on the droplet concentration in the frontal system was significant. An increase of the droplet concentration was obtained, the potential exists however for both positive and negative changes, as revealed by Feingold and Kreidenweis (2000), depending on the updraft velocity of the subsequent cloud cycle. The increased droplet concentrations resulted in suppression of the rain intensities in the less vigorous part of the system, while the effect on the maximum precipitation was insignificant.

Particle processing by collision-coalescence and aqueous-chemistry processing in the continental stratocumulus case resulted in a bi-modal distribution. The maximum impact was found below and downwind of the cloud. The occurrence of stratocumulus cloud with standing forcing (water-land contrast) and in steady horizontal airflow is common in the region of the Great Lakes. The modification of the particle spectrum in such conditions is easily identifiable and verifiable by field observations. The added sulfate mass by aqueous-phase oxidation of SO_2 increased the particle mean radius by up to 3-5 %. This increase was as significant as that by collision-coalescence processing alone. The initial trace-gas concentrations provide strong constraints on the chemical processing. For the case simulated here, characterized by high

concentrations of SO_2, beyond times of about 40 min the production of sulfate was oxidant (H_2O_2) limited. This limits the increase of the mean size of the processed particles.

The multi-modal representation of the aerosol and droplet spectra in the model was crucial to properly represent the collision-coalescence processing using the bulk approach. The results demonstrate the capability of mesoscale models to correctly simulate the modifications of the particle spectrum by clouds. Observational studies of cloud processing of aerosol would certainly be useful to verify the particle growth and the droplet concentration changes obtained by the model. Nevertheless, the obtained results are useful in that they provide guidance for in-situ measurements as to where to find the area of maximum impact of cloud processing. In addition, the implemented treatment of aerosol processing and the estimate of the effects are useful for air quality models.

There are still elements of the chemistry part of the model that can potentially be improved. This requires a true evaluation of the model on specific benchmarks through detailed comparisons with observations. Selected cases from field experiments can serve as such benchmarks. One example is the 2004 International Consortium for Atmospheric Research on Transport and Transformation (ICARTT) campaign. During this campaign, Meteorological Service Canada, Downsview, took cloud chemistry measurements in the Great Lakes region.

The aerosol processes included in a mesoscale model improved the regional simulation of marine stratus properties and affected the frontal precipitation. All cases discussed demonstrated significant variability in space of the cloud properties and of the aerosol impacts and illustrated the complexity of the coupled aerosol-cloud system at the cloud-system scales.

The objective of this study was to increase the understanding of the interactions between the aerosol and the clouds and precipitation in a regional model that display strong

inhomogeneity of cloud properties due to the dynamics of the system. We developed a benchmark including all processes and demonstrated a small flavor of the intricacy of the interactions and the inhomogeneity of the properties and the effects. If however in the future parameterizations of the regional effect of aerosol on clouds are to be developed, careful consideration is required to identify which processes may be omitted or simplified. This can be achieved through a systematic set of sensitivity tests investigating the individual components of the interaction for a variety of cases and synoptic conditions.

References

Abdul-Razzak, H., S. J. Ghan, and C. Rivera-Carpio, 1998: A parameterization of aerosol activation. Part I. Single aerosol types. *J. Geophys. Res.*, **103**, 6123–6131.

Abdul-Razzak, H., S. J. Ghan, and C. Rivera-Carpio, 2000: A parameterization of aerosol activation. Part II. Multiple aerosol types. *J. Geophys. Res.*, **105**, 6837–6844.

Ackerman, A. S., O. B. Toon, and P. V. Hobbs, 1995: A model for particle microphysics, turbulent mixing, and radiative transfer in the stratocumulus-topped marine boundary layer and comparison with measurements, *J. Atmos. Sci.*, **52**, 1204–1236.

Ackerman, A. S., O. B. Toon, D. E. Stevens, A. J. Heymsfield, V. Ramanathan, and E. J. Welton, 2000: Reduction of tropical cloudiness by soot. *Science*, **288**, 1042–1047.

Albrecht, B. A.,1989: Aerosols, Cloud Microphysics, and Fractional Cloudiness. *Science*, **245**, 1227–1230.

Banic, C. M., W. R. Leaitch, G. A. Isaac, M. C. Couture, 1996a: Transport of Ozone and sulfure to the North Atlantic atmosphere during the North-Atlantic Regional Experiment. *J. Geophys. Res.*, **101**, 29091-29104.

Banic, C.M., W.R. Leaitch, H.W. Barker, K.B. Strawbridge, A.V. Korolev, G.A. Isaac, M. C. Couture, J.I. MacPherson, J.W. strap and I. Gultepe, 1996b: Measurements of the Microphysics of Low Stratus Clouds and the Radiation above, in and below Cloud, *Proceedings Vol. 2, 12th International Conference on Clouds and Precipitation*, Zurich, Switzerland.

Baumgardner, D., and M. Spowart, 1990: Evaluation of the Forward Scattering Spectrometer Probe. Part III: Time response and laser inhomogeneity limitations. J. *Atmos. Oceanic Technol.*, **7**, 666-672.

Baumgardner, D., W. Strapp, and J. E. Dye 1985: Evaluation of the Forward Scattering Spectrometer Probe. Part II: Corrections for coincidence and dead-time losses. *J. Atmos. Oceanic Technol.*, **2**, 626-632.

Benoit, R., J. Cote, and J. Mailhot, 1989: Inclusion of a TKE boundary layer parameterization in the Canadian regional finit element model. *Mon. Wea. Rev.*, **117**, 1726-1750.

Beniot, R., M. Desgagne, P. Pellerin, S. Pellerin, and Y. Chartier, 1997 : The Canadian MC2 : A semi-Lagrangian, semi-implicit wideband atmospheric model suited for finescale process studies and simulation. *Mon. Wea. Rev.*, **125**, 2382-2415.

Berry, E. X., 1967: Cloud droplet growth by collection. *J. Atmos. Sci.*, **24**, 688-701.

Berry, E. X., and R. L. Reinhardt, 1974: An analysis of cloud drop growth by collection: Part II. Single initial distributions. *J. Atmos. Sci.*, **31**, 1825-1831.

Bluestein, H. B., 1992: Synoptic-dynamic meteorology in midlatitudes. Oxford University Press. Vol. 1.

Bower, K. N. and T. A. Hill, H. Coe, and T. W. Choularton, 1991: SO_2 oxidation in an entraining cloud model with explicit microphysics. *Atmos. Environ.*, **25**, 2401-2418.

Bower, K. N. and T. W. Choularton, 1993: Cloud processing of the cloud condensation nucleus spectrum and its climatological consequences. *Q. J. R. Meteorol. Soc.*, **119**, 655-679.

Bower, K. N. et al., 1997: Observations and modeling of the processing of aerosol by a hill cap cloud. *Atmos. Environ.*, **31**, 2527-2543.

Brenguier, J. L., 1989: Coincidence and dead-time corrections for particles counters. Part II: High concentration measurements with an FSSP. J. *Atmos. Oceanic Technol.*, **6**, 585-598.

Chameides, W. L., 1984: The photochemistry of remote marine stratiform cloud. *J. Geophys. Res.*, **89**, 4739-4755.

Chameides and Davis, 1982: The free radical chemistry of cloud droplets and its impact upon composition of rain, *J. Geophys. Res.*, **87**, 4863-4877.

Chang, S. G., R. Toossi and T. Novakov, 1981: The importance of soot particles and nitrous acid in oxidizing SO_2 in atmospheric aqueous droplets, *Atmos. Environ.*, **15**, 1287-1292.

Chen, J. P., and D. Lamb, 1994: Simulation of cloud microphysical and chemical processes using a multi-component framework I. Description of the microphysical model, *J. Atmos. Sci.*, **51**, 2613-2636.

Cohard, J.-M. and J.-P. Pinty, 2000a: A comprehensive two-moment warm microphysical bulk scheme. I: Description and tests. *Quart. J. Roy. Meteor. Soc.*, **126**, 1815-1842.

Cohard, J.-M. and J.-P. Pinty, 2000b: A comprehensive two-moment warm microphysical bulk scheme. II: 2D experiments with a non-hydrostatic model. *Quart. J. Roy. Meteor. Soc.*, **126**, 1843-1859.

Cohard, J.-M., J.-P. Pinty, and C. Bedos, 1998: Extending Twomey's Analytical Estimate of Nucleated Cloud Droplet Concentrations from CCN spectra. *J. Atmos. Sci.*, **55**, 3348-3356.

Collett, J. L. Jr., A. Bator, X. Rao, B. B. Demoz, 1994: Acidity variations across the cloud drop size spectrum and their influence on rates of atmospheric sulfate production. *Geophys. Res. Lett.*, **21**, 2393-2396.

Chuang, C. C., J. E. Penner, K. E. Taylor, A. S. Grossmas, 1997: An assessment of the radiative effects of anthropogenic sulfate. *J. Geophys. Res.*, **102**, 3761-3778.

Dye, J. E., and D. Baumgardner, 1984: Evaluation of the Forward Scattering Spectrometer Probe. Part I: Electronic and optical studies. J. *Atmos. Oceanic Technol.*, **1**, 329-344

Feingold, G., S. M. Kreindenweis, B. Stevens, and W. R. Cotton, 1996a: Numerical simulation of stratocumulus processing of cloud condensation nuclei through collision-coalescence. *J. Geophys. Res.*, **101**, 21391-21402.

Feingold, G., B. Stevens, W. R. Cotton, and A. S. Frisch, 1996b: On the relationships between drop in-cloud residence time and drizzle production in stratocumulus clouds. *J. Atmos. Sci.*, **53**, 1108-1122.

Feingold, G., R. Boers, B. Stevens, and W. R. Cotton, 1997: A modeling study of the effect of drizzle on cloud optical depth and susceptibility. *J. Geophys. Res.*, **102**, 13527-13534.

Feingold, G., R. K. Walko, B. Stevens, W. R. Cotton, 1998: Simulations of marine stratocumulus using a new microphysical parameterization scheme. *Atmos. Res.*, **47-48**, 505-528.

Feingold, G., S. M. Kreindenweis, and Y. Zhang, 1998: Stratocumulus processing of gases and cloud condensation nuclei, I, Trajectory ensemble model. *J. Geophys. Res.*, **103**, 19527-19542.

Feingold, G. and S. M. Kreindenweis, 2000: Does cloud processing of aerosol enhance droplet concentrations? *J. Geophys. Res.*, **105**, 24351-24362.

Feingold, G. and S. M. Kreindenweis, 2002: Cloud processing of aerosol as modeled by a large eddy simulation with coupled microphysics and chemistry. *J. Geophys. Res.*, **107**, 4687.

Flossmann, A. I., W. D. Hall, and H. R. Pruppacher, 1985: A theoretical study of the wet removal of atmospheric pollutants. Part I: The redistribution of aerosol particles captured through nucleation and impaction scavenging by growing cloud drops. *J. Atmos. Sci.*, **42**, 583-606.

Flossmann, A. I., 1994: A 2-D spectral model simulation of the scavenging of gaseous and particulate sulfate by a warm marine cloud. *Atmos. Res.*, **32**, 233-248

Fritsch J. M., and C. F. Chappel, 1980: Numerical prediction of convectively driven mesoscale pressure systems. Part I: Convective parameterization. *J. Atmos. Sci.*, **37**, 1722-1733.

Garand, L., and J. Mailhot, 1990: The influence of infrared radiation on numerical weather forecasts. *Reprints, 7th Conference of Atmospheric Radiation*, San Francisco, CA, Amer. Meteor. Soc., J146-J151.

Garrett, T. J. and P. V. Hobbs, 1995: Long-range transport of continental aerosol over the Atlantic ocean and their effects on cloud structures. *J. Atmos. Sci.*, **52**, 2977-2984.

Ghan S. J., L. R. Leung, and R. C. Easter, 1997: Prediction of cloud droplet number in a general circulation model. *J. Geophys. Res.*, **102**, 21777-21794.

Ghan, S. J., G. Guzman, and H. Abdul-Razzak, 1998: Competition between sea salt and sulfate particles as cloud condensation nuclei. *J. Atmos. Sci.*, **55**, 3340-3347.

Ghan S. J., R. C. Easter, J. Hudson, F.-M. Breon, 2001: Evaluation of aerosol indirect radiative forcing in MIRAGE. *J. Geophys. Res.*, **106**, 5317-5334.

Glazer, A. and H. G. Leighton, 1994: An evaluation of the ADOM cloud module, *Atmos. Ocean.*, **32**,645-661.

Golaz, J.-C., V. Larson, and W. Cotton, 2002: A PDF-based model for boundary layer clouds. Part I: Method and model description, *J. Atmos. Sci.*, **59**, 3540-3551.

Gong, S.L., L.A. Barrie, J.-P. Blanchet, K. von Salzen, U. Lohmann, G. Lesins, L. Spacek, L.M. Zhang, E. Girard, H. Lin, R. Leaitch, H. Leighton, P. Chylek, and P. Huang, 2003: Canadian Aerosol Module: A size segregated simulation of atmospheric aerosol processes for climate and air quality models: Part 1. Module development. *J. Geophys. Res.,* **108(D1)**, 4007, doi:10.1029/2001JD002002, 16 pp.

Guan, H., Tremblay, A., and Isaac, G. A., 2000: Numerical simulation of stratus clouds and their sensitivity to radiation – A RACE case study. *J. Appl. Meteor.*, **39**, 1881-1893.

Gurciullo, C. S. and S. N. Pandis, 1997: Effect of composition variations in cloud droplet populations on aqueous chemistry. *J. Geophys. Res.*, **102**, 9375-9385.

Hatzianastassiou, N., W. Wobrock, and A. I. Flossmann, 1998: The effect of cloud-processing of aerosol particles on clouds and radiation. *Tellus*, **50B**, 478-490.

Hegg, D. A. and P. V. Hobbs, 1982: Measurement of sulfate production in natural clouds. *Atmos. Environ.*, **16**, 2663-2668.

Hegg, D. A., L. F. Radke, and P.V. Hobbs, 1990: Particles production associated with marine clouds, *J. Geophys. Res.*, **95**, 13917-13926.

Hegg, D. A., and T. V. Larson, 1990: The effect of microphysical parameterization on model predictions of sulfate production in clouds, *Tellus*, **42B**, 272-284.

Hegg, D. A., R. Majeet, P. F. Yuen, M. B. Baker, and T. V. Larson, 1996: The impacts of SO2 oxidations in cloud drops and haze particles on aerosol light scattering and CCN activity, *Geophys. Res. Lett.*, 23, 2613-2616.

Hoppel, W. A., J. W. Fitzgerald, G. M. Frick, and R. E. Larson, 1990: Aerosol size distributions and optical properties found in the marine boundary layer over the Atlantic Ocean. *J. Geophys. Res.*, **95**, 3659-3686.

Hoppel, W.A., G.M. Frick, J.W. Fitzgerald, and B.J. Wattle, 1994: A cloud chamber study of the effect that nonprecipitating water clouds have on the aerosol size distribution. *Aerosol Sci. and Technol.,* **20**, 1-30.

Hudson, J. G., 1993: Cloud condensation nuclei new marine cumulus. *J. Geophys. Res.*, **98**, 2693-2702.

Hung, H.-M., P. A. Ariya, H. G. Leighton, 2005: The impact of organic properties on droplet activation, Submitted to *Atmos. Environ.*

Isaac, G. A., C. M. Banic, W. R. Leaitch, K. G. Anlauf, M. D. Couture, P. S. K. Liu, A. M. Macdonald, K. I. A. MacQuarrie, K. J. Puckett, and H. A. Weibe, 1998: Vertical profiles and horizontal transport of atmospheric aerosols and trace gases over central Ontario, *J. Geophys. Res.*, **103**, 22015-22037.

Jiang, H., G. Feingold, and W. R. Cotton (2002): Simulations of aerosol-cloud-dynamical feedbacks resulting from entrainment of aerosol into the marine boundary layer during the Atlantic Stratocumulus Transition Experiment. *J. Geophys. Res.*, **107**, 4813, doi:10.1029/2001JD001502.

Kessler, E., 1969: On the distribution of continuity of water substance on atmospheric circulation. *Meteor. Monorr.*, **10**, 84 pp.

Khain, J. S., and J. M. Fritsch, 1990: A one-dimensional entraining/detraining plume model and its application in convective parameterization. *J. Atmos. Sci.*, **47**, 2784-2802.

Khain, J. S., and J. M. Fritsch, 1993: Convective parameterization for mesiscale models: The Khain-Fritsch scheme. *The Representation of Cumulus Convection in Numerical Models, Meteor. Monogr.*, No. **46**, Amer. Meteor. Soc., 165-177.

Khairoutdinov, M. F., and Y. L. Kogan, 2000: A new cloud physics parameterization for large-eddy simulation model of marine stratocumulus. *Mon. Wea. Rev.*, **128**, 2115-2131.

Klein, S. A. and D. L. Hartmann, 1993: The seasonal cycle of low stratiform clouds. *J. Climate*, 6, 1587-1606.

Kogan, Y. L., M. P. Khairoutdinov, D. K. Lilly, Z. N. Kogan, and Qingfu Liu, 1995: Modeling of stratocumulus cloud layers in a large eddy simulation model with explicit microphysics . *J. Atmos. Sci.*, **52**, 2923-2940.

Kong, F.-Y., and M. K. Yau, 1997: An explicit approach of microphysics in MC2. *Atmos.-Ocean*, **35**, 257-291.

Kong, F.-Y., Huang, M.-Y., and Xu, H.-Y., 1990: Three-dimensional numerical simulation of ice-phase microphysics in cumulus clouds. Model establishment and ice-phase processes parameterization. Chinese J. Atmos. Sci., **14**, 437-450.

Kreidenweis, S. M., C. J. Walcek, G. Feingold, W. Gong, M. Z. Jacobson, C. Kim, X. Liu, J. E. Penner, A. Nenes, and J. H. Seinfeld, 2003: Modification of aerosol mass and size distribution due to aqueous-phase SO_2 oxidation in clouds: Comparison of several models. *J. Geophys. Res.*, **108**, 4213.

Kuo, H.L., 1974: Further study on the parameterization of the influence of convection on large-scale flow. *J. Atmos. Sci.*, **31**, 1232-1240.

Leighton, H. G., M. K. Yau, A. M. Macdonald, J. S. Pitre, and A. Giles, 1990: A numerical simulation of the chemistry of a rainband, *Atmos. Environ.*, **24A**, 1211-1217.

Leighton, H. G., L. Lauzon, and W. R. Leaitch, 1996: Evaluation of a three-dimensional cloud chemistry model. *Atmos. Evnviron.*, **30**, 3651-3665.

Liu, P. S. K., W. R. Leaitch, A. M. Macdonald, G. A. Isaac, J. W. Strapp, and H. A. Weibe, 1993: Sulfate production in summer cloud over Ontario, *Tellus*, Sr. B, **45**, 368-390.

Liu, P. S. K., W. R. Leaitch, C. M. Banic, S.-M. Li, and D. Ngo, 1996: Aerosol observations at Chebogue Point during the 1993 North Atlantic Regional Experiment: Relationships among cloud condensation nuclei, size distributions, and chemistry, *J. Geophys. Res.*, **101**, 28971-28990.

Lohmann, U. and E. Roeckner, 1996: Design and performance of a new cloud microphysics scheme developed for the ECHAM general circulation model. *Clim. Dyn.*, **12**, 557-572.

Lohmann, U., J. Feichter, C. C. Chuang, and J. E. Penner, 1999a: Predicting the number of cloud droplets in the ECHAM GCM, *J. Geophys. Res.*, **104**, 9169-9198.

Lohmann, U., J. Feichter, C. C. Chuang, and J. E. Penner, 1999b: Corrections to predicting the number of cloud droplets in the ECHAM GCM, *J. Geophys. Res.*, **104**, 24557-24563.

Lohmann, U., J. Feichter, J. E. Penner, and R. Leaitch, 2000: Indirect effect of sulfate and carbonaceous aerosols: A mechanistic treatment, *J. Geophys. Res.*, **105**, 12193-12206.

Lohmann, U., and J. Feichter, 2001: Can direct and semi-direct aerosol effect compete with the indirect effect on a global scale? *Geophys. Res. Lett.*, **28**, 159-161.

Lohmann, U., 2002: Possible aerosol effects on ice clouds via contact nucleation, *J. Atmos. Sci.*, **59**, 647-656.

Long, A. B., 1974: Solutions to the droplet collection equation for polynomial kernels. *J. Atmos. Sci.*, **31**, 1040-1057.

Mailhot, J., Sarrazin, R., Bilodeau, B., Brunet, N., Methot, A., Pellerin, G., Chouinard, C., Garand, L., Girard, C., and Hogue, R., 1995: Changes to the Regional Forecast System: Description and Evaluation of the 50-km Version, *Atmos.-Ocean.*, **33**, 55-80.

Mailhot, J., S. Bélair, R. Benoit, B. Bilodeau, Y. Delage, L. Lillion, L. Garand, C. Girard, and A. Tremblay, 1998: Scientific description of RPN physics library – Version 3.6. Technical Report. Atmospheric Environment Service, Dorval, Québéc, 188 pp.

Martin, L. R., D. E. Damschen, and H. S. Judeikis, 1981: The reactions of nitrogen oxides with SO_2 in aqueous aerosols, *Atmos. Environ.*, **15**, 191-195.

McCaa, J. R. and C. S. Bretherton, 2004: A new parameterization for shallow cumulus convection and its application to marine subtropical cloud-topped boundary layers. Part II: Regional simulations of marine boundary layer clouds. *Mon. Wea. Rev.*, **132**, 883-896.

Mcdonald, A. M., K. G. Anlauf, C. M. Banic; W. R. Leaitch, and H. A. Wiebe, 1995: Airborne measurements if aqueous and gaseous hydrogen peroxide during spring and summer in Ontario, Canada. *J. Geophys. Res.*, **100**, 7253-7262.

Mechem, D. B. and Y. L. Kogan, 2003: Simulating the transition from drizzling marine stratocumulus to boundary layer cumulus with a mesoscale model. *Mon. Wea. Rev.*, **131**, 2342-2360.

Milbrandt, J. and M. K. Yau, 2005: Analysis of the role of the shape parameter in bulk microphysics parameterizations and a proposed triple-moment approach. *J. Atmos. Sci.* (accepted).

Mitra, S. K., J. Brinkmann, and H. T. Pruppacher, 1992: A wind tunnel study on the drop-to-particle conversion. *J. Aerosol Sci.*, **23**, 245-256.

Mocko, D. M. and W. R. Cotton, 1995: Evaluation of fractional cloudiness parameterizations fir use in a mesoscale model. *J. Atmos. Sci.*, **52**, 2884-2901.

Nagarajan, B., M. K. Yau, and D.-L. Zhang, 2001: A Numerical Study of a Mesoscale Convective System during TOGA COARE. Part I: Model description and validation. *Monthly Weather Review*, **129**, 2501–2520.

Nash, T., 1979: The effect of nitrogen dioxide and some transition metals on the oxidation of dilute bisulfite solutions, *Atmos. Eviron.*, **13**, 1149-1154.

Nenes, A., S. Ghan, H. Abdul-Razzak, P. Y. Chuang, and J. H. Seinfeld, 2001: Kinetic limitations of cloud droplet formation and impact on cloud albedo, *Tellus*, 53B, 133-149.

Nicholls, S. 1984: The dynamics of stratocumulus. *Quart. J. Roy. Meteor. Soc.*, **110**, 783-820.

Noonkester, V. R., 1984: Droplet Spectra Observed in Marine Stratus Cloud Layers, *J. Atmos. Sci.*, **41**, 829-845.

Penkett, S. A., B. M. R. Jones, K. A. Brice, and A. E. J. Eggleton, 1979: The importance of atmospheric ozone and hydrogen peroxide in oxidizing sulfur dioxide in cloud and rainwater. *Atmos. Environ.*, **13**, 123-137.

Penner, J. E., R. J. Charlson, J. M. Hales, N. Laulainen, R. Leifer, T. Novakov, J. Ogren, L. F. Radke, S. E. Schwartz, and L. Travis, 1994: Quantifying and minimizing uncertainty of climate forcing by anthropogenic aerosols, *Bull. Am. Met. Soc.*, **75**, 375-400

Penner, J. E., M. Andreae, H. Annegarn, L. Barrie, J. Feichter, D. Hegg, A. Jayaraman, R. Leaitch, D. Murphy, J. Nganga, and G. Pitari, Chapter 5: Aerosols, their Direct and Indirect Effects, in *Climate Change 2001: The Scientific Basis*, Ed. by H.T. Houghton, Y. Ding, D.J. Griggs, M. Noguer, P.J. van der Linden, X. Dai, K. Maskell, C.A. Johnson, Report to Intergovernmental Panel on Climate Change

from the Scientific Assessment Working Group (WGI), 289-416, Cambridge University Press.

Phiney, L. A., Lohmann, U., and W. R. Leaitch, 2003: Limitations of using the equilibrium approximation in an aerosol activation parameterization. *J. Geophys. Res.*, **108**, doi:10.1029/2002JD002391.

Pinty, J.-P., S. Cosma, J.-M. Cohard, E. Richard, and J.-P. Chaboureau., 2001: CCN sensitivity of a warm precipitation event over fine scale orography with a advanced microphysical scheme. *Atmos. Res.*, **59-60**, 419-446.

Platnick, S. and S. Twomey, 1994: Determining the susceptibility of cloud albedo to changes in droplet concentrations with the Advanced Very High Resolution Radiometer, *J. Appl. Meteor.*, **33**, 334-347.

Ramanathan, V., R. D. Cess, E. F. Harrison, P. Minnis, B. R. Barkstrom, E. Ahmad, and D. Hartmann, 1989: Cloud radiative forcing and climate: Results from the Earth Radiation Budget Experiment, Science, **243**, 57-63

Robert, A.., 1993: Bubble Convection Experiments with a Semi-Implicit Formulation of the Euler Equations. *Journal of the Atmospheric Sciences*, **50**, 1865–1873.

Robert, A.., T. L. Yee, and H. Ritchie, 1985: A Semi-Lagrangian and Semi-Implicit Numerical Integration Scheme for Multilevel Atmospheric Models. *Monthly Weather Review*, **113**, 388–394.

Roelofs, G. J. H., 1993: A cloud chemistry sensitivity study and comparison of explicit and bulk cloud model performance. *Atmos. Environ.*, **27A**, 2255-2264.

Rogers R. R. and M. K. Yau, 1996: A short course in cloud physics: Third edition, Butterworth-Heinmann.

Rosenfeld, D. R., 2000: Suppression of rain and snow by urban and industrial air pollution. *Science*, **287**, 1793-1796.

Rosenfeld, D. R. Lahav, A. Khain, M. Pinsky, 2002: The role of sea spray in cleansing air pollution over ocean via cloud processes. *Science*, **297**, 1668-1670.

Schwartz, S. E., P. H. Daum, M. R. Hjemfelt and L. Newman, 1982: Cloud water acidity measurements and formation mechanisms—experimental design. Precipitation scavenging, dry deposition and resuspension. *H. R. Pruppacher, R. G. Semonin, and W. G. N. Slinn, Coords., Elsevier*, 15-30.

Schwartz, S. E., 1984: Gas-aqueous reactions of sulfur and nitrogen oxides in liquid water clouds. SO_2, NO, and NO_2 oxidation mechanisms: Atmospheric considerations. *J. G. Calvert, Ed., Butterworth*, 254 pp.

Seifert, A. and K. D. Beheng, 2001: A double-moment parameterization for simulating autoconversion, accretion, and self-collection. *Atmos. Res.*, **59-60**, 265-281.

Seinfeld, J. H., 1986: *Atmospheric Physics and Chemistry of Air Pollution.* 738 pp., John Wiley, N. Y.

Slingo, A., 1982: Aircraft observations of marine stratocumulus during JASIN, *Quart. J. R. Met. Soc.*, **108**, 833-888.

Slingo, A., 1990: Sensitivity of the Earth's radiation budget to changes in low clouds. *Nature*, **343**, 49-51.

Song, Q. and H. G. Leighton, 1998: A parameterization for sulfate production in convective clouds for use in large-scale models, *Atmos. Res.*, **47-48**, 555-572.

Sundqvist H., E. Berge, and J.E. Kristjiansson, 1989: Condensation and cloud parameterization studies with a mesoscale numerical weather prediction model. *Mon. Wea. Rev.*, **117**, 1641-1657.

Tanguay, M., A. Robert, and R. Laprise, 1990: A Semi-implicit Semi-Lagrangian Fully Compressible Regional Forecast Model. *Monthly Weather Review*, **118**, 1970–1980.

Tremblay, A. and H. G. Leighton, 1986: A three-dimensional cloud chemistry model. *J. Clim. Appl. Meteorol.*, 25, 652-671.

Trautmann, T., 1993: On the stochastic approach to the kinetics in polydisperse multi-component populations, *Atmos. Res.*, **29**, 99-113.

Twomey, S., 1959: The nuclei of natural cloud formation. Part II: The supersaturation in natural clouds and the variation of cloud droplet concentration, *Geophys. Pura Appl.*, **43**, 243-249.

Twomey, S., 1971: The composition of cloud nuclei. *J. Atmos. Sci.* **28**, 377-381.

Twomey, S., 1974: Pollution and the planetary albedo. *Atmos. Environ.* **8**, 1251-1256.

Twomey, S., 1977: The Influence of Pollution on the Shortwave Albedo of Clouds. *J. Atmos. Sci.*, **34**,1149-1152.

Twomey, S. A., M. Peipgrass, and T. L. Wolfe, 1984: An assessment of the impact of pollution on global cloud albedo, *Tellus* B**36**, 356–366.

Von der Emde, K. and U. Wacker, 1993: Comments on the relationship between aerosol spectra, equilibrium drop size spectra, and CCN spectra. *Beitr. Phys. Atmos.*, 66, 157-162.

Von Salzen, K., H. G. Leighton, P.A. Aria, L. A. Barrie, S. L. Gong, J.-P. Blanchet, L. Spasek, U. Lohmann, and L. I. Kleinman, 2000: Sensitivity of sulfate aerosol size distributions and CCN concentrations over North America to SO_x emissions and H_2O_2 concentrations. *J. Geophys. Res.*, **105**, 9741-9765.

Wang, S., 1993: Modeling marine boundary-layer clouds with a two-layer model: A one dimensional simulation. *J. Atmos. Sci.*, **50**, 4001-4021.

Wang, S., B. A. Albrecht, and P. Minnis, 1993: A regional simulation of marine boundary layer clouds. *J. Atmos. Sci.*, **50**, 4022-4042.

Warner, J., 1968: A reduction of rainfall associated with smoke from sugar-cane fires – An inadvertent weather modification?, *J. Appl. Meteor.*, **7**, 247-251.

Wurzler, S., T. G. Reisin, and Z. Levin, 2000: Modification of mineral dust particles by cloud processing and subsequent effects on drop size distributions, *J. Geophys. Res.*, **105**, 4501-4512.

Yau, M. K., 1980: The effect of evaporation, water load, and wind shear on cloud development in a three-dimensional numerical model, *J. Atmos. Sci.*, **37**, 488-494.

Ziegler, C. L., 1985: Retrieval of thermal and microphysical variables in observed convective storms: Part 1: Model development and preliminary testing. *J. Atmos. Sci.*, **42**, 1487-1509.